UNIVERSITY OF OKLAHOMA

GRADUATE COLLEGE

A STUDY OF THE INTERACTIONS OF NITRIC OXIDE AND NITRIC OXIDE

CONTAINING MOLECULES WITH HEME PROTEINS

A DISSERTATION

SUBMITTED TO THE GRADUATE FACULITY

in partial fulfillment of the requirements for the

degree of

Doctor of Philosophy

By

DANIEL MORRIS COPELAND

Norman, Oklahoma

2006

UMI Number: 3237581

UMI®

Dissertation Publishing

ProQuest®

A STUDY OF THE INTERACTIONS OF NITRIC OXIDE AND NITRIC OXIDE
CONTAINING MOLECULES WITH HEME PROTEINS

A DISSERTATION APPROVED FOR THE
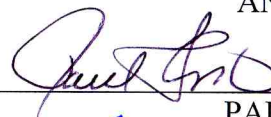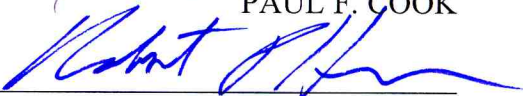DEPARTMENT OF CHEMISTRY AND BIOCHEMISTRY

BY

_____
GEORGE B. RICHTER-ADDO

_____
ANN H. WEST

_____
PAUL F. COOK

_____
ROBERT P. HOUSER

_____
JIMMY D. BALLARD

Acknowledgements

I would like to express my sincere gratitude to both of my major advisors, Dr. George B. Richter-Addo and Dr. Ann H. West for giving me the time and direction that was needed for the completion of this journey. From them I received skills and training that aided me in the completion of this project and will continue to benefit me in my future endeavors. I also want to thank the rest of my advisory committee, Dr. Paul F. Cook, Dr. Robert Houser, and Dr. Jimmy Ballard, for aiding me on this journey.

I also would be remiss if I did not thank all of the people that I have worked with in the time I have spent here. First and foremost I would like to thank Dr. Stace Porter and Dr. Fabiola Janiak-Spens who both took on the task of training me when I arrived and then were important collegues and friends as I continued my work here. I would also like to thank Dr. Lilian Chooback who joined the lab after I did, but once there provided the support and expertise in fields that I was not as strong in. I would also like to thank the rest of of the members of Dr. West and Dr. Cook's labs, especially, Hui Tan, Alla Dubrovska, Dr. Corey Johnson, Dr. Wael Rabeh and Dr. Babak Andi, who all provided assistance at some time or other, but were always available for discussion, whether related to science or not. I would additionally like to thank all the members of Dr. Richter-Addo's lab both past and present, even though I did not spend a whole lot of time with any of you because of geographic separation. I appreciated the time when we did get to work together, whether it be in discussion of back bonding and π orbitals, working on trying to solve X-ray structures or just shooting the breeze. Drs. Li Chen, Lin Cheng, and Jonghyuk Lee for all of their technical assistance in working with inorganic

List of Tables

List of Figures

Abbreviations

Mb	Myoglobin
hh Mb	horse heart myoglobin
sw Mb	sperm whale myoglobin
MbNO	nitrosyl myoglobin
P450BM-3	cytochrome P450 BM-3 heme domain
sGC	soluble guanylate cyclase
Hb	hemoglobin
P450	cytochrome P450
NOS	nitric oxide synthase
NIR	nitrite reductase
NOR	nitric oxide reductase
NAR	nitrate reductase
N_2OR	nitrous oxide reductase
NP	nitrophorin
NP1	nitrophorin-1
NP2	nitrophorin-2
NP4	nitrophorin-4
HO	heme oxygenase
legHb	leghemoglobin
RNO	nitrosoalkane/nitrosoarene
PhNO	nitrosobenzene
EtNO	nitrosoethane

MeNO	nitrosomethane
2-PrNO	2-nitrosopropane
i-PrNO	2-nitrosopropane
1-PrNO	1-nitrosopropane
1-MeIm	1-methylimidazole
4-MePip	4-methylpiperdine
Py	pyridine
4-dMAP	4-Dimethylaminopyridine
PPIX	protoporphyrin IX
Por	porphyrin
TPP	tetra-*meso*-substituted 5,10,15,20-tetraphenylporphyrin
TTP	5,10,15,20-tetra-*p*-tolylporphyrin
OEP	2,3,7,8,12,13,17,18-octaethylporphyrin
PPDME	Protoporphyrin IX dimethylester
TpivPP	picket fence porphyrin
OETAP	octaethyltetraazaporphyrinato
oxoOEP	2-oxo-3,3′,7,8,12,13,17,18-octaethylporphyrin
NADPH	nicotinamide adenine dinucleotide phosphate
BNL	Brookhaven National Laboratory
NSLS	National Synchrotron Light Source
CCP4	Collaborative Computing Project Number 4
EPR	Electron paramagnetic resonance
MS XAFS	multiple-scattering x-ray absorption fine structure

Abstract

The interactions of nitric oxide (NO), nitrite and organic nitroso compounds with heme proteins are biologically relevant. The formation of adducts between these NO-containing species and myoglobin (Mb) has served as a prototypical system for the interactions of nitroso compounds with heme proteins. We have prepared nitrosyl horse heart myoglobin using the two common synthetic routes, and we have determined that there are reproducible differences in the geometry of the FeNO moieties that depend on the synthetic method used. The 1.30 Å resolution structure of the complex formed from the reaction of reduced myoglobin with NO gas revealed an FeNO angle of 120° and an Fe-NO bond length of 2.13 Å. The 1.30 Å resolution structure of nitrosyl hh Mb formed using nitrite and sodium dithionite revealed an FeNO angle of 144° and an Fe-NO bond length of 1.87 Å. These differences are reproducible and suggest a role of the distal pocket in stabilizing conformational minima.

Recently, it has been shown that hemoglobin (Hb) and myoglobin catalyze the reduction of nitrite to NO under hypoxic conditions. Prior to our work, there was no reported crystal structure of a Hb-nitrite or Mb-nitrite complex. Therefore, obtaining the structure of the myoglobin nitrite adduct was an important goal in our research. In this thesis, we report the 1.20 Å resolution structure of hh Mb(ONO) complex. The nitrite ligand binds to the heme iron through its oxygen forming an Fe-O-N-O linkage, with an Fe-O bond length of 1.94 Å and an O-N-O angle of 113°. This complex was formed both by soaking a preformed metMb crystal with nitrite, as well as performing the Mb(ONO) adduct and crystallizing the complex. The only appreciable difference between the two

structures is the lower occupancy of the nitrite ligand and partial occupancy of a water molecule in the latter cocrystallization method.

Nitrosoalkane and nitrosoarenes are biologically significant compounds that are formed both by the oxidation of amine containing compounds (RNH_2) or the reduction of nitro compounds (RNO_2). The resulting RNO compounds are known to bind to heme iron. We determined the 1.70 Å resolution crystal structure of the Mb nitrosoethane complex (Mb(EtNO)), and the 1.60 Å resolution crystal structure of the related Mb nitrosomethane complex (Mb(MeNO)). To the best of our knowledge, these are the only two heme-nitrosoalkane structures to be reported. Both crystal structures reveal the N-binding mode (bound through nitrogen) of the nitrosoalkane to the heme iron, with the hydrophobic portion of the ligand oriented toward the interior of the protein and the NO moiety oriented toward the solvent and in hydrogen bonding distance to the distal histidine 64 residue. The 2.00 Å resolution structure of the myoglobin complex of a representative nitrosoarene, nitrosobenzene, was also determined. This is the second heme-PhNO crystal structure to be reported; the first was the leghemoglobin nitrosobenzene complex. The orientation of the PhNO in the heme pocket of the legHb structure reveals that the phenyl ring is oriented toward the exterior of the protein and the NO group toward the interior of the protein, opposite to the orientation that was determined here for Mb(PhNO). In the Mb(PhNO) complex, the phenyl ring is oriented toward the interior of the protein in a similar fashion to the nitrosoalkane complexes, which allows the NO to be oriented toward the exterior of the protein and allows hydrogen bonding between the O of PhNO and histidine 64 to help stabilize the complex.

1.   Introduction

The interactions of heme proteins with nitric oxide (NO), nitrite (NO_2^-) and C-nitroso compounds (RNO) have been studied for well over 100 years, and some of the earliest work dealt with nitrobenzene metabolites and their interactions with hemoglobin[1]. Throughout the 20th century these interactions were studied in greater detail as the biological importance of these molecules was discovered.

In this dissertation, I will examine the interactions of NO as well as several different nitric oxide containing molecules (NOX, X being oxygen or an R-group), namely nitrite and *C*-nitroso compounds, and their interaction with biological heme systems. Through these interactions we hope to add to the discussion on the biological chemistry of these adducts.

1.1 Nitric Oxide

Nitric oxide is a simple diatomic molecule with a bond order of 2.5 and is a gas at standard temperature and pressure. It can be identified using infrared spectroscopy by an absorbtion band at 1875 cm^{-1} [2]. In the last 20 years NO has returned to the forefront of research because of the many and varied biological functions of this simple diatomic molecule.

While it has been shown recently that NO is produced *in vivo*, NO can be made by various methods both environmentally and synthetically. One of the most common natural sources is the reaction of molecular nitrogen and oxygen at high temperatures caused by lightning[3, 4]. It is also a product of combustion in the presence of N_2, as occurs in internal combustion engines. As such, the increased number of cars on the road has drastically increased the NO levels in the lower atmosphere[5]. The NO released from car exhaust reacts with O_2 to form NO_2 (smog)[5]. Catalytic converters on cars are used in part to reduce the levels of NO that is released into the atmosphere[5, 6]. On a laboratory scale, NO can be made by the reaction of nitric acid with copper[7].

$$8HNO_3 + 3Cu \rightarrow 3Cu(NO_3)_2 + 4H_2O + 2NO$$
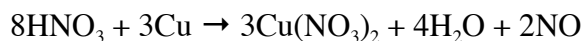
However, most commercially available NO is produced by the catalytic oxidation of ammonia over Pt at 800°C [5].

Once produced, NO can react with both metals and non-metals. One simple reaction was described above, the reaction with O_2 to produce NO_2. It has also been shown to react with various organic compounds to form so called X-NO compounds.

Usually the link for this type of compound is made through the nitrogen, but the less common isonitrosyl linkages have been observed.
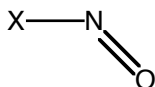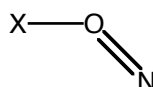
Nitrosyl linkage   Isonitrosyl linkage

One example of this is the reaction that was proposed between a cysteine on the β−subunit of hemoglobin and NO to form S-nitrosocysteine[8]. Other reactions have been observed that lead to N-linked, O-linked and C-linked nitroso compounds.

The other important type of reaction occurs between NO and metal centers. NO has been show to be a good ligand to both free metals and chelated metals as seen in porphyrin system. The affinity of NO for some metalloporphyrins has been shown to be ten orders of magnitude greater than the related CO affinity[2]. Whereas, there are only two major binding modes for nitric oxide with organic molecules, metal interactions offer many different modes of binding.
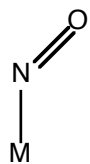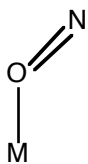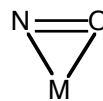
η^1-N η^1-O η^2-NO

There are three basic modes of binding that are available to the NO when binding to monometallic centers. The first available binding mode involves binding through the

nitrogen, η^1-N. This η^1-N binding mode has subgroups available, the MNO geometry can be either linear or bent.

$$
\begin{array}{ccc}
& O & O \\
& \diagup\diagup & \parallel \\
N & & N \\
| & & | \\
M & & M \\
\text{Bent} & & \text{Linear}
\end{array}
$$
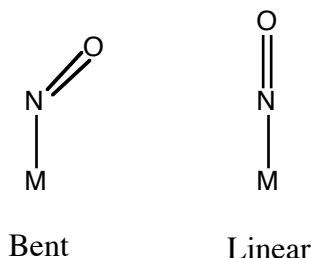
The geometry of this adduct depends greatly on the oxidation state of the metal, as well as the number of electrons available from the ligand. The second available binding mode involves binding through the oxygen, η^1-O. Similarly to the η^1-N binding mode, this mode also can be divided into linear and bent modes. Finally, we have the η^2-NO or side-on binding. This occurs when both the nitrogen and the oxygen are bound to the same metal center.

In porphyrin model complexes, the most significant model complexes relevant to this work, the main type of binding that has been observed is η^1-N. However, using flash photolysis metastable η^1-O binding has been observed [2].

1.2 Nitrite

The nitrite anion (NO_2^-) is a simple oxyanion of nitrogen with a pK_a in aqueous solution of 3.2 at 20 °C [9]. Nitrite is a common anion throughout the ecosystem. It is present in the ocean between 0.000005 to 0.00002 ppm throughout the surface levels and at greater concentrations in deeper water [10, 11]. Nitrite is also an important molecule for plant growth and is abundant in soil [12]. Nitrite is one of the major players in the global nitrogen cycle. The denitrification pathway is shown below.

$$NO_3^- \longrightarrow NO_2 \longrightarrow NO_2^- \longrightarrow NO \longrightarrow N_2O \longrightarrow N_2 \longrightarrow NH_4^+$$

Beyond the naturally occurring nitrite in the environment, nitrite is also used in the meat packing industry, as an additive to meat. It is added for both its antimicrobial activity and its ability to impart the color of fresh meat. The color derives from the heme-NO pigment that has a similar visible spectrum to Mb-O_2 [13-15].

Nitrite is formed as stated above as a normal part of the nitrogen cycle by bacteria, but it can also be formed by the reaction of NO with O_2. Historically, nitrite has been detected using the Griess reagent [16]. Johann Peter Griess developed a method to detect NO_2^- in 1858 and it has been used commonly to detect nitrite ever since. The Griess reagent is used to detect free nitrite in solution; however, in this study I am interested in metal-nitrite complexes, which are commonly detected using spectroscopy.

Nitrite, like NO can interact with both non-metals and metals in several different ways. One common reaction between nitrite and non-metals is the reaction between nitrous acid (in equilibrium with nitrite in solution) with C-H bonds adjacent to electron withdrawing groups which results in the C-nitrosation of organic molecules by replacing the –H with –NO [17-19].

The interaction of nitrite with metals can occur in multiple ways. Nitrite can bind to monometallic centers and multimetalic centers by bridging the metals. Similarly to NO, nitrite can bind metals through its nitrogen, η^1-N, through its oxygen, η^1-O. Additionally, it can bind through both oxygens, η^2-O or in a variety of bridging complexes[20].
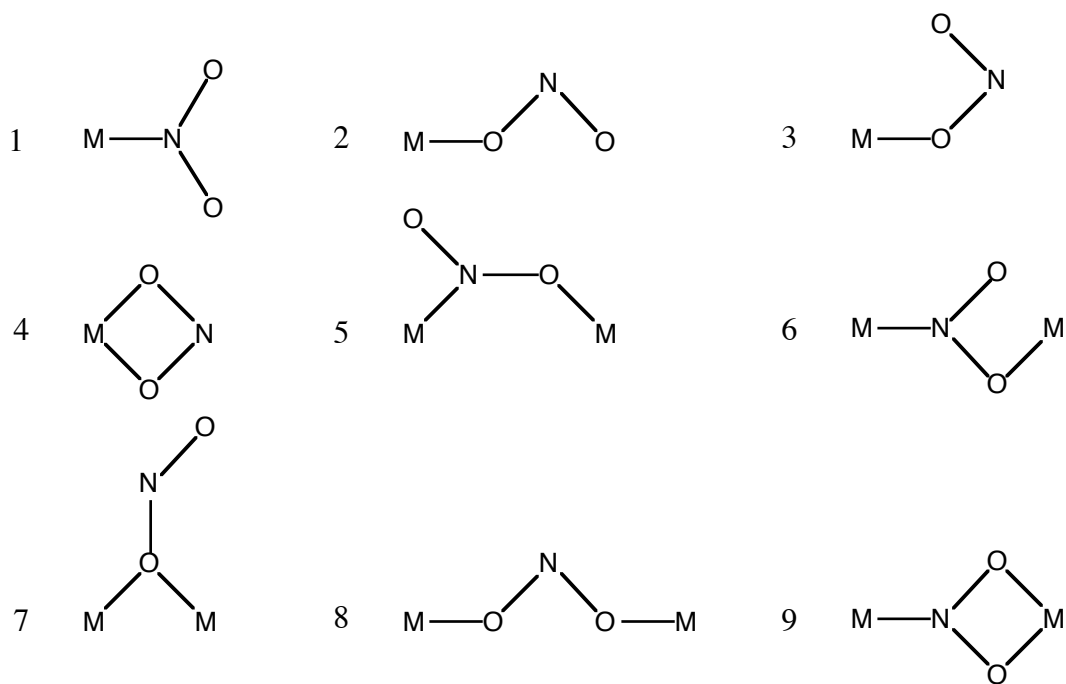
Figure 1.1   Schematic representation of possible binding modes of nitrite to metals.   1 Nitro; 2 Monodentate nitrito (trans); 3 Monodentate nitrito (cis); 4 Chelation; 5 Nitrito bridging μ(N,O) free O away from metal; 6 Nitrito bridging μ(N,O) free O adjacent to a metal; 7 Nitrito bridging μ(O); 8 Nitrito bridging (not yet observed); 9 Three coordinate nitrite (not yet observed). Figure from Hitchman review [20].

1.3 C-Nitroso Compounds

As previously mentioned, the reaction of NO with some organic compounds gives rise to so called X-NO species that display interesting reactions. There are four major types of organic nitroso compounds, *N*-nitroso, *O*-nitroso, *S*-nitroso, and *C*-nitroso. Each of these has different reactivities in biological and non-biological systems.

Many *N*-nitrosamines are carcinogenic, and are produced in the stomach and gut by the reaction of some amines with nitrite or NO [21-25]. They are also formed during the smoking process during the production of tobacco products (production, not consumption). S-nitroso compounds are often used as NO donors [17], and it has been proposed that S-nitroso-cysteine is a storage device for NO in vivo [8]. O-nitroso compounds are generally synthesized by nitrosating the precursor alcohol, and are commonly used as NO donors in organometallic chemistry [17].

In this thesis, the main focus of these X-NO compounds will be on the *C*-linked nitroso compounds. The biological significance of these RNO compounds stems from their ability to bind and inhibit the function of heme proteins. This inhibition is due to the binding of RNO compound to the heme metal[26].

The mode of RNO binding to the heme proteins is unclear, but the binding of RNO compounds to inorganic model systems has been reviewed recently [17]. In model complexes, the RNO ligand has the ability to bind through the nitrogen, η^1-N; the oxygen, η^1-O; as a dimer through the oxygens, η^1-O; side on through the nitrogen and the oxygen, η^2-NO; or through some other functional group in the R-group [17]. All of the above types of binding are to monometallic centers, which is most significant to this

work and shown below, but RNO ligands can bind to two or more metallic centers in multiple bridging modes (not shown) [17].

η^1-N η^1-O η^1-O Dimer η^2-N,O
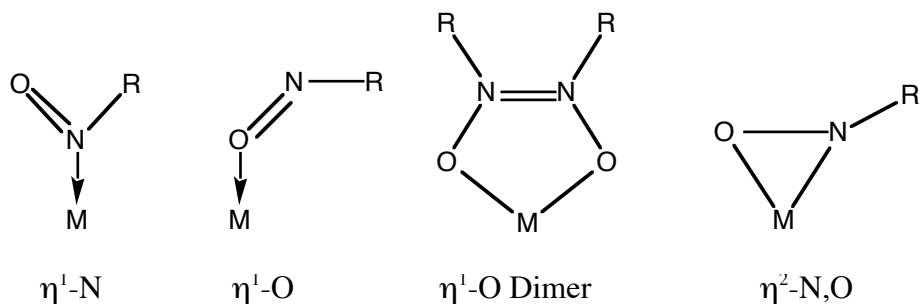
These C-nitroso compounds can be synthesized through multiple synthetic routes. The two most important to this work are: (i) the oxidation of amines or hydroxylamines,[27] and (ii) the direct reduction of nitro compounds to the nitroso compound [28-30]. Both of the above methods were employed in this research and will be discussed in Chapter 4. As described in the previous section on nitrite, nitrous acid or other nitrosating agents can react with C-H bonds adjacent to electron withdrawing groups, which results in the C-nitrosation of organic molecules by replacing the –H with –NO [18, 19]. The reaction of organometallic reagents with nitrosating agents, as well as the addition of nitrosating agents across double bonds, and reaction of NO with carbon radicals are also used to synthesize RNO compounds [31-33].

C-nitroso compounds exist as both monomers and dimers in solution. While the dimer is colorless, it can be detected by UV/Vis spectroscopy. Both the *cis-* and the *trans-* dimer absorb in the 260-290 nm range [17, 27, 32, 34]. The monomers for both alkyl and aryl nitroso compounds absorb in the visible region having either a slightly blue or green tint respectively [17, 27, 32, 34].

If there is an available hydrogen on the alpha carbon, the monomer is not stable in solution and can tautaumerize to the associated oxime [35], which will not bind to a metal center. For this reason, in this study we used the associated nitro compound and reduced it to the nitroso compound to form the nitrosoalkane complexes and used the hydroxylamine to form the nitrosoarene complex.
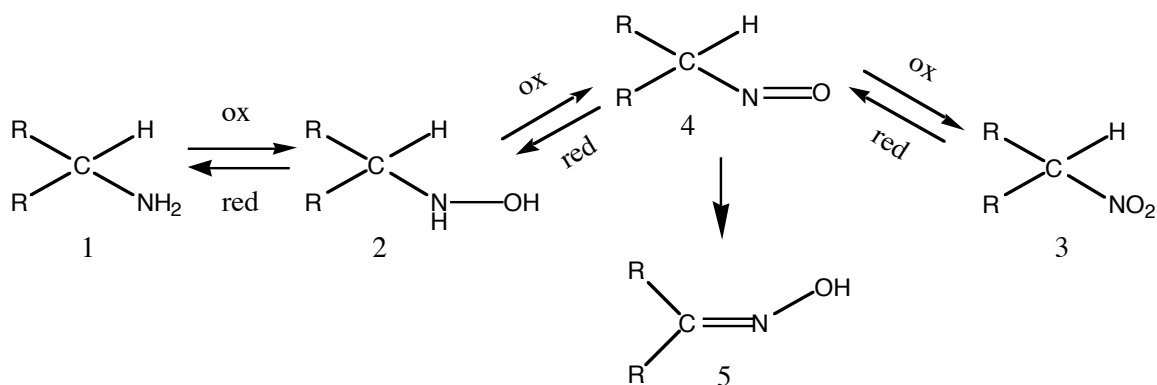
Figure 1.2   Two synthetic routes to make RNO compounds.   (1) amine can be oxidized to (2) hydroxylamine which can be oxidized to form the (4) nitroso compound. (3) the nitro compound can also be reduced to the (4) nitroso compound. If a hydrogen is available on the carbon through which the NO is linked the (4) nitroso compound can tautaumerize to the (5) oxime. Figure adapted from reference [35].

1.4   Heme and Heme Models

One of the commonalities between all of the above mentioned small molecules is that they bind to metals, and more specifically heme or heme model complexes. Heme is an important biological cofactor and is more appropriately named iron protoporphyrin IX (PPIX).

Iron Protoporphyrin IX
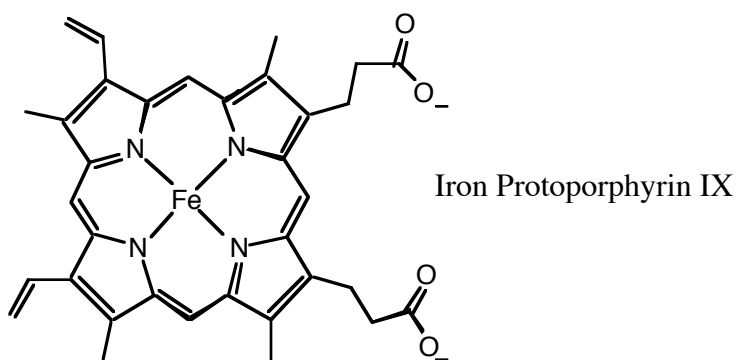
Heme is a hydrophilic, asymmetric porphyrin and is fairly difficult to work with by itself in solution. Therefore, inorganic chemists have devised ways to try to model the activity and functionality of heme with compounds that are easier to work with. These synthetic porphyrins are usually symmetrical and much more hydrophobic than PPIX. The most common synthetic porphyrins used are the tetra-*meso*-substituted 5,10,15,20-tetraphenylporphyrin (TPP) and 5,10,15,20-tetra-*p*-tolylporphyrin (TTP) and the octa-β-substituted 2,3,7,8,12,13,17,18-octaethylporphyrin (OEP) are shown below. Protoporphyrin IX dimethylester (PPDME) is also shown because of its similarity to protoporphyrin IX.

(TPP)Fe   (TTP)Fe   (OEP)Fe   (PPDME)Fe
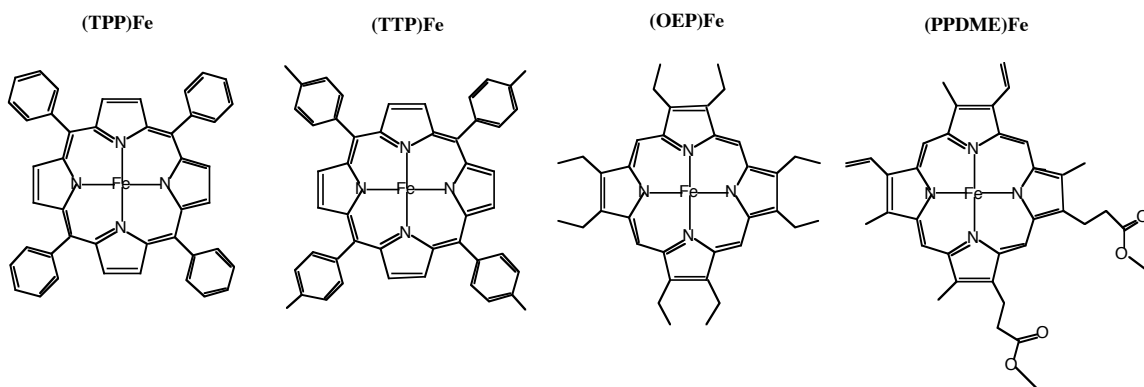
All of these compounds are much easier to synthesize and work with than are biological porphyrins. For the most part, they are reasonable biological porphyrin mimics, with the obvious limitations that they do not allow for interaction with the heme pocket, which is nonexistent and the complexes are studied for the most part in non-aqueous environments. In order to study the effects of the heme pocket two proteins were used.

1.5   *Myoglobin and Cytochrome P450 BM-3*

Horse heart myoglobin and Cytochrome P450 BM-3 were chosen because they are both good models for other proteins that are more difficult to work with. First, Myoglobin was chosen because it is a simple heme protein that has a molecular weight of 16,951 Da. This protein is small, stable and crystallizes readily. It is made up of 8 α-helices connected with short loops or turn regions. Heme b is incorporated into the fold and the heme iron is ligated by a histidine residue. Myoglobin has been used for decades as the prototypical histidine ligated heme protein and for that reason we chose it as the protein on which to perform our crystallography. We obtained the horse heart myoglobin from Sigma and it was used with little or no additional purification. The crystallization was performed using a method that was slightly modified for the method used in Ilme Schlichting's laboratory[36].
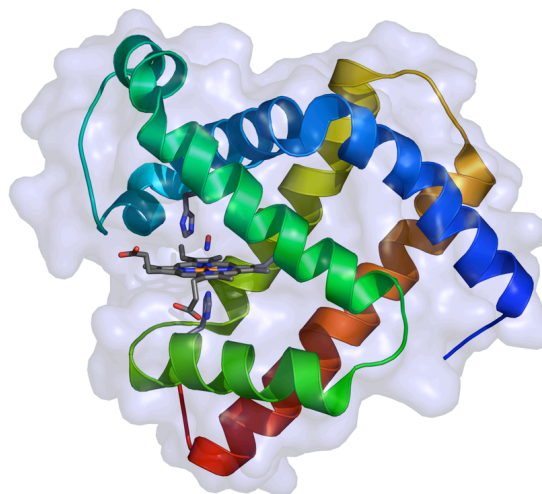
Figure 1.3 Typical horse heart myoglobin fold showing both the surface in shaded blue and the protein backbone with 8 α-helices in ribbon format colored in rainbow form from blue at the N-terminus to red at the C-terminus. The heme is shown with histidine 90 (below heme) ligating the heme and an NO molecule bound to the distal face of the heme, with His64 shown hydrogen bonding to the NO ligand. From 1NPF[37].

The heme domain of cytochrome P450BM-3 was chosen because of its sequence similarity to mammalian P450s, and that it is a soluble protein, unlike most mammalian P450s. It is classified as a Type II P450, the class that all mammalian P450s fall into; additionally it is the only P450 that contains all of the catalytic components on a single polypeptide chain. The figure below shows schematically the similarities between P450BM-3 and mammalian P450s, and the differences it has compared to other bacterial P450s.
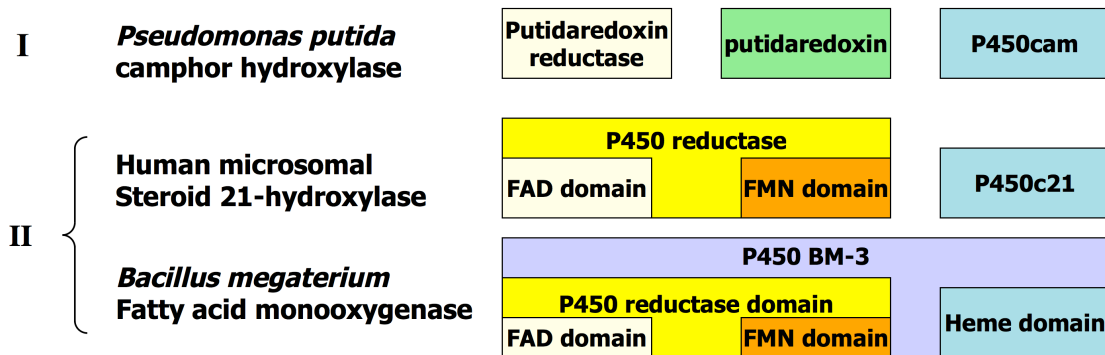
Figure 1.4 Schematic representation of the two major classes of P450s. Class I envelops bacterial P450s and Class II is constituted of mammalian P450s with the notable addition of P450BM-3 from the bacterium *Bacillus megaterium*.

The DNA for the heme domain was cloned into a pET21 expression vector, which we obtained from the Lab of Dr. Thomas Poulos. The protein was then expressed as in the paper which describes the initial characterization[38].

1.6 Research Focus

The aim of this research is to add structural information to the debate on the binding of NO and NO-containing ligands to heme proteins. X-ray crystallography and UV/Vis spectroscopy are the primary tools that were utilized in the performance of the research reported in this dissertation.

The geometries associated with nitrosyl heme interactions in biological systems are as varied as the proteins involved. In 6-coordinate, Fe(II) model complexes, with a reasonable histidine mimic as the sixth ligand, the metal nitrosyl geometry falls into a fairly tight range (137-140° (avg. ~138.5 °)), and the Fe-NO bond lengths range from 1.744(2)-1.758(1) Å (avg. ~1.753 Å) [39, 40]. In heme protein nitrosyl complexes that range expands dramatically (the $\angle$FeNO ranges from 112 – 160° and the Fe-N(O) bond length ranges from 1.5 Å to 2.2 Å). This expansion in the range is most likely due to the fact that the protein itself plays a major role in the binding of the ligand to the metal. The work discussed here adds to the discussion on the variety of FeNO geometries observed in biological nitrosyl complexes by showing that the method of formation of a horse heart myoglobin nitrosyl complex affects the final geometry of the complex.

Additionally, this dissertation will focus on the interaction of nitrite with heme proteins; specifically, we will focus on the mode of binding of nitrite to myoglobin. In all known cases the nitrite moiety binds to the heme iron with a nitro type binding. This has led to most of the current thinking on how enzymes that bind nitrite are able to convert it to NO. This work looks to add to this field by demonstrating an alternative binding mode for the nitrite ligand.

The final portion of this dissertation will focus on the interaction of RNO compounds with heme proteins. With the above techniques, I aimed to definitively answer questions on the mode of binding of nitrosoalkane and nitrosoarene ligands to myoglobin, as well as the effects that the protein sidechains in the heme pocket have on the geometry of the ligand and overall ability of the ligand to bind. This work is the logical extension of work begun over 100 years ago with the discovery of nitrobenzene poisoning[1, 41-50]. However, the interaction responsible for nitrobenzene poisoning was identified only 30 years ago by Mansuy and Chottard and has continued to be studied ever since [35, 49, 51-58]. These are the first reported crystal structures of heme nitrosoalkane complexes and an alternative PhNO conformation is shown to the leghemoglobin nitrosobenzene structure that was previously reported.

1.7 References

1. Filehne, W., *Arch. Exptl. Pathol. Pharmakol.* **1878,** 9, 329.

2. Cheng, L.; Richter-Addo, G. B., Binding and Activation of Nitric Oxide by Metalloporphyrins and Heme. In *The Porphyrin Handbook*, Guilard, R.; Smith, K.; Kadish, K. M., Eds. Academic Press: New York, 2000; Vol. 4 (Biochemistry and Binding: Activation of Small Molecules), pp 219-291.

3. Hill, R. D., Experimental study of the production of nitric oxide, nitrous oxide, and ozone in a simulated atmospheric corona. *Industrial & Engineering Chemistry Research* **1988,** 27, (7), 1264-9.

4. Hill, R. D., On the production of nitric oxide by lightning. . *Geophysical Research* **1979,** 6, (12), 945-7.

5. Richter-Addo, G. B.; Legzdins, P., *Metal Nitrosyls*. Oxford University Press: New York, 1992.

6. *Staff report on the hearing on controls of oxides of nitrogen*; south coast Air Quality Management District Ca., 1986.

7. Repa, A. G. G., L. M., Solubility of copper in nitric acid. *Zhurnal Prikladnoi Khimii* **1952,** 25, 1277-82.

8. Chan, N.-L.; Rogers, P. H.; Arnone, A., Crystal Structure of the S-Nitroso Form of Liganded Human Hemoglobin. *Biochemistry* **1998,** 37, 16459-16464.

9. Braida, W.; Ong, S. K., Decomposition of Nitrite Under Various pH and Aeration Conditions. *Water, Air, and Soil Pollution* **2000,** 118, 13-26.

10. Zafiriou, O. C.; McFarland, M., Determination of Trace Levels of Nitric Oxide in Aqueous Solution. *Anal. Chem.* **1980,** 52, 1662-1667.

11. Zafiriou, O. C. B., LA Hanley, Q, Trace Nitrite in Oxic waters. *Deep sea research Part A: Oceanographic research papers* **1992,** 39, (2), 1329-47.

12. Smil, V., Global Population and the Nitrogen Cycle. *Scientific American* **1997,** 277, (1), 76-82.

13. Keller, A., *Inorg Chim Acta* **1988,** 149, 165.

14. Keller, A., *Transition Met Chem (London)* **1987,** 12, 320.

15. Keller, A., *Inorg Chim Acta* **1987**, (133), 207.

16. Griess, P., *Liebigs. Ann. Chem.* **1858,** 106, 123.

17.   Lee, J.; Chen, L.; West, A. H.; Richter-Addo, G. B., Interactions of Organic Nitroso Compounds with Metals. *Chem. Rev.* **2002,** 102, (4), 1019-1065.

18.   Bosch, E.; Kochi, J. K., Direct Nitrosation of Aromatic Hydrocarbons and Ethers with the Electrophilic Nitrosonium Cation. *J. Org. Chem.* **1994,** 59, (19), 5573-5586.

19.   Jin, D.; Mendenhall, G. D., Ring-Nitrosation of a Secondary Aromatic Amine,.. *Tetrahedron Lett.* **1996,** 37, (28), 4881-4882.

20.   Hitchman, M. A.; Rowbottom, G. L., Transition Metal Nitrite Complexes. *Coord. Chem. Rev.* **1982,** 42, 55-132.

21.   Bartsch, H. O., H.; Pignatelli, B.; Calmels, Endogenously formed N-nitroso compounds and nitrosating agents in human cancer etiology. *Pharmacogenetics* **1992,** 2, (6), 272-7.

22.   Tannenbaum, S. R. W., John S. In *Endogenous nitrosation via nitric oxide.*, 217th ACS National Meeting, Anaheim, 1999; Anaheim, 1999.

23.   Shuker, D. E. G. In *The role of nitrosation: Exogenous vs. endogenous exposure to N-nitroso compounds.*, Carcinogenic and Anticarcinogenic Factors in Food, Symposium, germany, 2000; germany, 2000.

24.   Cross, A. J. P., Jim R. A.; Bingham, Sheila Anne, Haem, not protein or inorganic iron, is responsible for endogenous intestinal N-nitrosation arising from red meat. *Cancer Research* **2003,** 63, (10), 2358-2360.

25.   Bingham, S. A. H., Roisin; Cross, Amanda Jane, Effect of white versus red meat on endogenous N-nitrosation in the human colon and further evidence of a dose response. *Journal of Nutrition* **2002,** 132, (11s), 3522s-3525s.

26.   Fukuto, J. M.; Brady, J. F.; Burstyn, J. N.; VanAtta, R. B.; Valentine, J. S.; Cho, A. K., Direct Formation of Complexes between Cytochrome P-450 and Nitrosoarenes. *Biochemistry* **1986,** 25, (9), 2714-2719.

27.   Coombes, R. G., Nitro and Nitroso. *Comprehensive Org. Chem.* **1979,** 2, 305-317 (Chapter 7).

28.   Zerewitinoff, T.; Ostromisslensky, I., Uber Bariumoxyd als Reducknn.... *Ber.* **1911,** 44, 2402-2409.

29.   Alway, F. J.; Gortner, R. A., Ueber zwei Aromatische Nitrosover... *Ber.* **1905,** 38, 1899-1901.

30.   Bartoli, G., Conjugate Addition of Alkyl-Grignard Reagents to Mononitroarenes. *Acc. Chem. Res.* **1984,** 17, 109-115.

31.	Robson, E.; Tedder, J. M.; Woodcock, D. J., Nitrosoacetylenes. *J. Chem. Soc. (C)* **1968**, 1324-1328.

32.	Banus, J., Perfluoroalkyl Compounds of Nitrogen. Part 1. Perfluoroalkyl-nitroso- and -nitro-compounds. *J. Chem. Soc.* **1953**, 3755-3761.

33.	Beckham, L. J.; Fessler, W. A.; Kise, M. A., Nitrosyl Chloride. *Chem. Rev.* **1951,** 48, 319-396.

34.	Mason, J., Perfluoroalkyl Compounds of Nitrogen. Part 4. Electronic Absorption Spectra of Perfluoro-nitroso- and -nitro-alkanes, and Related Molecules. *J. Chem. Soc.* **1957**, 3904-3912.

35.	Mansuy, D.; Beaune, P.; Chottard, J. C.; Bartoli, J. F.; Gans, P., The Nature of the "455 nm Absorbing Complex" Formed During the Cytochrome P450 Dependent Oxidative Metabolism of Amphetamine. *Biochem. Pharmacol.* **1976,** 25, 609-612.

36.	Chu, K.; Vojtchovsky, J.; McMahon, B. H.; Sweet, R. M.; Berendzen, J.; Schlichting, I., Structure of a Ligand-Binding Intermediate in Wild-Type Carbonmonoxy Myoglobin. *Nature* **2000,** 403, 921-923.

37.	Copeland, D. M.; West, A. H.; Richter-Addo, G. B., Crystal Structures of Ferrous Horse Heart Myoglobin Complexed with Nitric Oxide and Nitrosoethane. *Proteins: Struct. Func. Genet.* **2003,** 53, 182-192.

38.	Li, H.; Darwish, K.; Poulos, T. L., Characterization of Recombinant Bacillus megaterium Cytochrome P450 BM3 and Its Two Functional Domains. *J. Biol. Chem.* **1991,** 266, (18), 11909-11914.

39.	Rath, S. P.; Koerner, R.; Olmstead, M. M.; Balch, A. L., Reversible Binding of Nitric Oxide and Carbon-Carbon Bond Formation in a Meso-hydroxylated Heme. *J. Am. Chem. Soc.* **2003,** 125, 11798-11799.

40.	Wyllie, G. R. A.; Schultz, C. E.; Scheidt, W. R., Five- to Six-Coordination in (Nitrosyl)iron(II) Porphyrinates: Effects of Binding the Sixth Ligand. *Inorg. Chem.* **2003,** 42, (18), 5722-5734.

41.	Loeb, R. F.; Bock, A. V.; Fitz, R., Acute Nitrobenzene Poisoning, With Studies On The Blood in Two Cases. *Am. J. Med. Sci.* **1921,** 161, 539-546. CA15:1761.

42.	Heubner, W.; Meier, R.; Rhode, H., Methemoglobin Formation. V. Phenylhydroxylamine. *Arch. Exptl. Pathol. Pharmakol.* **1923,** 100, 149-161. *Chem. Abs.* **18**:1306.

43.	Jung, F., Nitrosobenzene-Hemoglobin. *Naturwissenschaften* **1940,** 28, 264-265.

44.   Jung, F., Hemoglobin and Oxidation Products of Aniline (Nitrosobenzenehemoglobin). *Biochem. Z.* **1940,** 305, 248-260. *Chem. Abs.* **35**:472.

45.   Jung, F., Methemoglobin Formation. XVIII. The Phenylhydroxylamine-Nitrosobenzene Cycle. *Arch. Exptl. Pathol. Pharmakol.* **1940,** 195, 208-217. *Chem. Abs.* **35**:1865.

46.   Keilin, D.; Hartree, E. F., Reactions of Haemoglobin and its Derivatives with Phenyl Hydroxylamine and Nitrosobenzene. *Nature* **1943,** 151, (3831), 390-391.

47.   Murayama, M., The Combining Power of Normal Human Hemoglobin for Nitrosobenzene. *J. Biol. Chem.* **1960,** 235, (4), 1024-1028.

48.   Scheler, W., Formation of Nitrosobenzene Derivatives by Human Hemoglobin. *Naturwissenschaften* **1960,** 47, 399.

49.   Chottard, G.; Mansuy, D., Resonance Raman Studies of Hemoglobin Complexes With Nitric Oxide, Nitrosobenzene and Nitrosomethane: Observation of the Metal-Ligand Vibrations. *Biochem. Biophys. Res. Commun.* **1977,** 77, (4), 1333-1338.

50.   Kuranova, I. P.; Teplyakov, A. V.; Obmolova, G. V.; Voronova, A. A.; Popov, A. N.; Kheiker, D. M.; Arutyunyan, E. G., X-ray Diffraction Study of Leghemoglobin in Complexes with Nitrosobenzene, Nicotinic Acid, and Acetate, Fluoride, and Cyanide Ions. *Bioorg. Khim.* **1982,** 8, 1625-1636 (in Russian). *Chem. Abstr.* CA98:48994. PDB codes 1LH7 and 2LH7.

51.   Mansuy, D.; Chottard, J. C.; Chottard, G., Nitrosoalkanes as Fe(II) Ligands in the Hemoglobin and Myoglobin Complexes Formed from Nitroalkanes in Reducing Conditions. *Eur. J. Biochem.* **1977,** 76, 617-623.

52.   Mansuy, D.; Gans, P.; Chottard, J.-C.; Bartoli, J.-F., Nitrosoalkanes as Fe(II) Ligands in the 455-nm-Absorbing Cytochrome P-450 Complexes Formed from Nitroalkanes in Reducing Conditions. *Eur. J. Biochem.* **1977,** 76, 607-615.

53.   Mansuy, D.; Battioni, P.; Chottard, J. C.; Lange, M., Nitrosoalkanes and New Ligands of Iron(II) Porphyrins and Hemoproteins. *J. Am. Chem. Soc.* **1977,** 99, (19), 6441-6443.

54.   Mansuy, D.; Dreme, M.; Chottard, J. C.; Guilhem, J., 2-Methyl-2-nitrosopropane and Nitrosobenzene as Nitrogen-bonded Platinum(II) Ligands. Molecular Structure of {PtCl2[(CH33)3C(NO)]2}. *J. Organomet. Chem.* **1978,** 161, 207-220.

55.   Mansuy, D.; Battioni, P.; Chottard, J.-C.; Riche, C.; Chiaroni, A., Nitrosoalkane Complexes of Iron-Porphyrins: Analogy between the Bonding Properties of Nitrosoalkanes and Dioxygen. *J. Am. Chem. Soc.* **1983,** 105, (3), 455-463.

56. Mahy, J. P.; Mansuy, D., Formation of Prostaglandin Synthase-Iron-Nitrosoalkane Inhibitory Complexes upon in Situ Oxidation of N-Substituted Hydroxylamines. *Biochemistry* **1991,** 30, 4165-4172.

57. Renodon, A.; Boucher, J.-L.; Wu, C.; Gachhui, R.; Sari, M.-A.; Mansuy, D.; Stuehr, D., Formation of Nitric Oxide Synthase-Iron(II) Nitrosoalkane Complexes: Severe Restriction of Access to the Iron(II) Site in the Presence of Tetrahydrobiopterin. *Biochemistry* **1998,** 37, (18), 6367-6374.

58. Ricoux, R.; Boucher, J.-L.; Mansuy, D.; Mahy, J.-P., Formation of Iron(II) Nitrosoalkane Complexes: A New Activity of Microperoxidase 8. *Biochem. Biophys. Res. Commun.* **2000,** 278, 217-223.

2 Nitrosyl Horse Heart Myoglobin

2.1 Introduction

Nitric oxide is biosynthesized from L-arginine by the heme-containing enzyme NO synthase. This enzyme catalyzes the oxidation of L-arginine to citrulline and NO in two general steps utilizing NADPH and O_2 as additional substrates (Figure 2.1) [1]. The first step involves the conversion of L-arginine to N^ω-hydroxy-L-arginine, and the second step completes the oxidation to give citrulline and NO as final products.
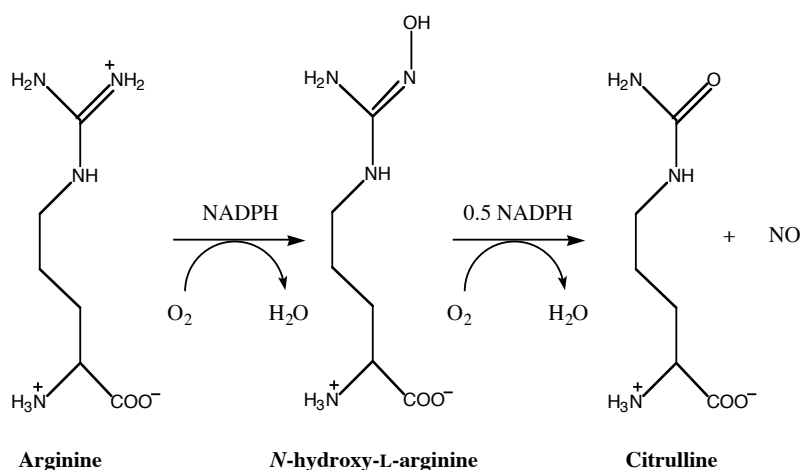
Figure 2.1 Biosynthesis of NO. Conversion of arginine to citrulline and NO carried out by nitric oxide synthase.

The identity of NO as the final gaseous product is generally accepted, however, some intriguing results have been presented in the literature that suggest that HNO (nitroxyl) is the initial product of this conversion [1,2].

The interactions of NO with the metal centers in heme-containing biomolecules are biologically important [3,4]. A primary role for NO *in vivo* is as a signaling molecule.

The heme-containing receptor, soluble guanylyl cyclase (sGC), contains histidine as a heme ligand, and the heme iron binds NO in a process that has been correlated with sGC activation and subsequent vasodilation [5-7]. NO is known to bind to other heme-containing biomolecules such as myoglobin (Mb), hemoglobin (Hb), cytochrome P450 (P450), and NO synthase (NOS), and the binding and activation of NO by metalloporphyrins and heme was reviewed in 2000 [3]. In the past ten years, NO has been implicated in a number of biological processes including apoptosis, leukemogenesis, asthma, G-protein signaling, abnormal T cell signal transduction, kidney function, diabetes, erectile dysfunction, chronic fatigue syndrome, and Parkinson's disease [8-17].

A primary mode of action of NO *in vivo* is its interaction with heme iron. The myoglobin nitric oxide complex has served as a prototype for the investigations of distal pocket effects on the FeNO conformations in solution. In this thesis, new findings concerning the binding of NO with myoglobin will be presented and discussed.

2.1.1 Nitric Oxide and Metals

Traditionally, metal-NO complexes that show a linear geometry have been described as containing an NO^+ moiety bound to the metal. In a similar manner, the bound NO in a bent metal-NO compound has been described as an NO^- ligand. The simple reason for these descriptions is that the linear NO is bound similarly to CO, and NO^+ is isoelectronic with CO. NO^- binds in a bent conformation much like O_2. This formalism is an oversimplification because it does not take into account the oxidation state of the metal[3].

The oxidation state of the metal plays a key role in determining the geometry of the FeNO moiety. These metal-NO complexes have been described as either "ferric" or "ferrous" complexes, however, like the NO^+ and NO^- description above, describing only the metal oxidation state also may be an oversimplification. The oxidation state of a metal is commonly known prior to a reaction with NO, but the definite oxidation state of a product complex is usually ambiguous. For example, iron porphyrin NO complexes are often described as $(por)Fe^{(II)}(NO)$ and as ferrous, low-spin, d^6 complexes. However, these formulations cannot be correct because these complexes are paramagnetic, they have an unpaired electron.

The idea of describing the complexes solely by their oxidation state or as NO^+/NO^- species are both overly simplistic, so Enemark and Feltham developed the so-called Enemark-Feltham notation[18]. This is a formalism that is used to describe metal-NO complexes. The notation is as follows: $\{M(NO)_x\}^n$ where x is the number of NO molecules bound to the metal, and n is the total number of d electrons of the metal and the π^* orbital of the NO.

$$Fe(III) \quad + \quad NO \quad = \quad \{Fe(NO)\}^6$$

$$5\ e^- \qquad\qquad 1\ e^- \qquad\qquad 6\ e^-$$
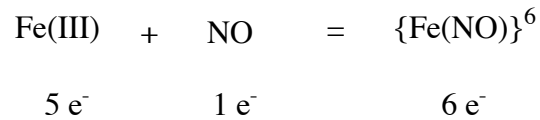
One added benefit to this notation is it simplifies the prediction of FeNO geometries in octahedral complexes. If $n \leq 6$ the M-NO geometry should be linear and if $n > 6$ the M-NO geometry will be bent. Most biochemists do not subscribe to this notation, so in this thesis the ferrous/ferric (Fe(II)/Fe(III)) notation will be primarily used, but will describe the oxidation state of the metal prior to the reaction, not the oxidation state of the complex. In this thesis, MbNO is taken to mean $\{Fe(NO)\}^7$ unless stated otherwise.

2.1.2 Nitric Oxide Complexes

2.1.2.1 Spectroscopy

The most widely used methods to study the interactions of nitric oxide with porphyrin model systems are spectroscopic methods. All of the major spectroscopic techniques have been used to study nitrosyl metal porphyrin complexes and a review was written on the topic in 1996 [19].

2.1.2.2 X-ray Crystal Structures

Synthetic metalloporphyrins are frequently used as models for the heme cofactor, and such model complexes containing NO have been studied over the past few decades. Studies on the NO adducts of Mo, Mn, Fe, Ru, Os, Rh and Co porphyrins synthesized prior to 2000 are reviewed by Cheng and Richter-Addo in The Porphyrin Handbook [3]. Another review in 2002 includes several new (por)M(NO) structures [20].

In this work, we will focus on six-coordinate Fe(II) porphyrins containing a reasonable histidine mimic for the sixth ligand. This limits the axial ligands to piperidines, pyridines, and imidazoles. A reasonable review that contains many of the 5-coordinate species ((por)Fe(NO)) was published by Wyllie in 2002 [20]. Selected structural data for synthetic five-coordinate and six-coordinate Fe(II) nitrosyl porphyrins are presented in Table 2.1.

Table 2.1 Selected X-ray Structural Data for Synthetic Ferrous Nitrosyl Heme Complexes

Complex	coord.no.	Fe-N(O) (Å)	N-O (Å)	∠FeNO (°)	Fe-L (Å)	ref
(TPP)Fe(NO)	5	1.717(7)	1.122(12)	149.2(6)		[21]
(TPPBr$_4$)Fe(NO)	5	1.734(8)	1.119(11)	147.9(8)		[22]
		1.726(9)	1.144(12)	146.9(9)		
		1.691(11)	1.145(16)	145(1)		
(OEP)Fe(NO)						[22]
monoclinic	5	1.722(2)	1.167(3)	144.4(2)		
triclinic	5	1.7307(7)	1.1677(11)	142.74(8)		
(T(2,6-Cl$_2$)PP)Fe(NO)	5	1.703(8)		138.8(9)		[23]
(T(β-Br$_8$)PP)Fe(NO)	5	1.75(6)	1.42(7)	146.4(24)		[23]
(TTP)Fe(NO)	5			149.2(6)		[23]
(TpivPP)Fe(NO)	5	1.65(5)	1.17(5)	149(4)		[24]
		1.74(6)	1.20(7)	137(4)		
[(TpivPP)Fe(NO)]· [K(NO$_2$)(18C6)]	5	1.716(15)	1.197(9)	143.8(17)		[20, 25]
(OETAP)Fe(NO)	5	1.721(4)	1.155(5)	143.7(4)		[26]
(oxoOEC)Fe(NO)	5	1.7320(13)	1.1696(19)	143.11(15)		[22]
(TPP)Fe(NO)(1-MeIm)	6	1.743(4)	1.121(8)	142.1(6)	2.180(4)	[27, 28]
(TPP)Fe(NO)(1-MeIm)	6	1.750	1.181	137.72	2.173	[29]
(TPP)Fe(NO)(4-MePip)	6	1.740(7)	1.112(9)	143.7(6)	2.463(7)	[30]
(TPP)Fe(NO)(4-MePip) ·CHCl$_3$	6	1.721(10)	1.141(13)	138.5(11)	2.328(10)	[30]
(oxoOEP)(Fe(NO)(Py)	6	1.740	1.190	138.33	2.310	[31]
(TPP)Fe(NO)(4-dMAP)	6	1.758	1.170	139.79	2.278	[29]
(TpivPP)Fe(NO)(Py)	6	1.740	1.194	133.37	2.261	[29]

TPP = 5,10,15,20-tetraphenylporphinato; OEP = octaethylporphyrinato; TTP = *meso*-tetra-*p*-tolylporphyrin; TpivPP = picket fence porphyrin; OETAP = octaethyltetraazaporphyrinato; oxoOEP = 2-oxo-3,3′,7,8,12,13,17,18-octaethylporphyrin; 1-MeIm = 1-methylimidazole; 4-MePip = 4-methylpiperdine; Py = pyridine; 4-dMAP = 4-Dimethylaminopyridine

26

The distances and geometries reported for these complexes fall into a reasonably tight range; furthermore, the nature of the porphyrin does not appear to cause significant changes in the FeNO geometry. The presence of the trans ligand (to NO) causes the largest effect on the metric data [20,29]. For example, in six-coordinate (porphyrin)Fe(NO)(*N*-base) compounds, the Fe-N-O bond angles range from 137-140° (avg. ~138.5 °), and the Fe-NO bond lengths range from 1.744(2)-1.758(1) Å (avg. ~1.753 Å) [29, 31]. The related canonical values for five-coordinate (porphyrin)Fe(NO) compounds also shown in Table 1.1 are 143.4° (avg.) for the $\angle$FeNO and 1.728 Å (avg.) for the Fe-N bond length [29].

2.1.3 Biological Nitric Oxide Complexes

2.1.3.1 Spectroscopy

As stated in the introduction, the importance of biological NO complexes was not seen until fairly recently, however, there has been an explosion of research in this field in the past 20 years. Because some of the proteins of interest could not be crystallized, myoglobin has been used as the prototypical system employed for the study of Fe-NO bond formation and reactivity in histidine-liganded heme centers[3, 32-34]. This is due, in part, to the fact that some myoglobins such as horse heart Mb (hh Mb) and recombinant sperm whale Mb (sw Mb) are commercially available and are readily purified. In addition to the study of its formation in meat curing processes [32, 35], MbNO has been studied with regard to the kinetics of NO binding to the ferrous ($k_{on}/k_{off} = 1.4$ x 10^{11} M^{-1})

and ferric heme (k_{on}/k_{off} = 1.4 x 10^4 M^{-1}) [36], photodissociation and geminate recombination of NO [37-39a], and NO dioxygenase and scavenging potential [40].

Valuable insights into the FeNO angle in MbNO have been provided by spectroscopy. In the case of MbNO, Hori and Yonetani [41] demonstrated a temperature-dependence of the Fe-N-O bond angle by single-crystal EPR spectroscopy demonstrating that the conformation of the FeNO moiety was altered upon freezing. This study complemented earlier single crystal EPR studies that revealed FeNO bond angles of 108-110° for MbNO at 77 K [42], and 119° for horse HbNO at 77 K [43]. The effect of temperature on the EPR spectra of nitrosyl hemes was examined in a computational study by Waleh *et al.*, who suggested that changes in ligand geometry in MbNO could explain the EPR spectral results [44]. Rich et al. [45] have reported MS XAFS data for a frozen solution of $Mb^{II}NO$, and they determined an Fe-N-O angle of 150° and an Fe-NO bond length of 1.75 Å. These values are similar to those observed in synthetic iron(II) nitrosyl porphyrins [20, 29].

2.1.3.2   X-ray Crystal Structures

Selected structural data for nitrosyl heme proteins are presented in Table 2.2. A much wider range of Fe-N-O bond angles is evident from these protein X-ray structures, ranging from 112 to 160° than is seen in the corresponding model complexes that were discussed above. A range of 1.5-2.1 Å for the associated Fe-N(O) distances is also observed in the crystal structures, and again much larger than the reported values in model complexes. While some of the reported crystal structures of nitrosyl heme proteins were not obtained at high resolution, even with those that were high resolution, there is a significant range of FeNO conformations that suggest a role of heme pocket

residues in influencing FeNO geometry through a combination of factors including steric and electrostatic effects. This has been illustrated very well for MbNO [33, 46, 47], and related studies are ongoing for heme proteins in general, as distal and proximal effects are likely determinants of ligand discrimination and selectivity in heme-based sensor proteins.

Table 2.2 X-ray crystal structural data for nitrosylated His-liganded heme proteins.^{a,b}

Nitrosylated protein	res (Å)^c	pdb^d	O.S.^{e}	Fe-N(O) (Å)	N-O (Å)	∠FeNO (°)	Fe-(L$_{ax}$) (Å)	ref
sw Mb	1.7	1HJT	II	1.89	1.15	112	2.18	[48]
L29F/D122N sw Mb	1.9^f	1JDO	II	1.86^f	1.14^f	127^f	2.31^f	[48]
hh Mb (MS XAFS)^h			II	1.75	1.12(2)	150(2)	2.05	[45]
			III	1.68(2)	1.13(2)	180(4)	2.04	[45]
NP1 from *Rhodnius prolixus*	2.3	4NP1	II	2.06^f	1.34^f	119.5^f	2.10^f	[49]
			III	2.02^f	1.32^f	145^f	2.0^f	
NP2	1.45	1T68		1.93^f	1.38^f	134^f	2.10^f	[50]
NP4 from *Rhodnium proxilus*								
WT (pH 7.4)	1.08	1X8Q	II	1.74(2)	1.20(2)	143.8(1.6)	2.06(1)	[51]
WT (pH 5.6)	1.01	1X8O	III	1.69(1)	1.09(1)	159.1(1.1)	1.994(7)	[51]
D129A/L130A mutant	1.0	1SXX	III	1.60(2)	1.35^f	155(2)	2.05^f	[52]
T121V mutant	1.0	1SY1	III	1.62(2)	1.29^f	158(2)	2.03^f	[52]
D30N mutant	1.0	1SY3	II	1.78(2)	1.38^f	132(2)	2.06^f	[52]
D30A mutant	1.05	1SXW	II	1.71(3)	1.35^f	139(2)	2.09^f	[52]
HO from *N. meningitides*	1.75	1P3U	II	1.58^f	1.17^f	147^f	2.13^f	[53]
HO-1 from rat	1.7	1JO2	II	2.10^f	1.14^f	125^f	2.17^f	[54]
Human HO-1 WT	1.55	1OZW	II	1.64^f	1.14^f	138^f	2.12^f	[55]
D140A mutant	2.59	1OZL	II	1.49^f	1.16^f	148^f	2.12^f	[55]
Verdoheme	2.10	1TWR		1.83^f	1.15^f	150.9^f	2.54^f	[56]
				1.98^f	1.16^f	150.4^f	2.37	
lupin legHb	1.8	1GDL	II	1.97^f	1.35^f	145^f	2.19^f	[57]
soybean legHb (MS XAFS)^g			II	1.77	1.12	147	1.98	[58]
			III	1.68	1.12	173	1.89	[58]
FixL from *B. japonicum*	2.5	1DP8	II	1.76^f	1.14^f	154^f	2.10^f	[59]
cyt *c'* from *Alcaligenes xylosoxidans*	1.35	1E85	II	2.03^f	1.16^f	125^f	5-Coord.	[60]
				1.92^f		132^f		
cyt *cd₁* NiR from *P. pantotropha*	1.8	1AOM	II	2.0	1.37^f	128^f	1.98^f	[61]
cyt *cd₁* NiR from *P. aeruginosa*	2.65	1NNO	II	1.8	1.15	140^f	1.98^f	[62]
cyt *c* peroxidase from yeast	1.85			1.8		125, 135	2.04	[63]
cyt *c* from *Rhodobacter sphaeroides*	2.20	1DW2	II	1.75^f	1.42^f	113^f	2.23^f	[64]
			II	1.82^f	1.37^f	112^f	2.16^f	
horse Hb	2.8			1.74	1.11	~145	(His)	[65]
Hb (βcysSNOH) α heme	1.8	1BUW	II	1.75	1.13	131	2.28	[66]
β heme			II	1.74	1.11	123	2.28	[66]
T-state human Hb α heme	2.15	1RPS	II	1.72	1.13	138	5-coord.	[67]
β heme			II	1.75	1.15	128	2.25	[67]
T-state human Hb (βcysSOH)	2.11	1RQ4						
α heme				1.72	1.15	138	5-coord.	[67]
β heme				1.76	1.17	138	2.19	[67]
T-state human Hb βW37E	2.11	1RQA						
α heme				1.71	1.16	135	2.24	[67]
β heme				1.76	1.18	126	2.19	[67]

^{a} all nitrosylated sites are hexacoordinate of the form (por)Fe(NO)(His), except those of (i) cyt c', and (ii) the α-hemes of T-state Hb, which are pentacoordinate. These are indicated in the Fe-(L$_{ax}$) column by the term "5-coord".

^{b} *abbreviations:* sw Mb = recombinant sperm whale myoglobin; hh Mb = horse heart myoglobin; NP = nitrophorin; NP1 = nitrophorin-1; NP2 = nitrophorin-2; NP4 = nitrophorin-4; HO = heme oxygenase; legHb = leghemoglobin; Hb = hemoglobin.

^{c} resolution. ^{d} pdb access code. ^{e} formal oxidation state of iron if known. ^{f} metric data were obtained from the Protein Data Bank. ^{g} data obtained from multiple-scattering X-ray absorption fine structure spectroscopic analyses.

The variety that is seen in the geometries of crystal structures that are reported in the above table lead to a simple question, *Is the heme pocket and its residues or the metal itself the major determinant of FeNO geometry, or is there another major factor that has not been studied?* The other important question raised is, *Are there other factors that help to determine the FeNO geometry?* We contributed to this on-going debate by determining the high-resolution X-ray crystal structures of hh MbNO prepared by two common routes: (i) reaction of metMb with nitrite/dithionite, and (ii) reaction of reduced Mb with NO gas.

2.2 Materials and Methods

2.2.1 Crystal Growth and Complex Formation

2.2.1.1 Sodium Nitrite/Dithionite Method

Ferric *aqua-met*Mb crystals were grown according to the method of Schlichting *et al.* [68] The crystals were grown anaerobically in a glove box under a nitrogen atmosphere at room temperature (21˚C) using the hanging drop vapor diffusion method. The droplets were prepared by mixing 5 µL of the 30 mg/mL protein solution in 100 mM Tris-HCl at pH 7.4 with 5 µL of 3.4-4.0 M ammonium sulfate, 100 mM Tris-HCl at pH 7.4. The droplets were suspended over reservoirs containing 1 mL of 3.1–3.3 M ammonium sulfate, 100 mM Tris-HCl at pH 7.4. The crystals grew in clusters of plates and reached a suitable size (0.5 x 0.2 x 0.05 mm) in 5 days.

The droplet containing the crystal cluster was transferred to 0.5 mL of artificial mother liquor containing 7.5% glycerol (v/v) as a cryoprotectant. Sodium nitrite crystals (~5 mg) and sodium dithionite (~10 mg) were added to this solution. During the ensuing 15 min period, the color of the crystal clusters changed from orange-brown to red. Single plates were then harvested anaerobically and flash-frozen in liquid nitrogen.

Later crystals were grown under an aerobic atmosphere after we determined that an anaerobic atmosphere was not necessary. Crystal growth was improved by placing the crystal trays in Styrofoam boxes to avoid large fluctuations in the temperature of the plates. Crystals reached approximately the same size as crystals described earlier in 5 days. The MbNO crystal for which data were collected at Brookhaven National Laboratory, National Synchrotron Light Source was produced as follows. Ferric aqua-

metMb crystals were grown as described above. The cover slip containing the drop was placed under a layer of mineral oil (Figure 2.2) and 20 μL of a degassed solution of artificial mother liquor with 15% glycerol (added as cryoprotectant) was
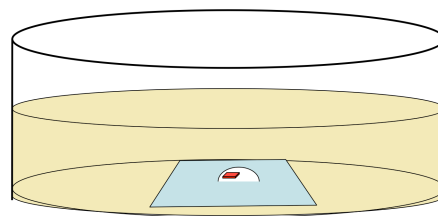
Figure 2.2 Coverslip submerged face up under mineral oil in a small Petri Dish.

added to the 10 μL drop containing the crystal and was carefully mixed. A portion of the droplet (20 μL) was then removed and 20 μL of degassed solution was added. The addition-removal cycle was repeated 5 more times in order to significantly reduce the amount of oxygen in the droplet containing the crystal. Degassed artificial mother liquor (10 μL) with 15% glycerol (cryosolution) and 250 mM sodium nitrite was added to the drop and allowed to soak for 10 minutes, during which time there was no visible color changes in the crystal. Degassed cryosolution (20 μL) containing 500 mM freshly dissolved sodium dithionite was added to the drop in order to reduce both the nitrite to nitric oxide and the heme iron from Ferric to Ferrous. The color of the crystals slowly changed over a 10 minutes period from brown (λ_{max} = 409 nm) to bright red (λ_{max} = 420 nm) and leaflets were harvested under the oil and flash frozen in liquid nitrogen.

2.2.1.2   NO Gas Method

*Met*Myoglobin crystals were grown by the same method as described in previous sections. The cover slip containing the drop was placed under a layer of mineral oil (Figure 2.2) and then the crystals were transferred to a degassed solution of artificial mother liquor containing 15% glycerol and 500 mM sodium dithionite to reduce the heme iron to the ferrous state. After the crystals changed colors from brown (λ_{max} = 409 nm) to deep red (λ_{max} = 435 nm) the artificial mother liquor was exchanged with

33

degassed cryosolution saturated with NO gas. The crystal was allowed to soak in the solution for 2–5 minutes, until a color change was seen shifting to a brighter red (λ_{max} = 420 nm). The crystal was then harvested and flash frozen in liquid nitrogen.

2.2.2 Data Collection and Processing

Data collection was carried out both at our home source and on two different beam lines at National Synchrotron Light Source (NSLS) at Brookhaven National Laboratory (BNL). The diffraction data were then processed using the stand alone version of *d*TREK* [69] or d*TREK as implemented in the *Crystal Clear* suite available from Molecular Structure Corporation [70].

2.2.2.1 Home Source Data Collection

X-ray data were collected at 100 K using CuKα radiation produced from a RigakuMSC RU-H3R X-ray generator operated at 50 kV/100 mA and a Rigaku R-AXIS IV++ image plate detector.

For the MbNO crystal formed from sodium nitrite reported in Copeland et al.[71], the crystal-to-detector distance was set at 70 mm and 180 frames of data were collected using a 1.0° oscillation and a 300 second exposure to a resolution of 1.9 Å.

For all other crystals for which data were collected on our home source the crystal to detector distance was set to 70 mm, and 180 - 250 images were collected with a 1.0° oscillation. The exposure time was determined for each crystal based on individual crystal diffraction quality, but was usually between 4 and 6 minutes per image.

2.2.2.2 Synchrotron Data Collection

High quality crystals were shipped to the National Synchrotron Light Source (NSLS) at Brookhaven National Laboratory (BNL) via the Mail-in Data Collection Program operated by the Protein Crystallography Research Resource (BNL-PXRR; www.px.nsls.bnl.gov/fedex.html) for high resolution X-ray data collection. X-ray data were collected at 100 K on beamlines X-12B (using an ADSC Quantum4 CCD detector) or X-29 (using an ADSC Quantum-315 CCD detector). For the MbNO crystal obtained from the nitrite/dithionite soak method, 1° oscillation images were collected over a range of 360° with an exposure time of 10 sec per image and a crystal-to-detector distance of 150 mm. For the MbNO crystal obtained from the dithionite/NO method, 1° oscillation images were collected over a range of 180° with an exposure time of 10 sec per image and a crystal-to-detector distance of 150 mm.

2.2.3   Structural Refinement

2.2.3.1   Synchrotron MbNO from Nitrite

The CCP4 suite [72] was used to solve and refine this structure. The search model chosen was the 1.9 Å resolution structure of hh MbNO (PDB access code 1NPF) [71] with the NO and solvent molecules removed from the structure.   After the rotation and translation search carried out using MOLREP,[73] the initial model had an *R-factor* of 33.9%. Restrained refinement was carried out for 20 cycles in Refmac5 prior to the addition of any solvent, which lowered the *R-factor* to 24.9%. At this point, the NO ligand and sulfate ions were added to the model based on density seen in an F_o-F_c electron density map, and the structure was checked for sidechains exhibiting low occupancy or multiple conformations. Lysine 47 was modeled in with low occupancy; however, no sidechains were seen with clear alternate positions in an F_o-F_c difference electron density map. After cycling with *ARP_waters* (as implemented in Refmac5) and 10 additional cycles of restrained refinement, 142 water molecules were added and the *R-factor* dropped to 21.5%. 100 more cycles of restrained refinement using data between 10 Å and 1.30 Å, and model manipulation with *Xfit*, resulted in an *R-factor* of 20.1%. Poor electron density was observed at the C-terminal of the protein for residues Gln 152 and Gly153; residue 153 was omitted from the structure. Up to this refinement stage, all refinement was performed with isotropic B-factor refinement.   Now, anisotropic B-factors were refined and the final *R-factor* decreased to 17.7% with an R_{free} of 22.0% calculated with 5% of the data. Coordinates have been deposited in the Protein Data Bank with the access code 2FRJ.

2.2.3.2 Synchrotron MbNO from NO(g) and Dithionite

Again, the search model chosen was the 1.9 Å resolution structure of hh MbNO (PDB access code 1NPF) [71] with the NO and solvent molecules removed from the structure. After molecular replacement the initial *R-factor* was 34.2%. After 30 cycles of restrained refinement with Refmac5 the *R-factor* dropped to 24.1% prior to the addition of ligand or solvent molecules. Nitric oxide and sulfate molecules were modeled into density based on an F_o-F_c difference electron density map. At this point the structure was checked for sidechains that had low occupancy or multiple positions and Lysine 47 was again modeled in with low occupancy, however no sidechains in multiple positions were clearly observed. Multiple cycles of *ARP_waters*, as implemented in Refmac5, were used to add a total of 147 water molecules to the structure and the *R-factor* dropped to 18.74%. At this point multiple cycles of refinement with Refmac5 followed by model adjustment with *Xfit* were performed to complete the major refinement of the structure. As stated in the previous structure poor electron density was seen for the two C-terminal residues and Gly153 was again omitted from the structure. The structure was refined initially using isotropic B-factors. Once all of the major structural refinement was complete, anisotropic B-factors were refined using data between 10 Å and 1.30 Å to complete refinement and lower the *R-factor* to a final value of 16.8% with an R_{free} of 20.5% calculated with 5% of the data. Coordinates have been deposited at the Protein Data Bank with the access code 2FRK.

2.3   Results

The data processing and refinement statistics for the two high resolution MbNO structures discussed in this chapter are shown in Table 2.3.

Table 2.3 X-ray Data Collection, Processing and Refinement Statistics

Method of prepn.	MbNO nitrite/dithionite	MbNO dithionite/NO$_{(g)}$
Data Collection[a]		
Space Group	P2$_1$	P2$_1$
Source	BNL, X-29	BNL, X-29
λ (Å)	1.0	0.9611
Cell Dimensions		
a, b, c (Å)	35.49,28.79,63.25	35.49,28.58,63.28
β (°)	105.97	105.59
Resolution(Å)	1.30	1.30
Mean $I/\sigma(I)$	17.8 (1.5)	9.9 (2.2)
No. Reflections		
Observed	129648 (12087)	105934 (10253)
Unique	35401 (2670)	30078 (3012)
Completeness (%)	91.4 (70.1)	98.7 (98.1)
R$_{merge}$ (%)[b]	5.2 (44.2)	5.5 (42.5)
Refinement Statistics[a]		
Resolution Range (Å)	9.78-1.30	9.89-1.30
R-factor (%)[c]	17.7 (35.9)	16.8 (26.8)
R$_{free}$ (%)[d]	22.0 (40.6)	20.5 (32.5)
r.m.s.d. bond distances (Å)	0.009	0.008
r.m.s.d. angles (°)	1.189	1.138
B factor (Å^2)		
Mean	20.71	20.35
r.m.s.d. mainchain	0.912	0.935
r.m.s.d. sidechain	3.348	3.720
Ramachandran Plot[e]		
% Residues in		
Most Favored	93.2	92.5
Allowed	6.8	7.5

[a] Values in parentheses correspond to the highest resolution shells for MbNO(BNL) (nitrite/dithionite) and MbNO (BNL) (dithionite/NO$_{(g)}$) (1.333-1.30 Å).

[b] R$_{merge}$ = $\Sigma|I - <I>|/\Sigma(I)$ where I is the individual intensity observation and $<I>$ is the mean of all measurements of I.

[c] R-factor = $\Sigma||F_o| - |F_c||/\Sigma|F_o|$ where F$_o$ and F$_c$ are the observed and calculated structure factors, respectively.

[d] R$_{free}$ is calculated using randomly selected reflections comprising 5% of the data not used throughout refinement.

[e] As calculated using PROCHECK. [74]

2.3.1 MbNO from Sodium Nitrite and Dithionite

Reaction of *met*Mb with nitrite and dithionite results in MbNO formation as demonstrated previously. X-ray diffraction data was obtained for this hh MbNO complex at 1.30 Å resolution. The heme environment is shown in Figure 2.3. The Fe-N bond length is 1.87 Å, and the Fe-N-O angle is 144°. The NO ligand, oriented away from the distal His64 residue, is stabilized by electrostatic interactions with the N^ε-atom of His64; the nitrosyl N-atom is located at a distance of 3.05 Å from the N^ε-atom, whereas the nitrosyl O-atom is located 3.35 Å away. No other significant interactions are apparent between the NO ligand and other distal amino acid residues; the closest contacts (ignoring hydrogen atoms) are with the $C\gamma^2$ of Val68, at a distance of 3.25 Å (nitrosyl O-atom) and 3.40 Å (nitrosyl N-atom). All other contacts are ≥ 3.6 Å from the NO ligand.

The Fe-N(His93) distance is 2.08 Å, and the (His93)N-Fe-N(O) axial bond angle is 170°. The imidazole plane of the proximal His93 ligand essentially eclipses a diagonal (por)N-Fe-N(por) bond, displaying only a 10° deviation with this diagonal. The angle between the plane of the imidazole and the FeNO plane is 42°, and the nitrosyl N-atom is tilted 9° from the normal to the heme 4N-plane.
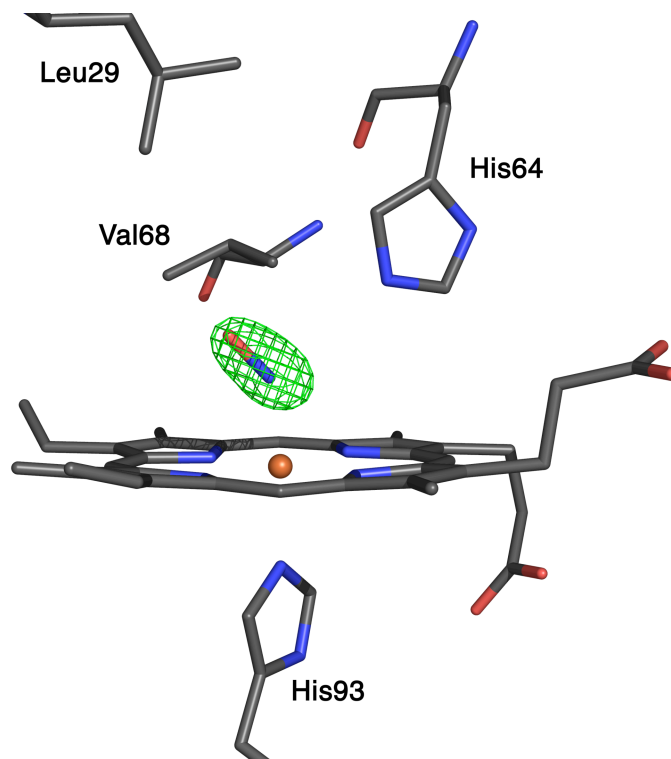
Figure 2.3 Final model and F_o-F_c omit electron density map contoured at 3σ showing a side view of the heme environment in hh MbNO. Carbon, oxygen, nitrogen and iron atoms are colored grey, red, blue, and brown, respectively.

2.3.2 MbNO from NO$_{(g)}$

Crystals of hh MbNO were also obtained by exposure of reduced myoglobin to NO gas. Diffraction data for this MbNO crystal were collected to 1.1 Å, but the crystal suffered radiation decay, and the structure was solved to 1.30 Å resolution. The bulk features of the FeNO group are similar to that described for the MbNO structure of the complex obtained from the nitrite/dithionite method and the heme environment is shown in Figure 2.4. Notable differences lay in the FeNO conformation. Thus, the Fe-N(O) distance is 2.13 Å, and the Fe-N-O angle is 120°. The nitrosyl N-atom is located 2.72 Å away from the N$^{\varepsilon}$-atom of His 64, indicating a stronger hydrogen bonding interaction with this residue than that observed in the MbNO crystal structure described in the previous section (i.e., MbNO from nitrite/dithionite). The distance between the nitrosyl O-atom and the N$^{\varepsilon}$ atom of His64 is 3.33 Å. As the MbNO structure described in the previous section, the nitrosyl N-atom is also tilted 9° off-axis from the normal to the heme 4-N plane of this derivative. Importantly, the Fe atom is displaced 0.13 Å below the mean porphyrin 4N-plane towards the proximal His93 residue. The (His93)N-Fe-N(O) axial angle is 175°, and the angle between the proximal imidazole plane and the FeNO plane is 43°.
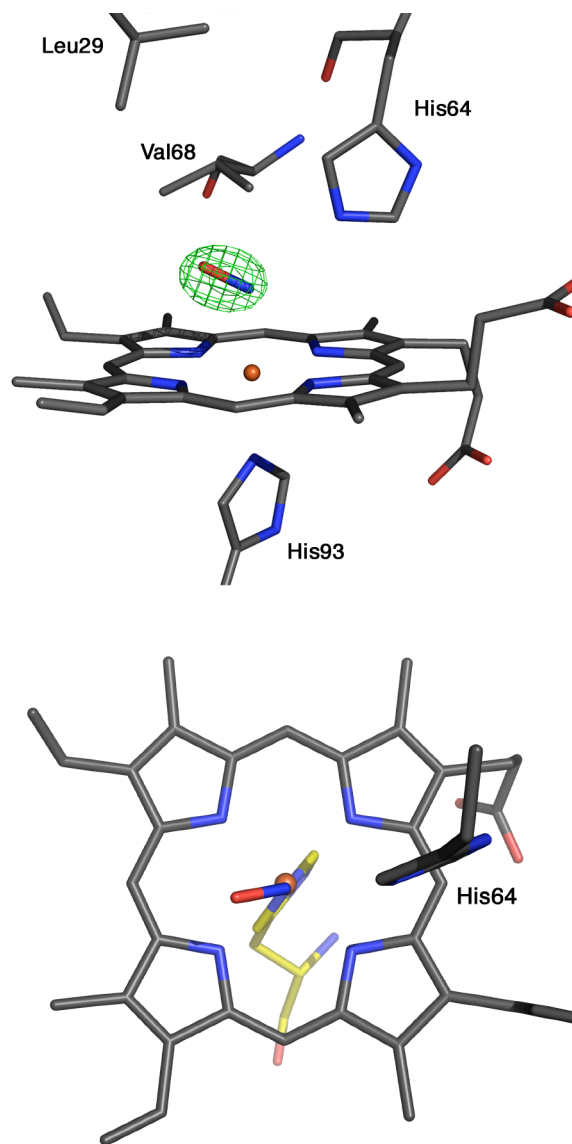
Figure 2.4 (a) Final model and F_o-F_c omit electron density map contoured at 3σ showing a side view of the heme environment in hh MbNO. The hydrogen bond between N^ε of the distal His64 residue and the N atom of the nitrosyl ligand is 2.72 Å. The Fe-N(O) bond length in this complex is 2.13Å, slightly longer than in the complexes made from the nitrite/dithionite method. Carbon, oxygen, nitrogen and iron atoms are colored grey, red, blue, and brown, respectively. (b) Top view of the heme in the hh MbNO, with the NO ligand on the side of the porphyrin ring facing the viewer. The coloring scheme is same as in (a) with the exception of the proximal His93 ligand which is drawn in yellow for clarity.

2.3.3 Reproducibility of FeNO Conformations

The issue of reproducibility regarding the observation of the two FeNO bond conformations described above was examined and multiple data sets collected on these samples gave confirmatory results regarding our observed clustering of the FeNO angles at ~143° and at ~118°. For example, five separate determinations of the structure of MbNO from nitrite/dithionite, from separate preparations, in the 1.9-2.6 Å resolution range (with three at 1.9 Å resolution) yielded FeNO angles in the 139-147° range (avg. 143°). In contrast, the related five independent structural determinations of MbNO from NO gas, in the 1.7-2.35 Å resolution range (with three at 1.7 Å) yielded FeNO bond angles in the 117-121° range (avg. 118°).

We next explored the possibility that temperature differences during sample preparation were responsible for the observed difference in the FeNO angles produced by the two synthetic routes. Specifically, dissolution of solid nitrite in water is endothermic, resulting in a lowering of the temperature of the droplet containing the crystals during the crystal soak with solid nitrite. Three methods of MbNO formation from nitrite were thus carried out, as were two methods of formation of MbNO from the use of NO gas: (i) addition of solid nitrite to the soak solution at room temperature (~21 °C) followed by dithionite addition, (ii) addition of pre-dissolved nitrite (in buffer; equilibrated at room temperature) to the soak solution at room temperature followed by dithionite addition, (iii) addition of pre-dissolved nitrite (in buffer; equilibrated at 4 °C) to the soak solution equilibrated at 4 °C followed by dithionite addition at 4 °C, (iv) addition of NO-saturated buffer to the soak solution containing reduced Mb at room temperature, and (v) addition of NO-saturated buffer (equilibrated at 4 °C) to the soak solution containing reduced Mb

equilibrated at 4 °C. In-house X-ray data were collected on the MbNO crystals from duplicate preparations for each of the five methods above (data not shown). All the nitrite-derived MbNO structures exhibited FeNO angles in the 144-147° range, whereas those derived from NO exhibited FeNO angles in the 118-120° range.

2.4   Discussion

FeNO Conformations in Nitrosylated Heme Proteins

The nature of the interaction between NO and heme proteins has intrigued structural chemists and biochemists for many decades. Prior to the ready availability of appropriate cryocrystallography instrumentation for the determination of high-resolution protein crystal structures, the related crystal structures of bioinorganic heme model compounds played a key role in providing information on binding modes and associated geometrical parameters for small molecule ligands when bound to heme.

As stated in the introduction, (porphyrin)Fe(NO)(N-base) compounds have a very tight range of FeNO geometries [20, 29]. In these complexes the Fe-N-O bond angles range from 137-140° (avg. ~138.5 °), and the Fe-NO bond lengths range from 1.744(2)-1.758(1) Å (avg. ~1.753 Å) [29, 31]. The situation is less clear, however, for nitrosyl heme proteins that have been structurally characterized by X-ray crystallography. Selected structural data for nitrosyl heme proteins are presented in Table 2.2.

A much wider range of Fe-N-O bond angles is evident from these protein X-ray structures, ranging from 112 to 160°. A range of 1.5-2.1 Å for the associated Fe-N(O) distances is also evident. This suggests a role of distal residues in influencing FeNO geometry through a combination of factors including steric and electrostatic effects. Studies are ongoing for heme proteins in general, as distal and proximal effects are likely determinants of ligand discrimination and selectivity in heme-based sensor proteins. The method of preparation of each of the complexes in Table 2.2 was also examined to determine if there was a correlation between the method of formation of the complexes with the FeNO geometry. There were 12 complexes synthesized using nitrite and 29

complexes synthesized using NO gas and the average FeNO angles were 138.5° and 137.5° respectively. There is clearly no trend observed when comparing different proteins, but because of the differences in the heme sites of these proteins one should not have been expected. Brucker and coworkers showed that even with minor changes to the heme pocket there was a modest change in the FeNO geometry from 112° in wild type nitrosyl sperm whale myoglobin to 127° in the L29F/D122N sw MbNO mutant[48].

In the case of MbNO, Hori and Yonetani [41] demonstrated a temperature-dependence of the Fe-N-O bond angle by single-crystal EPR spectroscopy. They showed that for sw MbNO, the Fe-N-O angle was 153±5° at 293 K, but was 109±5 at 77 K,
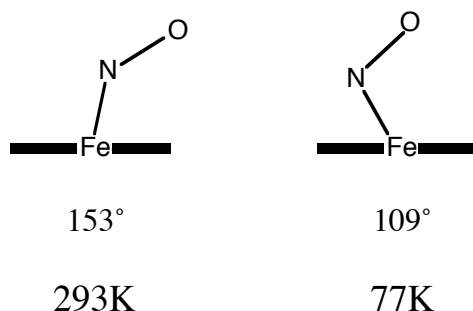
Figure 2.5 Representations of the two conformations of the Fe-NO moiety as calculated using single-crystal EPR spectroscopy at two different temperatures which showed that temperature can play a large role in the conformation of the nitrosyl moiety.

demonstrating that the conformation of the FeNO moiety was altered upon freezing. The nitrogen atom in both of the complexes showed severe deflection from the heme normal, ~20° off of the heme normal in the structure at 293 K and an even larger 30° in the 77 K structure. This study complemented earlier single crystal EPR studies that revealed FeNO bond angles of 108-110° for MbNO at 77 K, [42] and 119° for horse HbNO at 77 K[43]. In the Brucker et al. [48] structure of a nitrosyl sperm whale myoglobin at 1.7 Å the

46

reported Fe-N-O bond angle of 112° was far more acute that the Fe-N-O bond angles observed in nitrosyl heme model compounds. The authors indicate that subtle distal pocket effects may cause the acute angle. Their crystal of sw MbNO was prepared by NO-induced reduction (reductive nitrosylation) of a pre-formed ferric Mb crystal. We subsequently reported the 1.9 Å resolution crystal structure of hh MbNO, generated by the addition of nitrite and dithionite, and determined an Fe-N-O bond angle of 147° for this compound [71]. Because the MbNO complex is an $\{Fe(NO)\}^7$ complex, the angle of 147° fits quite nicely with the expected values of ~145° that $\{M(NO)]^7$ species are predicted to have[3]. When comparing only the nitrosyl myoglobin complexes, there is a wide range observed in the FeNO geometry. For ease of comparison, the metric data for the 5 published MbNO structures are shown in Table 2.4. Interestingly, Rich et al.[45] have reported MS XAFS data for a frozen solution of $Mb^{II}NO$, and they determined an Fe-N-O angle of 150° and an Fe-NO bond length of 1.75 Å. These values are similar to those observed in synthetic iron(II) nitrosyl, $\{Fe(NO)\}^7$, porphyrins[20, 29]. Oldfield and coworkers [75] have reported that geometry optimization of the heme environment of sw MbNO (using the data from the X-ray structure as the initial model) results in the generation of a "normal" heme-NO geometry (Fe-N-O = 138.1°; Fe-N(O) = 1.781 Å) that is similar to structural data from model heme-NO compounds.

Table 2.4 Metric Data of Published MbNO Structures

	sw	sw	hh	hh	hh
Molecular Description	wt	L29F/D122N	wt	wt	wt
PDB ID	1HJT	1JDO	1NPF	2FRJ	2FRK
Method of Formation	NO gas	NO gas	NO_2/Dithionite	NO_2/Dithionite	NO/Dithionite
Temperature	RT	RT	100 K	100 K	100 K
Space Group	$P2_1$	P6	$P2_1$	$P2_1$	$P2_1$
Resolution (Å)	1.7	1.9	1.9	1.3	1.3
Fe-N (Å)	1.89	1.86	2.03	1.88	2.13
∠Fe-N-O (°)	112	127	147	144	120
Fe-N(por) (Å)	2.03-2.13	1.95-1.99	1.98-2.02	2.03-2.05	2.04-2.08
Fe-N(His) (Å)	2.11	2.31	2.11	2.08	2.15
H64(N)-N(O) (Å)	2.78	3.23	2.98	3.05	2.72
H64(N)-O(N) (Å)	3.38	2.98	3.18	3.34	3.33
Fe out of plane (Å)	+0.04	+0.09	-0.06	+0.02	-0.13
∠N(por)-Fe-N-O (°)	25.1	-10.9	14.7	36.9	35.9

abbreviations: sw Mb = recombinant sperm whale myoglobin, *Phyester catadon*; hh Mb = horse heart myoglobin, *Equus cabalus*; wt = wild type
Metric data were obtained from PDB files

These studies raise an important question: *What is the geometry of the FeNO group in MbNO?* Or perhaps a more appropriate question is: *What are the possible geometries of the FeNO group in MbNO?* We sought to contribute to this on-going debate by determining the high-resolution X-ray crystal structures of hh MbNO prepared by two common routes: (i) reaction of metMb with nitrite/dithionite, and (ii) reaction of reduced Mb with NO gas.

The structure with the FeNO bond angle at 144° also shows an Fe-NO distance of 1.87 Å; the bond angle is similar to that seen for synthetic ferrous nitrosyl porphyrins, however, the Fe-NO bond length is ~0.1 Å longer than that observed in the model compounds. In contrast, the structure with the FeNO bond angle of 120° shows an Fe-NO distance of 2.13 Å; the bond angle is more acute that that seen for the nitrosyl heme models, and the Fe-NO distance is long. Interestingly, in the 144° structure, the Fe was calculated to be in the plane of the porphyrin ring (with less than 0.02 Å deviation from

the 4-N plane), whereas in the 120° structure, the Fe atom was calculated to be 0.12 Å *below* the 4-N porphyrin plane, away from the NO ligand. This latter feature suggests or reinforces the notion of a weaker bond between the NO ligand and the Fe center in this structure. Consistent with this view is the occurrence of a slightly longer Fe-NO bond and more acute Fe-N-O angle. Indeed, the N-atom of the nitrosyl group is thus situated closer to the distal His64 ligand suggesting a stronger hydrogen bonding interaction between the NO and His64 residue. We can also see, in Figure 2.6 that there is ~9° off axis tilt in both of the complexes, however the tilt in the two structures are in the opposite direction. This is very similar to what Hori and Yonetani saw with their temperature dependent EPR structures [41].

Our current thinking, therefore, is that the pre-formed distal pocket in the precursor *aqua-met*Mb crystals of hh Mb imposes some constraints in the geometry of the heme distal pocket during and after formation of the MbNO derivative. Nitrosylation of the *aqua-met*Mb crystals by the two methods employed here involve different intermediates along the reaction pathways, and the observed MbNO product geometries probably reflect distal pocket stabilizations of local minima on the ground state potential energy surface. In this scenario, the distal His64 residue must play an important role. Such a possibility is reinforced by the MS XAFS work on frozen solutions of hh MbNO that reveal more "normal" FeNO geometries reflective of perhaps the global minimum structure [45]. The geometry optimization work by Oldfield and coworkers [75] appears to support this hypothesis.

Fe-N(O)   1.87Å
∠Fe-N-O   144°

Fe-N(O)   2.13Å
∠Fe-N-O   120°
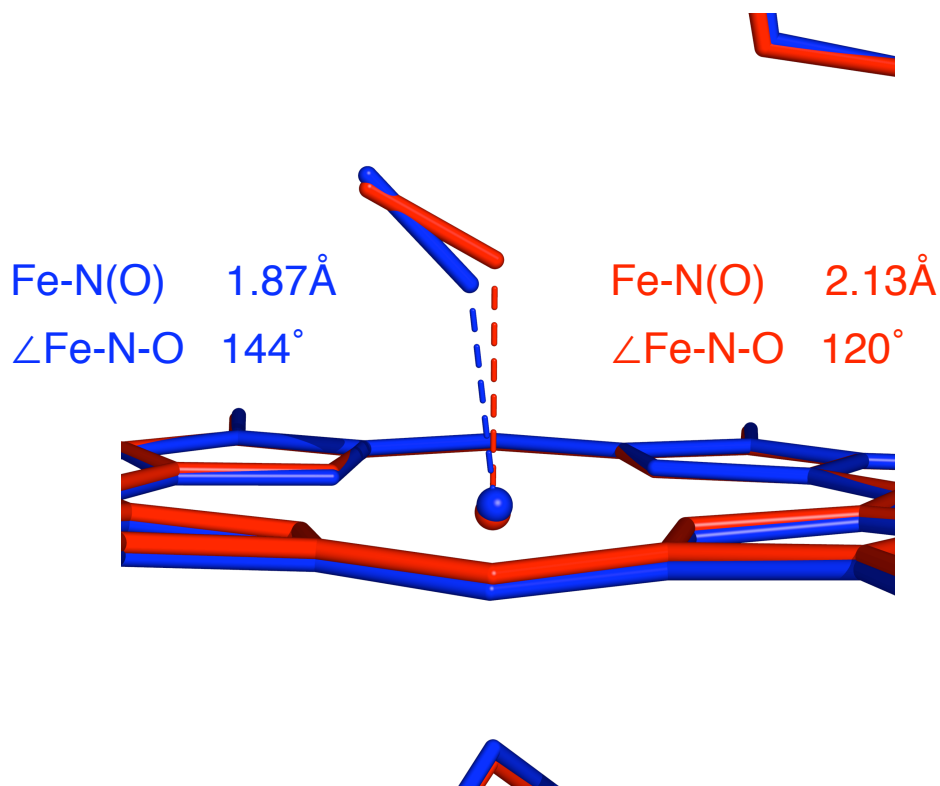
Figure 2.6   Overlay of the atomic coordinates of 2FRJ (1.3Å structure of MbNO formed using the nitrite/dithionite method) shown in blue and 2FRK (1.3Å structure of MbNO formed using the NO/dithionite method) shown in red.

It is important to note that the two native MbNO complexes (both hh and sw) that display the most acute FeNO angles were generated in a way that is consistent with the final step in the mechanism for reductive nitrosylation[39a]. In the case of sw MbNO, NO itself was the reducing agent[48], and in the formation of hh MbNO, sodium dithionite was the reductant. The mechanism for reductive nitrosylation proceeds as follows. Initially, an NO molecule binds to the Fe(III) center and transfers an electron to the metal. The electrophilic NO$^+$ species then undergoes a nucleophilic attack by a hydroxide ion. The rate constant (k_{OH}) for this, the rate limiting step in the reaction, is $(3.2 \pm 0.2) \times 10^2$ M^{-1} s^{-1}

in solution at pH > 7.2 [39b]. This forms nitrous acid (HNO_2), which dissociates from the reduced metal. After the dissociation of the HNO_2 species, the active site is free for another NO molecule to bind to the five coordinate Fe(II) species. However, in this mechanism for reductive nitrosylation, the identity of the reductant is not significant to the binding of the NO ligand in the final step.
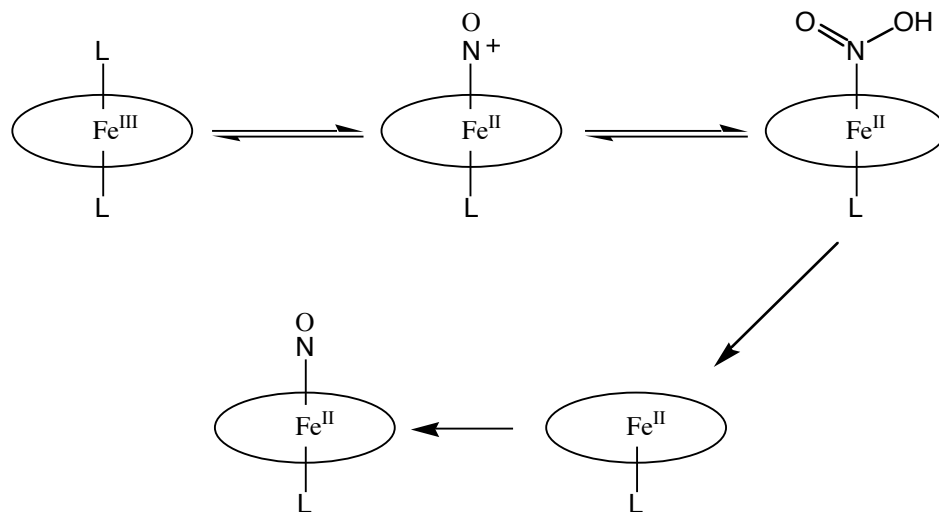
Mechanism for reductive nitrosylation

In both, sw and hh MbNO prepared from NO gas, the FeNO geometry is similar, 112° for the sw MbNO and 120° for the hh MbNO, because the NO ligand encounters a five-coordinate Fe(II) species.

The same cannot be said for the mechanism for the formation of the MbNO species using nitrite to generate the NO ligand. As will be seen in the following chapter the nitrite moiety itself can bind to the heme iron. Therefore, it is not clear which species the NO ligand encounters as it approaches the heme iron, or if in fact it is an NO species that approaches the heme site. If the nitrite binds to the heme iron and is converted to NO while still on the metal, it is reasonable to expect that there could be a different FeNO

geometry than what was just described above. Furthermore, the FeNO geometry observed in the final structure of the hh MbNO complex formed from nitrite and dithionite suggests that there is some difference in the mechanism, but more studies are needed to determine what the mechanism of formation actually is.

It is also interesting to note that *all the heme NO structures reported to date have been obtained from nitrosylation of preformed crystals of the protein.* Put another way, the "NO" equivalent is added to a preformed distal pocket in the crystal, usually by the replacement of an iron-bound water ligand, although this is not always the case. It is thus tempting to speculate that the wide range of FeNO geometries observed in the crystal structures of heme-NO proteins to date may be reflective of the distal pocket stabilizations of various local minima in these nitrosylated derivatives, something that is not available to the synthetic iron nitrosyl porphyrins. In other words, the observed FeNO geometries in crystals of heme-NO compounds prepared from nitrosylation of precursor crystals may not necessarily represent the global minimum conformations of the FeNO moiety.

2.5   Conclusions

We have determined the crystal structure of ferrous hh MbNO at high resolution, and we have shown that the FeNO bond angle clusters around two values depending on the mode of preparation of the complex, ~120° for complexes made with $NO_{(g)}$/dithionite and ~144° for those made with nitrite/dithionite. To date, all heme-NO crystal structures reported in the literature have been on compounds that have been derived from nitrosylation of precursor crystals. Several previous studies have demonstrated that the FeNO geometry in MbNO may depend on temperature of the crystal or on distal pocket effects. We have now shown that the method of preparation of MbNO from *aqua-met*Mb crystals is a determining factor in the observed FeNO geometry. Nitrosylation of pre-formed Mb crystals may therefore impose limitations on the attainment of global FeNO conformation minima, and may enable variable FeNO conformations that are stabilized by subtle electrostatic and steric effects imposed by the pre-formed distal pockets.

At this time it is difficult to say that the differences in FeNO geometry have direct biological significance, however this work is an important starting point that determined that there is a difference. One possible future area of research may be to try to determine if NO derived from nitrite and NO gas are discriminated between *in vivo*. If this is the case the binding modes seen here may play an important role in that discrimination, only time will tell.

2.6   References

1.   Alderton, W. K.; Cooper, C. E.; Knowles, R. G., Nitric Oxide Synthases: Structure, Function and Inhibition. Biochem. J. 2001, 357, 593-615.

2.   Ishimura, Y.; Gao, Y. T.; Panda, S. P.; Roman, L. J.; Masters, B. S. S.; Weintraub, S. T., Detection of Nitrous Oxide in the Neuronal Nitric Oxide Synthase Reaction by Gas Chromatography-Mass Spectrometry. Biochem. Biophys. Res. Commun. 2005, 338, 543-549.

3.   Cheng, L.; Richter-Addo, G. B., Binding and Activation of Nitric Oxide by Metalloporphyrins and Heme. In The Porphyrin Handbook, Guilard, R.; Smith, K.; Kadish, K. M., Eds. Academic Press: New York, 2000; Vol. 4 (Biochemistry and Binding: Activation of Small Molecules), pp 219-291.

4.   Lee, J.; Chen, L.; West, A. H.; Richter-Addo, G. B., Interactions of Organic Nitroso Compounds with Metals. Chem. Rev. 2002, 102, (4), 1019-1065.

5.   Zhao, Y.; Hoganson, C.; Babcock, G. T.; Marletta, M. A., Structural Changes in the Heme Proximal Pocket Induced by Nitric Oxide Binding to Soluble Guanylate Cyclase. Biochemistry 1998, 37, (36), 12458-12464.

6.   Ballou, D. P.; Zhao, Y.; Brandish, P. E.; Marletta, M. A., Revisiting the Kinetics fo Nitric Oxide (NO) Binding to Soluble Guanylate Cyclase: The Simple NO-Binding Model is Incorrect. Proc. Natl. Acad. Sci., USA 2002, 99, (19), 12097-12101, and references therein.

7.   Cary SP, W. J., Marletta MA, Tonic and acute nitric oxide signaling through soluble guanylate cyclase is mediated by nonheme nitric oxide, ATP, and GTP. Proc Natl Acad Sci U S A. 2005, 102, (37), 13064-9.

8.   Burkitt, M. J. R., Alaeddin, Nitric oxide generation from hydroxyurea: significance and implications for leukemogenesis in the management of myeloproliferative disorders. American Society of Hematology 2006, 107, (6), 2219-2222.

9.   Shaw, C. A. M., Ian L.; Rossi, Adriano G., Apoptosis and atherosclerosis: the role of nitric oxide. Anti-Inflammatory & Anti-Allergy Agents in Medicinal Chemistry 2006, 5, (1), 27-33.

10.   Bilodeau, M. L. H., Heidi E., Endothelial nitric-oxide synthase reveals a new face in G protein signaling. Molecular Pharmacology 2006, 69, (3), 677-679.

11.   Redington, A. E., Modulation of nitric oxide pathways: Therapeutic potential in asthma and chronic obstructive pulmonary disease. European Journal of Pharmacology 2006, 533, (1-3), 263-276.

12.   Araujo, M. W., William J., Oxidative stress and nitric oxide in kidney function. Current Opinion in Nephrology & Hypertension 2006, 15, (1), 72-77.

13. Nagy, G. P., Andras., The role of nitric oxide in abnormal T cell signal transduction in systemic lupus erythematosus. Clinical Immunology 2006, 18, (2-3), 145-151.

14. Christ, G. J. H., Steve., Molecular mechanisms of detrusor and corporal myocyte contraction: identifying targets for pharmacotherapy of bladder and erectile dysfunction. British Journal of Pharmacology 2006, 147, (2), s41-s55.

15. Prabhakar, S. S., Pathogenic role of nitric oxide alterations in diabetic nephropathy. . Current Diabetes Reports 2005, 5, (6), 449-454.

16. Nijs, J. D. M., Kenny, Nitric oxide and chronic fatigue syndrome: Are we caring for our patients or are we practicing selfcare? Medical Hypotheses 2005, 66, (2), 449-450.

17. Zhang, L. D., Valina L.; Dawson, Ted M., Role of nitric oxide in Parkinson's disease. Pharmacology & Therapeutics 2006, 109, (1-2), 33-41.

18. Feltham, R. D.; Enemark, J. H., Structures of Metal Nitrosyls. Top. Stereochem. 1981, 12, 155-215.

19. Methods in Nitric Oxide Research. John Wiley and Sons: 1996.

20. Wyllie, G. R. A.; Scheidt, W. R., Solid-State Structures of Metalloporphyrin NOx Compounds. Chem. Rev. 2002, 102, (4), 1067-1089.

21. Scheidt, W. R.; Frisse, M. E., Nitrosylmetalloporphyrins. II. Synthesis and Molecular Stereochemistry of Nitrosyl-a,b,g,d-tetraphenylporphinatoiron(II). J. Am. Chem. Soc. 1975, 97, (1), 17-21.

22. Scheidt, W. R.; Duval, H. F.; Neal, T. J.; Ellison, M. K., Intrinsic Structural Distortions in Five-Coordinate (Nitrosyl)iron(II) Porphyrinate Derivatives. J. Am. Chem. Soc. 2000, 122, 4651-4659, and references therein.

23. Bohle, D. S.; Hung, C.-H., Ligand-Promoted Rapid Nitric Oxide Dissociation from Ferrous Porphyrin Nitrosyls. J. Am. Chem. Soc. 1995, 117, (37), 9584-9585.

24. Cheng, L.; Powell, D. R.; Khan, M. A.; Richter-Addo, G. B., The First Unambiguous Determination of a Nitrosyl-to-Nitrite Conversion in an Iron Nitrosyl Porphyrin. Chem. Commun. 2000, 2301-2302.

25. Nasri, H.; Haller, K. J.; Wang, Y.; Huynh, B. H.; Scheidt, W. R., Reactions of Bis(nitro)[a,a,a,a-meso-tetrakis(o-pivalamidophenyl)porphinato]iron(III) with 2,3,5,6-Tetrafluorothiophenol and 2,3,5,6-Tetrafluorothiophenolate. EPR and Mössbauer Spectra and Molecular Structures. Inorg. Chem. 1992, 31, (16), 3459-3467.

26. Bohle, D. S.; Debrunner, P.; Fitzgerald, J. P.; Hansert, B.; Hung, C.-H.; Thomson, A. J., Electronic Origin of Variable Denitrosylation Kinetics From Isostructural {Fe(NO)}7 Complexes: X-ray Crystal Structure of [Fe(oetap)(NO)]. Chem. Commun. 1997, 91-92.

27. Piciulo, P. L.; Rupprecht, G.; Scheidt, W. R., Stereochemistry of Nitrosylmetalloporphyrins. Nitrosyl-a,b,g,d-tetraphenylporphinato(1-

methylimidazole)iron and Nitrosyl-a,b,g,d-tetraphenylporphinato(4-methylpiperidine)manganese. J. Am. Chem. Soc. 1974, 96, (16), 5293-5295.

28. Scheidt, W. R.; Piciulo, P. L., Nitrosylmetalloporphyrins. III. Synthesis and Molecular Stereochemistry of Nitrosyl-a,b,g,d-tetraphenylporphinato(1-methylimidazole)iron(II). J. Am. Chem. Soc. 1976, 98, (7), 1913-1919.

29. Wyllie, G. R. A.; Schultz, C. E.; Scheidt, W. R., Five- to Six-Coordination in (Nitrosyl)iron(II) Porphyrinates: Effects of Binding the Sixth Ligand. Inorg. Chem. 2003, 42, (18), 5722-5734.

30. Scheidt, W. R.; Brinegar, A. C.; Ferro, E. B.; Kirner, J. F., Nitrosylmetalloporphyrins. 4. Molecular Stereochemistry of Two Crystalline Forms of Nitrosyl-a,b,g,d-tetraphenylporphinato(4-methylpiperidine)iron(II). A Structural Correlation with u(NO). J. Am. Chem. Soc. 1977, 99, (22), 7315-7322.

31. Rath, S. P.; Koerner, R.; Olmstead, M. M.; Balch, A. L., Reversible Binding of Nitric Oxide and Carbon-Carbon Bond Formation in a Meso-hydroxylated Heme. J. Am. Chem. Soc. 2003, 125, 11798-11799.

32. Moller, J. K. S.; Skibsted, L. H., Nitric Oxide and Myoglobins. Chem. Rev. 2002, 102, 1167-1178.

33. Springer, B. A.; Sligar, S. G.; Olson, J. S.; George N. Phillips, J., Mechanisms of Ligand Recognition in Myoglobin. Chem. Rev. 1994, 94, 699-714.

34. Arnold, E. V.; Bohle, D. S., Isolation and Oxygenation Reactions of Nitrosylmyoglobins. Methods Enzymol. 1996, 269, 41-55.

35. Skibsted, L. H., Cured Meat Products and Their Oxidative Stability. In The Chemistry of Muscle-Based Foods, Johnson, D. E.; Knight, M. K.; Ledward, D. A., Eds. Royal Society of Chemistry: Cambridge, 1992; pp 266-286.

36. Hoshino, M.; Laverman, L.; Ford, P. C., Nitric Oxide Complexes of Metalloporphyrins. An Overview of Some Mechanistic Studies. Coord. Chem. Rev. 1999, 187, 75-102, and references therein.

37. Carlson, M. L.; Regan, R.; Elber, R.; Li, H.; Phillips, G. N.; Olson, J. S.; Gibson, Q. H., Nitric Oxide Recombination to Double Mutants of Myoglobin: Role of Ligand Diffusion in a Fluctuating Heme Pocket. Biochemistry 1994, 33, (35), 10597-10606.

38. Miller, L. M.; Pedraza, A. J.; Chance, M. R., Identification of Conformational Substrates Involved in Nitric Oxide Binding to Ferric and Ferrous Myoglobin through Difference Fourier Transform Infrared Spectroscopy (FTIR). Biochemistry 1997, 36, (40), 12199-12207.

39. (a) Ford, P. C.; Lorkovic, I. M., Mechanistic Aspects of the Reactions of Nitric Oxide with Transition-Metal Complexes. Chem. Rev. 2002, 102, 993-1017. (b) Hoshino, Mikio, Masahiro Maeda, Reiko Konishi, Hiroshi Seki, Peter C. Ford, Studies on the Reaction Mechanism for Reductive Nitrosylation of Ferrihemoproteins in Buffer Solutions. J. Am. Chem. Soc. 1996, 118, 5702-5707

40. Brunori, M., Nitric Oxide, Cytochrome-c Oxidase and Myoglobin. Trends Biochem. Sci. 2001, 26, (1), 21-23.

41. Hori, H.; Ikeda-Saito, M.; Yonetani, T., Single Crystal EPR of Myoglobin Nitroxide. J. Biol. Chem. 1981, 256, (15), 7849-7855.

42. Dickinson, L. C.; Chien, J. C. W., An Electron Paramagnetic Resonance Study of Nitrosylmyoglobin. J. Am. Chem. Soc. 1971, 93, (20), 5036-5040.

43. Chien, J. C. W., Electron Paramagnetic Resonance Study of the Stereochemistry of Nitrosylhemoglobin. J. Chem. Phys. 1969, 51, (10), 4220-4227.

44. Waleh, A.; Ho, N.; Chantranupong, L.; Loew, G. H., Electronic Structure of Nitrosyl Ferrous Heme Complexes. J. Am. Chem. Soc. 1989, 111, (8), 2767-2772.

45. Rich, A. M.; Armstrong, R. S.; Ellis, P. J.; Lay, P. A., Determination of the Fe-Ligand Bond Lengths and Fe-N-O Bond Angles in Horse Heart Ferric and Ferrous Nitrosylmyoglobin Using Muliple-Scattering XAFS Analyses. J. Am. Chem. Soc. 1998, 120, 10827-10836.

46. Tomita, T.; Hirota, H.; Ogura, T.; Olson, J. S.; Kitagawa, T., Resonance Raman Investigation of Fe-N-O Structure of Nitrosylheme in Myoglobin and Its Mutants. J. Phys. Chem. B 1999, 103, 7044-7054.

47. Coyle, C. M.; Vogel, K. M.; Rush, T. S., III; Kozlowski, P. M.; Williams, R.; Spiro, T. G.; Dou, Y.; Ikeda-Saito, M.; Olson, J. S.; Zgierski, M. Z., FeNO Structure in Distal Pocket Mutants of Myoglobin Based on Resonance Raman Spectroscopy. Biochemistry 2003, 42, 4896-4903.

48. Brucker, E. A.; Olson, J. S.; Ikeda-Saito, M.; Philips, G. N., Jr., Nitric Oxide Myoglobin: Crystal Structure and Analysis of Ligand Geometry. Proteins: Structure, Function, and Genetics 1998, 30, (4), 352-356.

49. Ding, X. D.; Weichsel, A.; Andersen, J. F.; Shokhireva, T. K.; Balfour, C.; Pierik, A. J.; Averill, B. A.; Montfort, W. R.; Walker, F. A., Nitric Oxide Binding to the Ferri- and Ferroheme States of Nitrophorin 1, a Reversible NO-Binding Heme Protein from the Saliva of the Blood-Sucking Insect, Rhodnius prolixus. J. Am. Chem. Soc. 1999, 121, 128-138.

50. Weichsel, A.; Montfort, W. R., to be published.

51. Kondrashov, D. A.; Roberts, S. A.; Weichsel, A.; Montfort, W. R., Protein Functional Cycle Viewed at Atomic Resolution: Conformational Change and Mobility in NItrophorin 4 as a Function of pH and NO Binding. Biochemistry 2004, 43, 13637-13647.

52. Maes, E. M.; Weichsel, A.; Andersen, J. F.; Shepley, D.; Montfort, W. R., Role of Binding Site Loops in Controlling Nitric Oxide Release: Structure and Kinetics of Mutant Forms of Nitrophorin 4. Biochemistry 2004, 2004, 6679-6690.

53. Friedman, J.; Lad, L.; Deshmukh, R.; Li, H.; Wilks, A.; Poulos, T. L., Crystal Structures of the NO- and CO-bound Heme Oxygenase from Neisseriae meningitidis. Implications for O2 Activation. J. Biol. Chem. 2003, 278, (36), 34654-34659.

54.   Sugishima, M.; Sakamoto, H.; Noguchi, M.; Fukuyama, K., Crystal Structures of Ferrous and CO-, CN--, and NO-bound Forms of Rat Heme Oxygenase-1 (HO-1) in Complex with Heme: Structural Implications for Discrimination between CO and O2 in HO-1. Biochemistry 2003, 42, 9898-9905.

55.   Lad, L.; Wang, J.; Li, H.; Friedman, J.; Bhaskar, B.; Ortiz de Montellano, P. R.; Poulos, T. L., Crystal Structures of the Ferric, Ferrous, and Ferrous-NO Forms of the Asp140Ala Mutant of Human Heme Oxygenase-1: Catalytic Implications. J. Mol. Biol. 2003, 330, 527-538.

56.   Lad, L.; Ortiz de Montellano, P. R.; Poulos, T. L., Crystal Structures of Ferrous and Ferrous-NO Forms of Verdoheme in a Complex With Human Heme Oxygenase-1: Catalytic Implications for Heme Cleavage. J. Inorg. Biochem. 2004, 98, 1686-1695.

57.   Harutyunyan, E. H.; Safonova, T. N.; Kuranova, I. P.; Popov, A. N.; Teplyakov, A. V.; Obmolova, G. V.; Vainshtein, B. K.; Dodson, G. G.; Wilson, J. C., The Binding of Carbon Monoxide and Nitric Oxide to Leghaemoglobin in Comparison with Other Haemoglobins. J. Mol. Biol. 1996, 264, 152-161.

58.   Rich, A. M.; Ellis, P. J.; Tennant, L.; Wright, P. E.; Armstrong, R. S.; Lay, P. A., Determination of Fe-Ligand Bond Lengths and the Fe-N-O Bond Angles in Soybean Ferrous and Ferric Nitrosylleghemoglobin a Using Multiple-Scattering XAFS Analyses. Biochemistry 1999, 38, 16491-16499.

59.   Gong, W.; Hao, B.; Chan, M. K., New Mechanistic Insights from Structural Studies of the Oxygen-Sensing Domain of Bradyrhibozium japonicum FixL. Biochemistry 2000, 39, 3955-3962.

60.   Lawson, D. M.; Stevenson, C. E. M.; Andrew, C. R.; Eady, R. R., Unprecedented Proximal Binding of Nitric Oxide to Heme: Implications for Guanylate Cyclase. EMBO Journal 2000, 19, (21), 5661-5671.

61.   Williams, P. A.; Fulop, V.; Garman, E. F.; Saunders, N. F. W.; Ferguson, S. J.; Hajdu, J., Haem-ligand Switching During Catalysis in Crystals of a Nitrogen-cycle Enzyme. Nature 1997, 389, 406-412.

62.   Nurizzo, D.; Cutruzzola, F.; Arese, M.; Bourgeois, D.; Brunori, M.; Cambillau, C.; Tegoni, M., Conformational Changes Occurring upon Reduction and NO Binding in Nitrite Reductase from Psudomonas aeruginosa. Biochemistry 1998, 37, (40), 13987-13996.

63.   Edwards, S. L.; Kraut, J.; Poulos, T. L., Crystal Structure of Nitric Oxide Inhibited Cytochrome c Peroxidase. Biochemistry 1988, 27, 8074-8081.

64.   Leys, D.; Backers, K.; Meyer, T. E.; Hagen, W. R.; Cusanovich, M. A.; Van Beeumen, J. J., Crystal Structures of an Oxygen-binding Cytochrome c from Rhodobacter sphaeroides. J. Biol. Chem. 2000, 275, (21), 16050-16056.

65.   Deatherage, J. F.; Moffat, K., Structure of Nitric Oxide Hemoglobin. J. Mol. Biol. 1979, 134, 401-417.

66. Chan, N.-L.; Rogers, P. H.; Arnone, A., Crystal Structure of the S-Nitroso Form of Liganded Human Hemoglobin. Biochemistry 1998, 37, 16459-16464.

67. Chan, N. L.; Kavanaugh, J. S.; Rogers, P. H.; Arnone, A., Crystallographic Analysis of the Interaction of Nitric Oxide with Quaternary-T Human Hemoglobin. Biochemistry 2004, 43, 118-132.

68. Chu, K.; Vojtchovsky, J.; McMahon, B. H.; Sweet, R. M.; Berendzen, J.; Schlichting, I., Structure of a Ligand-Binding Intermediate in Wild-Type Carbonmonoxy Myoglobin. Nature 2000, 403, 921-923.

69. Pflugrath, J. d*TREK, 7.2beta; Molecular Structure Corporation: 2001.

70. Jacobson, R. CrystalClear, Rigaku Corporation: 1999.

71. Copeland, D. M.; West, A. H.; Richter-Addo, G. B., Crystal Structures of Ferrous Horse Heart Myoglobin Complexed with Nitric Oxide and Nitrosoethane. Proteins: Struct. Func. Genet. 2003, 53, 182-192.

72. Project, C., The CCP4 Suite: Programs for Protein Crystallography. Acta Crystallogr., Section D 1994, D50, 760-763.

73. Vagin, A.; Teplyakov, A., MOLREP: An Automated Program for Molecular Replacement. J. Appl. Crystallogr. 1997, 30, 1022-1025.

74. Laskowski, R. A.; MacArthur, M. W.; Moss, D. S.; Thornton, J. M., PROCHECK: A Program to Check the Stereochemical Quality of Protein Structures. J. Appl. Cryst. 1993, 26, 283-291.

75. Zhang, Y.; Gossman, W.; Oldfield, E., A Density Functional Theory Investigation of Fe-N-O Bonding in Heme Proteins and Model Systems. J. Am. Chem. Soc. 2003, 125, 16387-16396.

3 Crystal Structures of Horse Heart Myoglobin Complexed with Nitrite

3.1 Introduction

3.1.1 Nitrite and Biological Systems

The nitrite anion (NO_2^-) is a simple oxyanion of nitrogen with a pK_a of 3.2 at 20 °C[1]. The nitrite anion has long been considered, in mammalian systems, a "dead end" species that results from oxidation of nitric oxide produced by the nitric oxide synthase (NOS) enzymes. As a consequence, its role in human physiology has been neglected until very recently[2, 3]. Nitrite is a key species in the global nitrogen cycle. In dissimilatory denitrification (eq 1)[4, 5], nitrate is converted to nitrite by the nitrate reductase (NaR) enzymes. Nitrite is then converted to nitric oxide by nitrite reductase (NiR) enzymes. Follow-up conversions by nitric oxide reductases (NOR) and nitrous oxide reductases (N_2OR) result in the generation of dinitrogen.

$$NO_3^- \xrightarrow{\text{NaR}} NO_2^- \xrightarrow{\text{NiR}} NO \xrightarrow{\text{NOR}} N_2O \xrightarrow{\text{N}_2\text{OR}} N_2 \quad (1)$$
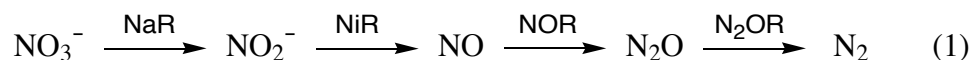
Two types of dissimilatory NiR enzymes are known, and they both carry out the one-electron reduction of nitrite to NO (eq 2).

$$NO_2^- + 2H^+ + 1e^- \rightarrow NO + H_2O \quad (2)$$
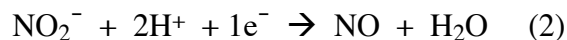
One is the periplasmic heme-containing cytochrome cd_1 NiR which is present in about two-thirds of denitrifying bacteria[4, 6]. The crystal structure of product obtained when nitrite was added to the reduced cytochrome cd_1 NiR from *Paraccocus pantotrophus* reveals N-binding of the nitrite ligand to the metal center (structure I).
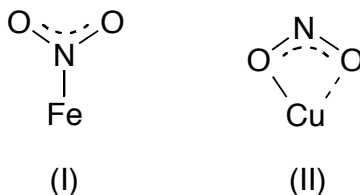
A second class of dissimilatory NiR enzymes contain copper in the active site[7]. Recent high-resolution crystal structures of the nitrite adducts of the copper-containing NiR[8] from *Alcaligenes xylosoxidans* (the His313Gly mutant)[9] and the soil bacterium *Achromobacter cycloclastes*[10] reveal an asymmetric *O,O'*-bidentate binding of the nitrite ligand (structure II).

In addition, nitrite can be reduced by the assimilatory (pentaheme) cytochrome *c* NiR (ccNiR) directly to ammonia without the detection of intermediates[11]. The active site heme contains lysine as a proximal ligand to iron, and the crystal structure of the nitrite-bound complex from *Wolinella succinogenes* reveals an N-binding of this group to iron (i.e., structure I)[12]. In fact, there are only three published structures of protein nitrite complexes, and selected metric data are shown below in Table 3.1 and the heme sites are shown in Figure 3.1.

Table 3.1 Biological Heme Nitrite Complexes

Complex	M-N	O1-N(avg)	∠O1-N-O2	∠Fe-N-O[1]	∠Np-M-N-O	Ref
Sulfite reductase[a]	2.024	1.245	118.25	110.73	66.51	[13]
Cytochrome cd_1 nitrite reductase[a]	2.00	1.215	120.5	118.72	42.68	[14]
Cytochrome c nitrite reductase[b]	1.88	1.66	98.66	116.97	43.12	[12]

[a] Metric data obtained from the PDB files 3GEO = Sulfite reductase and 1AOQ = Cytochrome cd_1 nitrite reductase.

[b] PDB file not in protein data bank, obtained from author.
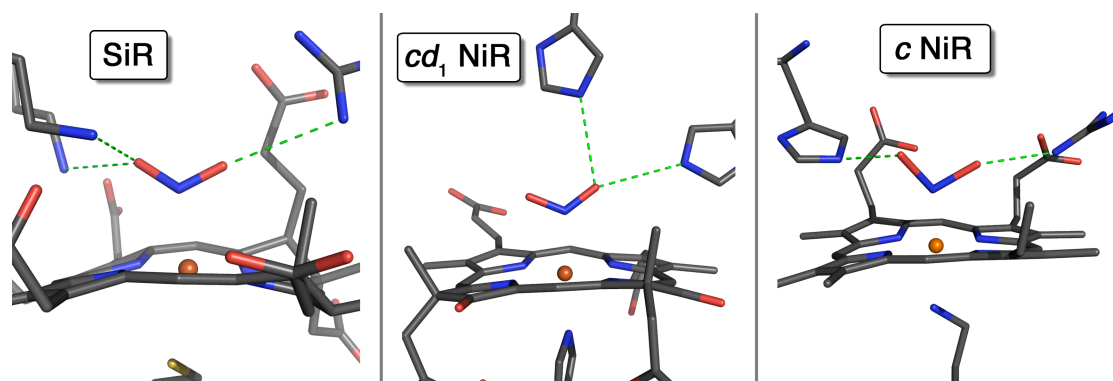
Figure 3.1   Side views of the heme sites of the three previously known biological heme nitrite complexes. (Left) Sulfite reductase from *Escherichia coli*. (Center) Cytochrome cd_1 Nitrite Reductase from *Paraccocus pantotrophus*. (Right) Cytochrome *c* Nitrite Reductse from *Wolinella succinogenes*. All three complexes show an N-binding mode as well as hydrogen-bonds shown in green to other heme pocket sidechains.

Recently, in September 2005, a two-day symposium at the US National Institutes of Health was held to highlight the increased recognition of nitrite as a bioactive small molecule that plays important roles in physiology and therapeutics[2]. The results of several studies support these proposed roles. For example, it has been known for some time that deoxyHb will reduce nitrite to NO[15].

$$NO_2^- + deoxyHb(Fe^{II}) + H^+ \rightarrow NO + metHb(Fe^{III}) + OH^- \quad (3)$$
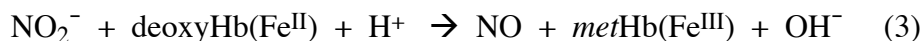
Myoglobin and xanthine oxidoreductase are also known to reduce nitrite to NO[2]. The NiR activity exhibited by deoxyHb has now been shown to be physiologically relevant under hypoxic conditions, generating an O_2-independent pool of NO (NOS enzymes require O_2) [16-18]. A related role for the NiR activity of deoxyMb (in the myocardium and skeletal muscles) and mitochondrial cytochrome oxidase and microsomal cytochrome P450 in tissues has been proposed [19]. Indeed, recent studies suggest a key role for myoglobin in the conversion of nitrite to NO in tissue, where endogenous nitrite levels can reach concentrations of 20 μM (c.f. 121 nM in plasma and 288 nM in erythrocytes[20]), and that this NiR activity may minimize ischemia-reperfusion injury during exercise[17, 21]. In addition, nitrite has been recognized as a biological signaling molecule that influences cGMP production, cytochrome P450 activities, and heat shock protein 70 and heme oxygenase-1 expression in various tissues[22].

Nitrite has long been utilized as an additive in meat products due to its antimicrobial and antioxidative activity[23, 24]. Addition of nitrite to meats during the curing process also restores the pink color due to the formation of the heme-NO pigment[25]. The

kinetics of reversible binding of nitrite to *met*Mb has been studied by van Eldik and coworkers; at pH 7.4 and 20 °C, k_{on} = 156±3 $M^{-1}s^{-1}$, with K_{eq} (k_{on}/k_{off}) of 60 M^{-1} which is two orders of magnitude smaller than that for NO binding to *met*Mb[26]. Ford and coworkers have shown that nitrite catalyzes the reductive nitrosylation of synthetic iron porphyrins and *met*Mb to produce the FeNO derivatives; it was suggested that the proposed ferric-nitrite species may be inhibitory in these reactions[27]. The electrocatalytic reduction of nitrite to NO by myoglobin[28] and synthetic iron porphyrins[29] has been demonstrated.

As mentioned above, nitrite reductase activity has been ascribed to Hb and Mb. Despite the importance of the heme-nitrite interaction in these proteins, however, no structural information exists to date on how nitrite interacts with their heme centers. We were thus interested in determining the structures of the nitrite derivative of a representative globin, namely myoglobin.

3.1.2 Nitrite and Synthetic Metalloporphyrins as Heme Models

The binding of nitrite to heme model systems has been studied with metalloporphyrins containing several different metals. Those systems can be subdivided into two major groups. The first group contains Fe and Co porphyrin model systems. All of the nitrite complexes with these two metals (with one exception discussed below) show nitro binding, binding through the nitrogen atom of the nitrite molecule [30-42].

The second group of crystal structures of nitrite complexes shows nitrito binding, binding through an oxygen atom of the nitrite molecule, and has been observed with Ru[43-45], Mn[46, 47], Cr[48], and Os[49] porphyrins. The two tables below lists all of the above mentioned complexes. Table 3.2 lists the nitro complexes and Table 3.3 lists the nitrito complexes. However, because the biological system, myoglobin, that was used in the study reported here contains a six coordinate Fe porphyrin, heme, with a histidine in the position trans to the nitrite ligand, iron porphyrin complexes that contain a reasonable histidine mimic for a sixth ligand are shown in bold in Table 3.2.

Table 3.2 Porphyrinate Nitro Complexes

Complex	M-N	O1-N(avg)	∠O1-N-O2	∠Fe-N-O[a]	∠Np-M-N-O	Ref
Nitro Complexes						
Iron(III)						
[Fe(TpivPP)(NO$_2$)$_2$]$^-$	2.001(6)	1.233	117.80	120.24	39.43	34
	1.970(5)	1.239	119.51	121.09	55.29	34
[Fe(TpivPP)(NO$_2$)(Py)]	**1.960(5)**	**1.233**	**119.87**	**120.06**	**37.29**	**35**
[Fe(TpivPP)(NO$_2$)(Py)]	**1.947**	**1.233**	**120.38**	**119.80**	**38.47**	**36**
[Fe(TpivPP)(NO$_2$)(Py)]	**1.970**	**1.213**	**123.40**	**118.28**	**37.86**	**36**
[Fe(TpivPP)(NO$_2$)(Py)]	**1.920**	**1.222**	**117.51**	**121.24**	**52.87**	**36**
[Fe(TpivPP)(NO$_2$)(HIm)]	**1.949(10)**	**1.191**	**116.16**	**121.91**	**37.47**	**35**
[Fe(TpivPP)(NO$_2$)(SC$_6$HF$_4$)]-	1.990(7)	1.223	118.74	119.36	50.88	38
[Fe(TpivPP)(NO)(NO$_2$)]	2.002(2)	1.270	120.87	119.56	41.01	42
[Fe(TpivPP)(NO)(NO$_2$)]	1.998(2)	1.223	121.39	118.59	45.73	42
[Fe(TpivPP)(NO)(NO$_2$)]	1.852	1.195	113.6	123.18	46.16	42
[Fe(TpivPP)(NO)(NO$_2$)]	1.91	1.246	120.87	119.56	46.50	42
[Fe(TpivPP)(NO)(NO$_2$)]	1.846	1.270	115.8	122.09	49.19	42
[Fe(TpivPP)(CO)NO$_2$)]	2.06	1.249	117.86	120.83	43.95	50
Iron(II)						
[Fe(TpivPP)(NO$_2$)]$^-$	1.849(4)	1.243	119.5	119.72	50.28	37
[Fe(TpivPP)(NO$_2$)(Py)]$^-$	**1.951(5)**	**1.257**	**116.60**	**121.46**	**42.92**	**40**
[Fe(TpivPP)(NO$_2$)(PMS)]$^-$	1.937(3)	1.242	118.40	120.53	44.26	40
[Fe(TpivPP)(NO)(NO$_2$)]$^-$ ⊥	**2.086(8)**	**1.245**	**117.80**	**120.53**	**44.36**	**39**
[Fe(TpivPP)(NO)(NO$_2$)]$^-$ ||	**2.060(7)**	**1.243**	**113.09**	**122.86**	**45.02**	**39**
Cobalt (III)						
[Co(TPP)(NO$_2$)(3,5-Lut)]	1.948(4)	1.156(4)	115.16	122.41	1.39	31
[Co(TPP)(NO$_2$)(Pip)]	1.897(11)					32
[Co(TpivPP)(NO$_2$)(1-MeIm)]	1.898(4)	1.223(3)	119.90	120.05	38.16	30
[Co(TpivPP)(NO$_2$)(1,2MeIm)]	1.917(4)	1.227(3)	120.42	119.78	35.57	30
[Co(Tpp)(NO$_2$)(Py)]	1.920(4)	1.200	118.98	116.72	48.73	33
[Co(TPP)(NO$_2$)(Py)]		1.219				33
[Co(TPP)(NO$_2$)(Cl$_2$Py)]	1.912(3)	1.217	119.64	119.64	40.51	33
[Co(TPP)(NO$_2$)]	2.000	1.211	123.95	117.05	37.55	51
[Co(TPP)(NO$_2$)]	1.88	1.215	123.35	117.75	59.19	52
[Co(TPP)(NO$_2$)(H$_2$O)]	1.863	1.235	120.15	119.92	43.42	52
[Co(TPP)(NO$_2$)$_2$]	1.948	1.200	126.40	115.41	38.53	52
[Co(TPP)(NO$_2$)(H$_2$O)]	1.963	1.234	115.83	120.89	32.57	53

[a] Measurement is of the most acute angle

⊥ and \|\| describe perpindicular vs parallel orientations of ligands seen in two structures

Table 3.3   Porphyrinate Nitrito Complexes

Complex	M-O	O1-N	∠O1-N-O2	∠Fe-O-N	∠Np-M-O-N	Ref
Nitrito Complexes						
Ruthenium(III)						
[Ru(TPP)(NO)(ONO)][b]	2.00(2)	109(5)	0.94(5)	1.33(4)	40.56	[43]
[Ru(pTol)(NO)(ONO)][b]	1.90(2)	108.0(30)	1.16(2)	1.23(2)	45.28	[44]
[Ru(OEP)(NO)(ONO)]	1.984(6)	117.3(9)	1.214	1.188(9)	33.06	[45]
[Ru(TPP)(NO)(ONO)][b]	1.988(6)	110.9(20)	1.15(2)	1.13(3)	34.62	[45]
Manganese(III)						
[Mn(TPP)(ONO)]	2.059(4)	114.8(5)	1.301(7)	1.202(8)	30.45	[46]
[Mn(Phth)(NO)(ONO)][c]	1.952	108.1	1.166	1.189	46.17	[47]
Osmium(III)						
[Os(pTol)(NO)(ONO)]	2.000	113.8	1.295	1.188	33.17	[49]
[Os(Mes)(NO)(ONO)]	1.996	113.27	1.258	1.154	55.60	[49]
Chromium(III)						
[Cr(Phth)(ONO)$_2$]	1.990	113.74	1.305	1.206	48.01	[54]

[b] Nitrite moiety is highly disordered
[c] Phth = Phthalocyaninate

All Fe(por) model systems show N-binding of the nitrite ligand to the metal, with the exception of the structure of [(TpivPP)Fe(NO$_2$)(NO)]$^-$ that shows the nitrite ligand disordered between the two binding modes[39]. The disordered component that shows nitrito binding sits at about 30° off of a diagonal N-Fe-N axis of the porphyrin and has a Fe-O bond length of 2.08 Å. The importance of this nitrito form was apparently not recognized and the occupancy of this "unusual linkage isomerism" was refined to 60% and then not commented on further. The nitro nitrogen and the nitrito oxygen (of the disordered component) were modeled into the same position and even though the nitrito complex was the major component in the complex the scattering factors for the nitro nitrogen were used to complete the structure. The ligand trans to the nitrite in this complex is NO, which was also disordered. As stated above, all of the other iron porphyrin nitrite complexes contain an N-bound NO$_2$ Ligand.

3.2 Materials and Methods

3.2.1 Crystallization and Complex Formation

Two methods were used to prepare the O-bound nitrite complexes. The first method was to soak preformed *met*myoglobin crystals in artificial mother liquor containing nitrite. The second method used to generate the complex was to preform the Mb(ONO) complex and then crystallize it. Both methods are described in detail below.

3.2.1.1 Nitrite Soaked metMb Crystals

Crystals of *aqua-met*Mb grown as previously described[55] were transferred into artificial mother liquor consisting of ~10 μL of 100 mM Tris-HCl, pH 7.4, 3.10-3.30 M ammonium sulfate containing 15% glycerol as cryoprotectant and then the coverslip was submerged in mineral oil under an atmosphere of nitrogen. A solution of sodium nitrite (10 μL, 250 mM) in artificial mother liquor was added to the droplet and allowed to soak into the crystals for ~10 min. The crystals were harvested with cryoloops and flash frozen in liquid nitrogen.

3.2.1.2 Cocrystallization of Mb Nitrite Complex

Solid sodium nitrite (~ 9 mg) was added to 1 mL of a 30 mg/mL *met*Mb solution (100 mM, Tris-HCl, pH 7.4; [nitrite] = 130 mM) and incubated on ice for ten minutes. The protein solution was then centrifuged for 1 min (at 10,000 x g). Crystal trays were then set up as previously described for Mb(EtNO)[55]. Suitable crystals formed in three

days, and they were harvested with cryoloops and passed through the cryosolution consisting of artificial mother liquor containing 15% glycerol and flash frozen in liquid nitrogen.

3.2.2 Data Collection, Processing and Refinement

The frozen crystals were initially screened for diffraction quality at our home source. X-ray data sets were collected at 100 K on a RigakuMSC RU-H3R X-ray generator operated at 50 kV/100 mA to produce Cu Kα radiation (λ = 1.5418 Å). Diffracted X-rays were detected using an R-AXIS 4^{++} dual image plate detector system. For the cocrystallized Mb(ONO) crystal data collected in-house, 1° oscillation images were collected over a range of 216° with the crystal-to-detector distance of 70 mm and an exposure time of 300 sec.

The data for the Mb(ONO) formed by soak was collected at the National Synchrotron Light Source (NSLS) at Brookhaven National Laboratory (BNL) via the Mail-in Data Collection Program operated by the Protein Crystallography Research Resource (BNL-PXRR; www.px.nsls.bnl.gov/fedex.html). X-ray data were collected at 100 K on beamline X-12B (using an ADSC Quantum4 CCD detector), 1° oscillation images were collected over a range of 180° with an exposure time of 120 sec per image and a crystal-to-detector distance of 100 mm.

All data sets collected at our home source were processed using the stand-alone d*TREK program (Macintosh v.2D)[56] from Molecular Structure Corporation. The synchrotron-derived data set was initially processed at BNL using Denzo and Scalepack as contained in the HKL2000 suite[57], and then reprocessed with d*TREK.

3.2.2.1 Nitrite Soaked Metmyoglobin Crystals

After molecular replacement using the 1.9 Å structure of hhMbNO (1NPF)[55] with the NO and solvent molecules removed as the search model, the *R-factor* was 27.7%. After 10 cycles of restrained refinement, nitrite and sulfate molecules were modeled into the structure based on F_o-F_c difference electron density maps. After 30 cycles of refinement the *R-factor* dropped to 24.9%, and the model was checked for residues with low occupancy or multiple conformations. Several cycles of model manipulation with *Xfit*[58] and refinement were carried out to refine the multiple positions/conformations of several sidechains (Lys47, Lys50, Lys 77, Gln91) where electron density was clearly observed for these multiple conformations. In addition, several sidechains (of Glu21, Glu27, Asp44, Glu54, Glu59, Lys78, His81, Glu83, Glu85, Glu148) were modeled with low occupancy due to disorder of the sidechains. Solvent molecules were then added to the structure with *ARP_waters* as implemented in Refmac5. After the addition of 187 water molecules, the *R-factor* was lowered to 19.5%. The C-terminal residue Gly153 was poorly defined and was omitted from the structure. After an additional 100 cycles of refinement with B-factors refined anisotropically, the final *R-factor* is 17.0% with an R_{free} of 21.1% calculated with 5% of the data. Coordinates have been deposited at the Protein Data Bank with the access code 2FRF.

3.2.2.2 Cocrystallized of Mb Nitrite Complex

The initial *R-factor* was 31.4% after molecular replacement using the 1.9 Å structure of hhMbNO (1NPF) with the NO and solvent molecules removed as the search

model, with *MOLREP* as implemented in the CCP4 suite. Nitrite and sulfate molecules were modeled into well-defined electron density after 10 cycles of restrained refinement with Refmac5 based on an F_o-F_c difference electron density map, and 40 additional cycles of refinement reduced the *R-factor* to 23.3%. Water molecules were added to the structure using *ARP/warp* as implemented in the CCP4 suite. 196 water molecules were added to the structure and the *R-factor* dropped to 19.2%. Additional cycles of model adjustment with *Xfit* and refinement yielded no major drops in *R-factor* or R_{free}. The F_o-F_c electron density map, with the nitrite ligand modeled in at full occupancy, showed slight negative density around the N and O2 atoms of the ligand. The ligand was then modeled in at a final lower occupancy of 65%, to remove the occurrence of the negative density. However, positive density was observed around the O1 atom of the ligand. A water molecule was modeled into the density as an alternate ligand at an occupancy of 35% at which point no more positive or negative density was seen in the vicinity of the ligand. The electron density of the C-terminus residue (Gly 153) was poorly defined, and this residue was omitted from the structure. For the final cycles of refinement were carried out using anisotropic refinement of B-factors, and the *R-factor* dropped to 14.6% with an R_{free} of 20.6% as calculated with 5% of the data. Coordinates have been deposited at the Protein Data Bank with the access code 2FRI.

3.3 Results

3.3.1 Spectroscopic Results Showing the Formation of the Nitrite Complex

The only report in the literature of spectroscopic data for a Mb(ONO) complex was reported by Sono and Dawson in 1982[59]. In that study there is a shift in the Soret band from 409 nm to 412 nm upon the addition of saturating nitrite. This experiment was performed at 4° C in 100 mM potassium phosphate buffer pH 7.0 with *sperm whale* myoglobin. When UV/Vis spectra were taken of our *horse heart* myoglobin in 100 mM Tris-HCl at pH 7.4 no clear shift in the UV/Vis spectra was observed to show the difference between the *aqua*-metmyoglobin complex and the O-bound nitrite myoglobin. Both have peaks at 409 nm when measured with an HP 8453 spectrophotometer with the above conditions.

3.3.2 Crystallographic Results

The data collection, data processing and refinement statistics for the two structures discussed in this chapter are presented in Table 3.4.

Table 3.4 X-ray Data Collection, Processing and Refinement Statistics

	Mb(ONO)	Mb(ONO)
Method of prepn.	Nitrite soak	cocrystallization
Data Collection[a]		
Space Group	$P2_1$	$P2_1$
Source	BNL, X-12B	Home source
λ (Å)	0.90	1.5418
Cell Dimensions		
a, b, c (Å)	35.24,28.61,62.94	35.22,28.59,62.84
β (°)	105.75	106.03
Resolution(Å)	1.20	1.60
Mean $I/\sigma(I)$	7.8 (3.0)	15.7 (3.6)
No. Reflections		
Observed	153540 (17881)	85985 (7421)
Unique	45327 (4948)	21705 (2179)
Completeness (%)	98.3 (99.8)	98.5 (95.8)
R_{merge} (%)[b]	7.3 (31.8)	4.7 (24.7)
Refinement Statistics[a]		
Resolution Range (Å)	9.94-1.20	19.96-1.60
R-factor (%)[c]	17.0 (30.0)	14.6 (25.4)
R_{free} (%)[d]	21.1 (39.1)	20.6 (38.6)
r.m.s.d. bond distances (Å)	0.007	0.010
r.m.s.d. angles (°)	1.076	1.135
B factor (Å^2)		
Mean	16.68	16.34
r.m.s.d. mainchain	0.839	0.523
r.m.s.d. sidechain	2.472	1.829
Ramachandran Plot[e]		
% Residues in		
Most Favored	91.7	94.0
Allowed	8.3	6.0

[a] Values in parentheses correspond to the highest resolution shells for Mb(ONO) (BNL) (nitrite soak) (1.231-1.20 Å), Mb(ONO) (Home) (nitrite cocrystalized) (1.641-1.60 Å).

[b] $R_{merge} = \Sigma|I - <I>|/\Sigma(I)$ where I is the individual intensity observation and $<I>$ is the mean of all measurements of I.

[c] R-factor $= \Sigma||F_o| - |F_c||/\Sigma|F_o|$ where F_o and F_c are the observed and calculated structure factors, respectively.

[d] R_{free} is calculated using randomly selected reflections comprising 5% of the data not used throughout refinement.

[e] As calculated using PROCHECK[60].

3.3.2.1 Nitrite Soaked Metmyoglobin Crystals

Multiple data sets were collected on crystals using our in-house diffractometer and one high-resolution data set was collected at NSLS/BNL. Native metmyoglobin crystals were grown, and nitrite was soaked into the crystal to form the complex. Because all of the data sets show the same result, the high-resolution data set collected at NSLS/BNL is discussed below.

Similarly to other myoglobin/ligand structures, the protein backbone of the Mb(ONO) structure has a typical myoglobin fold and therefore will not be discussed any further. The most chemically interesting feature of this structure is the heme nitrite moiety. To the best of our knowledge, this is the first crystal structure that displays O-bound nitrite complexed to a heme iron in any protein. The position of the nitrite ligand was modeled into clearly defined electron density in the initial F_o-F_c difference electron density map, and the ONO ligand did not move significantly during the remainder of the refinement. The primary interaction of the nitrite ligand with this heme protein is through O-binding to the iron center, with an Fe-O1 distance of 1.94 Å. The O1-N and N-O2 distances are 1.32 and 1.31 Å, respectively. The angle made by the Fe-O1-N moiety is 116°, and the O1-N-O2 angle is 113°. The (His93)N-Fe bond length is 2.07 Å. The top view of the heme site is shown in Figure 3.2 (bottom). The iron-nitrite torsion angle, as defined by the Fe-O1-N-O2 group, is 11°. The proximal imidazole plane lies almost directly along a (por)N-Fe-N(por) bond, with a deviation of only 4.5°, and the nitrite ligand plane is oriented ~77° to the proximal imidazole (of His64) plane.

The nitrite ligand is oriented away from the distal His64 residue. The distance between the nitrite O1 atom (bound to Fe) and the N^{ε}-atom of His64 is 2.83 Å, whereas

the related distance between the nitrite O2 atom (not bound to Fe) and the N^ε-atom is 3.20 Å. Thus, the nitrite ligand is likely stabilized in the distal pocket by hydrogen bonding between the O1 atom and the distal His64 residue. No other close contacts between the nitrite and the distal residues are observed. Thus, the next closest contacts of the nitrite ligand with the distal residues (other than with His64, and ignoring hydrogen atoms) are between the $C\gamma^2$ atom from Val68 and the nitrite O2 atom (3.12 Å), the nitrite N atom (3.24 Å) and the nitrite O1 atom (3.25 Å). All other distal residues are located ≥ 3.5 Å away from the nitrite ligand.

The iron atom in Mb(ONO) is located essentially in the mean plane of the four porphyrin N-atoms (i.e., the 4N-plane). The axial (His93)-Fe-O1 angle is 179°, exhibiting near perfect linearity, and the O1 atom of the nitrite is tilted 3° from the normal to the heme 4N-plane.
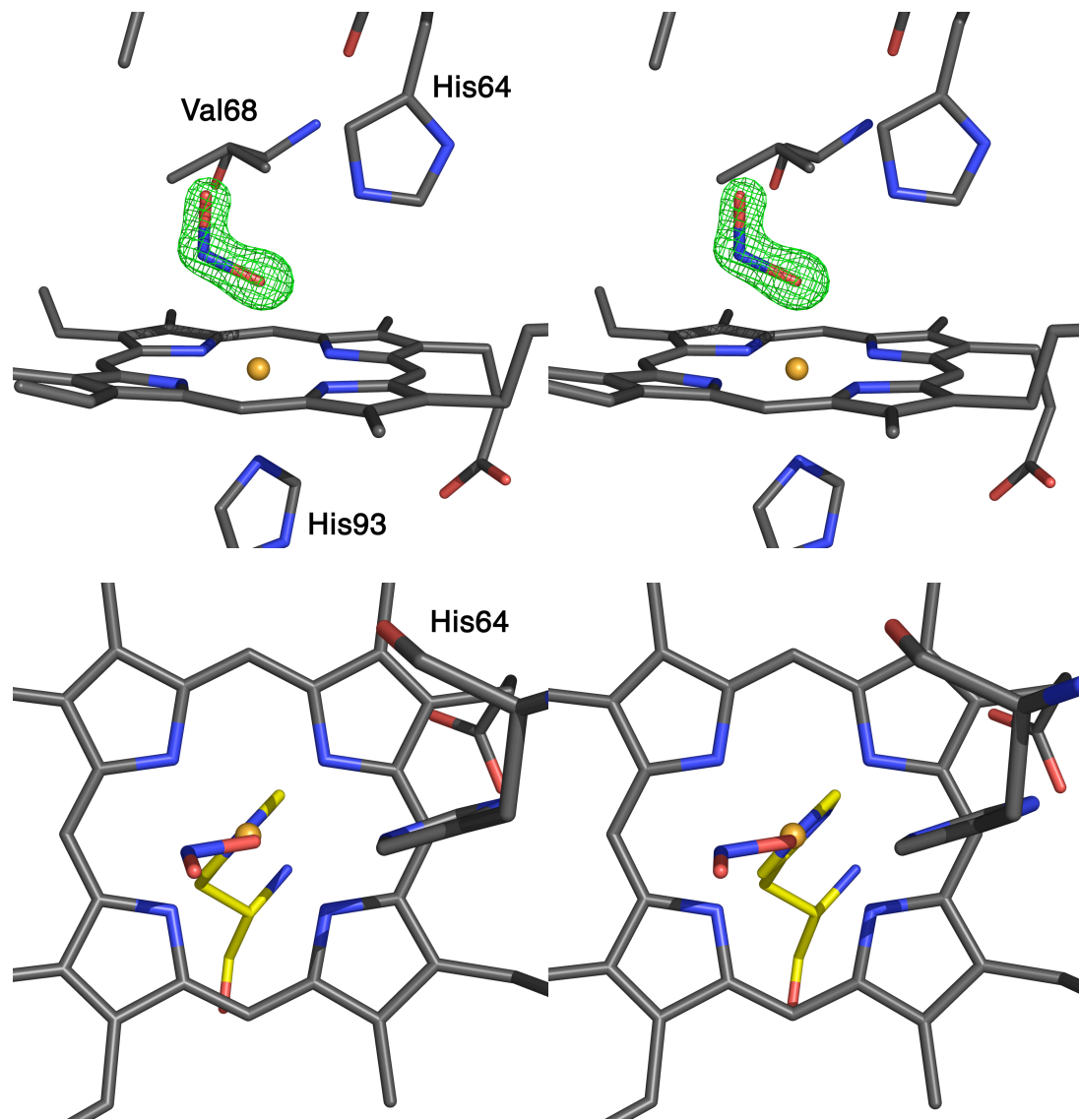
Figure 3.2 (top) Stereoview of the final model of the heme site in horse heart myoglobin. Density is form the F_o-F_c omit electron density map and is contoured at 3σ. Carbon, nitrogen, oxygen, and iron atoms are colored grey, blue, red, and orange respectively. (bottom) Stereoview from distal side of heme showing the orientation of the nitrite. His93, on the proximal side of the heme is shown in yellow for clarity.

3.3.2.2 Cocrystallized Mb Nitrite Complex

The Mb(ONO) complex made by forming the complex in solution and then crystallizing it has essentially the same structure. We considered the possibility that soaking the nitrite ligand into the distal cavity of pre-formed *met*Mb crystals influenced the preference for the O-binding mode. Consequently, we prepared a solution of ferric Mb(ONO) and were able to obtain suitable crystals of the compound prepared by this method. The structure reveals the O-binding mode of the nitrite ligand as described above. The occupancy of the ONO ligand, however, was only ~65%, with the remaining ~35% being an aqua ligand; the Fe-O(aqua) distance is 2.25 Å. Figure 3.3 shows the ONO and aqua ligands in the heme active site. We conclude that, in our hands and under the experimental conditions used here, soaking a pre-formed *met*Mb crystal with nitrite does not bias the ONO ligand towards the O-binding mode.
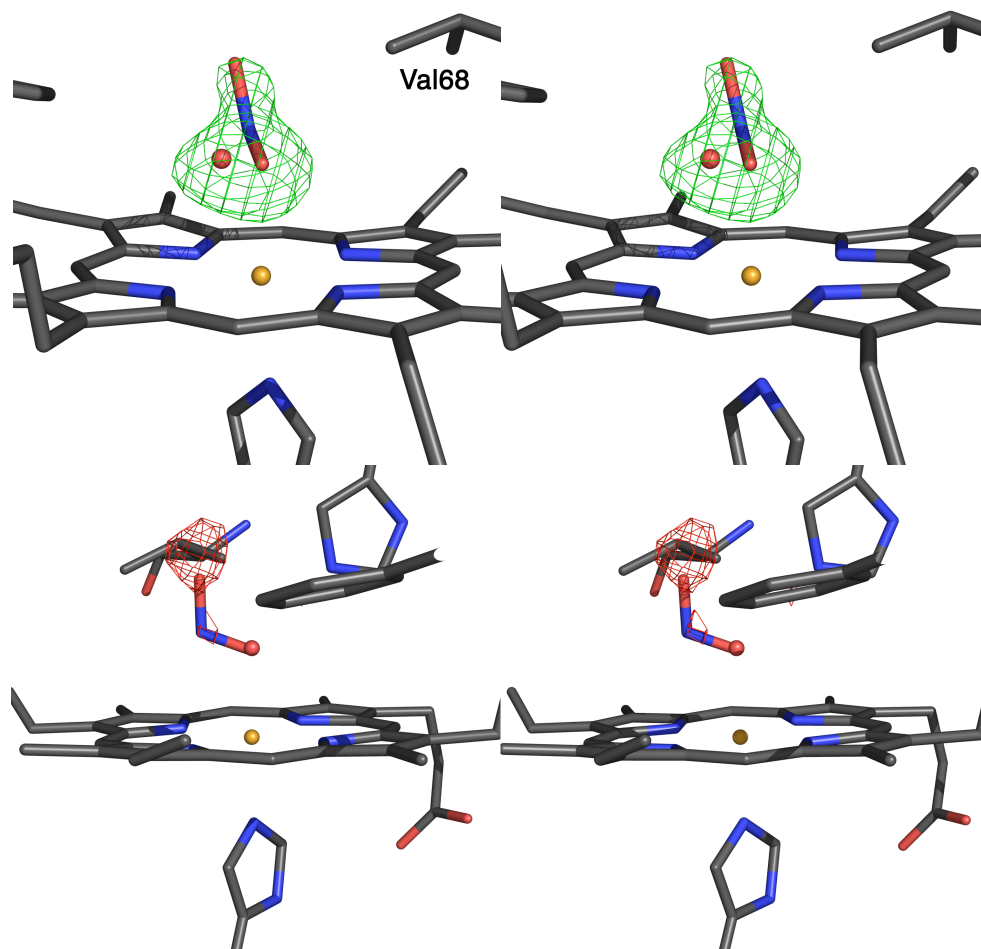
Figure 3.3 (top) Stereoview of the heme environment from the Mb(ONO) structure that was prepared by cocrystallization shown from the propionate side of the porphyrin. Electron density is contoured at 3σ and is the initial F_o-F_c electron density map after molecular replacement. A bulge in the electron density can clearly be seen and was modeled as a low occupancy water. The model is the final refined model and all of the colors are consistent with those in figure 1. (bottom) Stereoview showing the negative electron density that appears when nitrite is modeled at full occupancy. This led to modeling the nitrite at reduced occupancy and the addition of a water molecule in the alternate position sown in the top figure.

3.3.2.3 Attempts at Obtaining an N-bound form of Mb(NO$_2$)

We considered the possibility that N-binding might be favored for the reduced (i.e, ferrous) form of Mb. Two methods to obtain a ferrous Mb(NO$_2$) derivative were attempted: (i) addition of dithionite to the ferric Mb(ONO) complex, and (ii) addition of nitrite to ferrous Mb.

We exposed ferric Mb(ONO) crystals to dithionite for 15 sec, and subjected a suitable crystal to crystallographic analysis. The O-bound nitrite form was retained in the structure, but the occupancy of the ligand was reduced to ~85%. In separate experiments, exposure of the ferric Mb(ONO) crystals to dithionite for 35 and 45 seconds resulted in structures with O-bound nitrite occupancies of ~60% and ~30%, respectively. No secondary ligand was observed/present bound to the iron center. Addition of excess dithionite to the ferric Mb(ONO) crystals in the presence of excess nitrite produced the ferrous MbNO derivative with full occupancy of the NO ligand.

Table 3.5 Effect of Dithionite Soak Time on the Occupancy of Nitrite Ligand

Soak time (s)	15[a]	30[a]	35[a]	40[a]	45[a]	60[a]	60[b]
Occupancy of NO$_2^-$ (%)	80-90	60-65	~ 60	~ 40	~ 30	< 20	100 (NO)

[a] Crystal soaked first in droplet containing 500 mM sodium nitrite, then transferred to drop containing 500 mM dithionite.
[b] Crystal soaked first in droplet containing 500 mM sodium nitrite, then 500 mM dithionite was added to drop. NO gas was produced and bound to Mb.

We also added nitrite to crystals of reduced Mb in an attempt to obtain a ferrous Mb(NO$_2$/ONO) structure. The crystal structure of the product was identical to that of the ferric Mb(ONO) described above, displaying an O-binding mode of the nitrite ligand. Nitrite is known to oxidize reduced Mb, hence it is conceivable that we generated the

ferric nitrite complex. In summary, we have not been successful to date at generating the

N-bound nitrite form.

3.4   Discussion

Comparison with Model and Protein Structures

Several binding modes of nitrite to metals are known[61] and are shown schematically in Figure 1.1. However, the structures reported for heme protein nitrite compounds have been limited to the N-binding mode (structure 1 in Figure 1.1). The three structures are those of the nitrite adducts of cyt cd_1 NiR from *P. pantotrophus*[14], SiR from *E. coli* [13], and cyt *c* NiR from *W. succinogenes*[12]. It is interesting to note that in all synthetic iron porphyrin nitrite compounds whose X-ray structures have been reported, *the nitrite anion has been shown to bind to both ferric and ferrous centers via the N-binding mode*[41, 62].   The only exception is for a disordered component of nitrite in a crystal form of $[(TpivPP)Fe(NO_2)(NO)]^-$ (TpivPP = picket fence porphyrin) where both N-binding and O-binding were observed in the same crystal due to disorder of the nitrite group[39]. O-binding of nitrite has been observed to result from photoirradiation of the ground-state nitrosyl-nitro compound $(TPP)Fe(NO)(NO_2)$ (TPP = tetraphenylporphyrin) to give its metastable nitrosyl-nitrito linkage isomer $(TPP)Fe(NO)(ONO)$[63, 64].
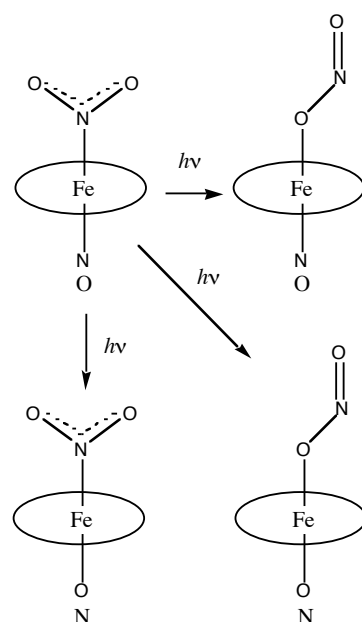
Figure 3.4 Scheme for linkage isomerism of (TPP)Fe(NO)(ONO)

Such nitrito binding has been observed in the crystal structures of other metalloporphyrin nitrite complexes of Mn[46], Ru[43-45], and Os[49].

To date, only the nitrite N-binding mode has been observed for heme protein systems or for synthetic iron (ferrous or ferric) porphyrins containing nitrite ligands. Thus, the nitrite O-binding mode determined for ferric hh Mb(ONO) reported here represents the first such example for a structurally characterized heme protein.

It is important to recognize that the previously reported N-binding modes in nitrite heme proteins have laid a foundation for understanding the mechanism of NiR activity for the classical NiR enzymes[6, 11]. For example, the crystal structure of the cyt cd_1 NiR enzyme complexed with nitrite reveals a conformation of the N-bound nitrite that places one of the nitrite O-atoms within hydrogen-bonding distance of two distal His residues that could play the role of proton donors[14]; presumably setting the stage for conversion of the bound NO_2 ligand to NO (structure III).

$$
\begin{array}{c}
H_{His} \\
/ \\
O \cdots O --- H_{His} \\
N \\
| \\
\text{— Fe —}
\end{array}
$$

(III)
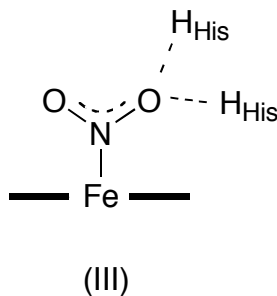
Similarly, the crystal structure of the ferric cytochrome c NiR enzyme complexed with nitrite reveals hydrogen bonding interactions between the N-bound nitrite O-atoms with distal residues[12].

Silaghi-Dumitrescu[65] has recently determined, using density functional theoretical calculations, that the N-bound nitrite isomer in cytochrome cd_1 NiR is favored over the O-bound isomer by 4.5 kcal/mol in the ferric form (6 kcal/mol in the ferrous form).

However, the author proposed that the O-bound nitrite isomer in this enzyme is energetically feasible, and that NO release can be facile in such O-bound ferrous nitrite compounds. For example, optimization of the geometry of the O-bound ferrous form (structure IV) resulted in convergence of the structure to a form that involved cleavage of the O-NO bond to result in an even more facile release of NO (structure V) [65].
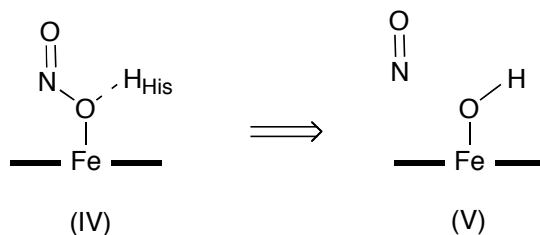
Thus, the author suggests that O-bound nitrite complexes are perhaps as catalytically competent as their N-bound analogues.

Interestingly, brief speculation of such an O-binding mode of nitrite to ferric heme proteins was presented more than two decades ago by Garber and Hollocher[66], who suggested that O-binding of nitrite (or HONO after protonation) might account for subsequent nitrosyl transfer reactions observed with dissimilaratory nitrite reductases. More recently, Herold and Rehmann have shown using a stopped-flow UV/Vis spectrophotometer with rapid scanning monochrometer that a Mb-nitrite species, formulated as ferric Mb(ONO), is generated as an intermediate during the reaction of the ferryl compound MbFe^{IV}=O with NO[67]. A similar ferric Hb(ONO) intermediate is formed in the corresponding reaction involving ferryl hemoglobin[68].

It is thus reasonable to assume that a 1-electron reduction and subsequent protonation of the O-bound nitrite in a heme protein will generate coordinated nitrous

acid, which could then release NO. Indeed, such a binding mode for HONO has structural precedence as shown by our previously demonstrated interaction mode of alkyl nitrites (RO-N=O; R = alkyl) and alkyl/arylthionitrites (RS-N=O) with synthetic metalloporphyrins of Fe , Ru, and Os[69-71].
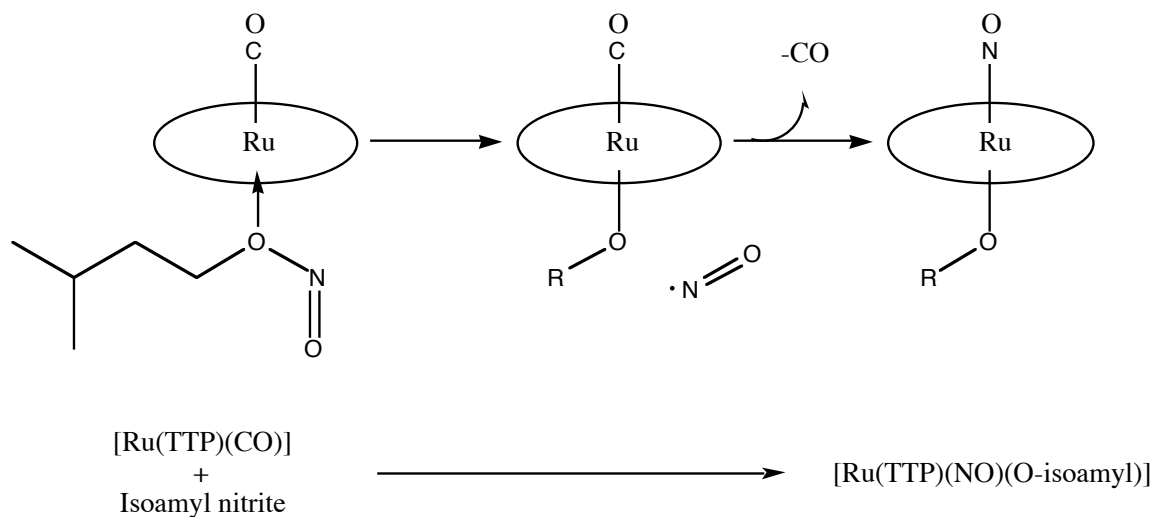
Figure 3.5 Reaction of [Ru(TTP)(CO)] with isoamyl nitrite to yield [Ru(TTP)(NO)(O-isoamyl)] from Yi and Richter-Addo[72].

In these reactions, we have determined experimentally that O-binding of the RONO group to group 8 metalloporphyrins (structure VI; M = Fe, Ru, Os) results in hemolytic cleavage of the RO-NO bond to release NO (analogous reactivity was observed with RSNO).

84
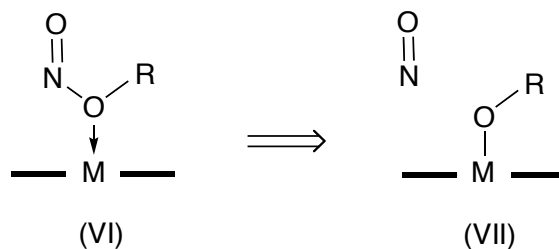
The bound nitrite in hh Mb(ONO) (Figure 3.2) is stabilized by hydrogen-bonding between the iron-bound O-atom and the distal His64 residue. It thus is tempting to speculate that reduction of the ferric heme to the ferrous state and subsequent protonation of the O1 atom of the nitrite ligand will result in efficient O-NO bond cleavage to release NO. Whether this O-binding mode of nitrite observed in the crystal structure of ferric Mb(ONO) is the precursor to catalytic nitrite reduction under hypoxic conditions (after proton-coupled electron transfer) remains to be firmly established. However, we note that anaerobic dithionite reduction of this complex does lead to NO production.

3.5 Conclusion

Nitrite is now recognized as an oxyanion of nitrogen that has important physiological roles in addition to its role in denitrification. Here we report the first structural study of the nitrite adduct of myoglobin. The high-resolution crystal structure reveals that the nitrite ligand is bound to the ferric heme center via the O-binding mode. This is the first non-disordered determination of such a binding mode in synthetic metalloporphyrins or heme proteins. The three heme protein nitrite crystal structures reported to date show the N-binding mode of nitrite to the heme centers. The observation of an O-binding mode of nitrite to a heme protein provides support for this binding mode as a viable intermediate in nitrite reductase activity by heme proteins.

In our lab, two studies are being performed to determine if the metal or the sidechains in the heme pocket are responsible. First, one member of our lab, Zaki Zahran, is using myoglobin with metal substituted porphyrins to try to force N-bound and O-bound conformations. Concurrently, another member of our lab, Lilian Chooback, is working on heme site mutation to attempt to stabilize the N-bound nitrite with additional hydrogen bonding. The outcome of these combined experiments should shed some light on why nitrite binds through the oxygen in myoglobin.

3.6 References

1. Braida, W.; Ong, S. K., Decomposition of Nitrite Under Various pH and Aeration Conditions. *Water, Air, and Soil Pollution* **2000,** 118, 13-26.

2. Gladwin, M. T.; Schechter, A. N.; Kim-Shapiro, D. B.; Patel, R. P.; Hogg, N.; Shiva, S.; Cannon III, R. O.; Kelm, M.; Wink, D. A.; Espey, M. G.; Oldfield, E. H.; Pluta, R. M.; Freeman, B. A.; Lancaster Jr., J. R.; Feelisch, M.; Lundberg, J. O., The Emerging Biology of the Nitrite Anion. *Nat. Chem. Biol.* **2005,** 1, (6), 308-314, and references therein.

3. Dejam, A.; Hunter, C. J.; Schechter, A. N.; Gladwin, M. T., Emerging Role of Nitrite in Human Biology. *Blood Cells, Molecules, and Diseases* **2004,** 32, 423-429.

4. Eady, R. R.; Hasnain, S. S., Denitrification. In *Comprehensive Coordination Chemistry II*, Que Jr., L.; Tolman, W. B., Eds. Elsevier: San Diego, CA, 2004; Vol. 8 (Bio-coordination chemistry), pp pp 759-786.

5. Wasser, I. M.; de Vries, S.; Moenne-Loccoz, P.; Schroder, I.; Karlin, K. D., Nitric Oxide in Biological Denitrification: Fe/Cu Metalloenzyme and Metal Complex NO_x Redox Chemistry. *Chem. Rev.* **2002,** 102, (4), 1201-1234.

6. Allen, J. W. A.; Ferguson, S. J.; Fülöp, V., Cytochrome cd1 Nitrite Reductase. In *Handbook of Metalloproteins*, Messerschmidt, A.; Huber, R.; Poulos, T.; Wieghardt, K., Eds. John Wiley & Sons: Chichester, 2001; Vol. 1, pp 424-439.

7. Suzuki, S.; Kataoka, K.; Yamaguchi, Y.; Inoue, T.; Kai, Y., Structure-Function Relationships of Copper-Containing Nitrite Reductases. *Coord. Chem. Rev.* **1999,** 190-192, 245-265.

8. Tocheva, E. I.; Rosell, F. I.; Mauk, A. G.; Murphy, M. E. P., Side-On Copper-Nitrosyl Coordination by Nitrite Reductase. *Science* **2004,** 304, (7), 867-870.

9. Barrett, M. L.; Harris, R. L.; Antonyuk, S.; Hough, M. A.; Ellis, M. J.; Sawers, G.; Eady, R. R.; Hasnain, S. S., Insights into Redox Partner Interactions and Substrate Binding in Nitrite Reductase from Alcaligenes xylosoxidans: Crystal Structures of the Trp138His and His313Gln Mutants. *Biochemistry* **2004,** 43, 16311-16319.

10. Antonyuk, S. V.; Strange, R. W.; Sawers, G.; Eady, R. R.; Hasnain, S. S., Atomic Resolution Structures of Resting-State, Substrate- and Product-Complexed Cu-Nitrite Reductase Provide Insight Into Catalytic Mechanism. *Proc. Natl. Acad. Sci. U.S.A.* **2005,** 102, (34), 12041-12046.

11. Einsle, O., Cytochrome c Nitrite Reductase. In *Handbook of Metalloproteins*, Messerschmidt, A.; Huber, R.; Poulos, T.; Wieghardt, K., Eds. John Wiley & Sons: Chichester, 2001; Vol. 1, pp 440-453.

12. Einsle, O.; Messerschmidt, A.; Huber, R.; Kroneck, P. M. H.; Neese, F., Mechanism of the Six-Electron Reduction of Nitrite to Ammonia by Cytochrome c Nitrite Reductase. *J. Am. Chem. Soc*. **2002,** 124, 11737-11745.

13. Crane, B. R.; Siegel, L. M.; Getzoff, E. D., Probing the Catalytic Mechanism of Sulfite Reductase by X-ray Crystallography: Structures of the *Escherichia coli* Hemoprotein in Complex with Substrates, Inhibitors, Intermediates, and Products. *Biochemistry* **1997,** 36, 12120-12137.

14. Williams, P. A.; Fulop, V.; Garman, E. F.; Saunders, N. F. W.; Ferguson, S. J.; Hajdu, J., Haem-ligand Switching During Catalysis in Crystals of a Nitrogen-cycle Enzyme. *Nature* **1997,** 389, 406-412.

15. Doyle, M. P.; Pickering, R. A.; DeWeert, T. M.; Hoekstra, J. W.; Pater, D., Kinetics and Mechanism of the Oxidation of Human Deoxyhemoglobin by Nitrites. *J. Biol. Chem*. **1981,** 256, (23), 12393-12398.

16. Cosby, K.; Partovi, K. S.; Crawford, J. H.; Patel, R. P.; Reiter, C. D.; Martyr, S.; Yang, B. K.; Waclawiw, M. A.; Zalos, G.; Xu, X.; Huang, K. T.; Shields, M.; Kim-Shapiro, D. B.; Schechter, A. N.; Cannon III, R. O.; Gladwin, M. T., Nitrite Reduction to Nitric Oxide by Deoxyhemoglobin Vasodilates the Human Circulation. *Nature Medicine* **2003?**, online: doi:10.1038/nm954.

17. Huang, Z.; Shiva, S.; Kim-Shapiro, D. B.; Patel, R. P.; Ringwood, L. A.; Irby, C. E.; Huang, K. T.; Ho, C.; Hogg, N.; Schechter, A. N.; Gladwin, M. T., Enzymatic Function of Hemoglobin as a Nitrite Reductase That Produces NO Under Allosteric Control. *J. Clin. Invest*. **2005,** 115, (8), 2099-2107.

18. Nagababu, E.; Ramasamy, S.; Abernethy, D. R.; Rifkind, J. M., Active Nitric Oxide Produced in the Red Cell under Hypoxic Conditions by Deoxyhemoglobin-mediated Nitrite Reduction. *J. Biol. Chem*. **2003,** 278, (47), 46349-46356.

19. Reutov, V. P., Nitric Oxide Cycle in Mammals and the Cyclicity Principle. *Biochemistry (Moscow)* **2002,** 67, (3), 293-311.

20. Dejam, A.; Hunter, C. J.; Pelletier, M. M.; Hsu, L. L.; Machado, R. F.; Shiva, S.; Power, G. G.; Kelm, M.; Gladwin, M. T.; Schechter, A. N., Erythrocytes are the Major Intravascular Storage Sites of Nitrite in Human Blood. *Blood* **2005,** 106, (2), 734-739.

21. Duranski, M. R.; Greer, J. J. M.; Dejam, A.; Jaganmohan, S.; Hogg, N.; Langston, W.; Patel, R. P.; Yet, S.-F.; Wang, X.; Kevil, C. G.; Gladwin, M. T.; Lefer, D. J., Cytoprotective Effects of Nitrite During In vivo Ischemia-Reperfusion of the Heart and Liver. *J. Clin. Invest*. **2005,** 115, (5), 1232-1240.

22. Bryan, N. S.; Fernandez, B. O.; Bauer, S. M.; Garcia-Suara, M. F.; Milson, A. B.; Rassaf, T.; Maloney, R. E.; Bharti, A.; Rodriguez, J.; Feelisch, M., Nitrite is a Signaling Molecule and Regulator of Gene Expression in Mammalian Tissues. *Nat. Chem. Biol*. **2005,** 1, (5), 290-?

23. Arendt, B.; Skibsted, L. H.; Andersen, H., Antioxidative Activity of Nitrite in Metmyoglobin Induced Lipid Peroxidation. *Z. Lebensm. Unters. Forsch A* **1997,** 204, 7-12, and references therein.

24. Carlsen, C. U.; Møller, J. K. S.; Skibsted, L. H., Heme-Iron in Lipid Oxidation. *Coord. Chem. Rev.* **2005,** 249, 485-498.

25. Møller, J. K. S.; Skibsted, L. H., Nitric Oxide and Myoglobins. *Chem. Rev.* **2002,** 102, 1167-1178.

26. Wanat, A.; Gdula-Argasinska, J.; Rutkowska-Zbik, D.; Witko, M.; Stochel, G.; van Eldik, R., Nitrite Binding to Metmyoglobin and Methemoglobin in Comparison to Nitric Oxide Binding. *J. Biol. Inorg. Chem.* **2002,** 7, 165-176, and references therein.

27. Fernandez, B. O.; Lorkovic, I. M.; Ford, P. C., Mechanisms of Ferriheme Reduction by Nitric Oxide: Nitrite and General Base Catalysis. *Inorg. Chem.* **2004,** 43, 5393-5402.

28. Immoos, C. E.; Chou, J.; Bayachou, M.; Blair, E.; Greaves, J.; Farmer, P. J., Electrocatalytic Reductions of Nitrite, Nitric Oxide, and Nitrous Oxide by Thermophilic Cytochrome P450 CYP119 in Film-Modified Electrodes and an Analytical Comparison of Its Catalytic Activities with Myoglobin. *J. Am. Chem. Soc.* **2004,** 126, 4934-4942.

29. Chi, Y.; Chen, J.; Aoki, K., Electrochemical Generation of Free Nitric Oxide from Nitrite Catalyzed by Iron meso-Tetrakis(4-N-methylpyridiniumyl)porphyrin. *Inorg. Chem.* **2004,** 43, 8437-8446.

30. Jene, P. G.; Ibers, J. A., Structural Characterization of the Picket Fence (TpivPP) Porphyrins Co(TpivPP), co(TpivPP)(NO2)(1-MeIm), and Co(TpivPP)(NO2)(1,2-Me2Im). *Inorg. Chem.* **2000,** 39, 3823-3827.

31. Kaduk, J. A.; Scheidt, W. R., Stereochemistry of Low-Spin Cobalt Porphyrins. V. Molecular Stereochemistry of Nitro-α,β,γ,δ-tetraphenylporphinato(3,5-lutidine)cobalt(III). *Inorg. Chem.* **1974,** 13, (8), 1875-1880.

32. Yamamoto, K.; Iitaka, Y., The Structure of Nitro-5,10,15,20-tetraphenylporphyrinato(piperidine)cobalt(III). *Chem. Lett.* **1989**, 697-698.

33. Goodwin, J.; Bailey, R.; Pennington, W.; Rasbery, R.; Green, T.; Shasho, S.; Yongsavanh, M.; Echevarria, V.; Tiedeken, J.; Brown, C.; Fromm, C.; Lyerly, S.; Watson, N.; Long, A.; De Nitto, N., Structural and Oxo-Transfer Reactivity Differences of Hexacoordinate and Pentacoordinate (Nitro)(tetraphenylporphinato)cobalt(III) Derivatives. *Inorg. Chem.* **2001,** 40, 4217-4225.

34. Nasri, H.; Goodwin, J. A.; Scheidt, W. R., Use of Protected Binding Sites for Nitrite Binding to Iron(III) Porphyrinates. Crystal Structure of the Bis(nitro)(tetrakins..... *Inorg. Chem.* **1990,** 29, (2), 185-191.

35. Nasri, H.; Wang, Y.; Huynh, B. H.; Walker, F. A.; Scheidt, W. R., Reactions of Bis(nitro)(a,a,a,a-tetrakis(o-pivalamidophenyl)porphinato)ferrate(III) with

Pyridine and Imidazole. EPR and Mossbauer Spectra and Molecular Structures of the Mixed-Ligand Species. *Inorg. Chem.* **1991,** 30, (7), 1483-1489.

36.   Cheng, L.; Powell, D. R.; Khan, M. A.; Richter-Addo, G. B., The First Unambiguous Determination of a Nitrosyl-to-Nitrite Conversion in an Iron Nitrosyl Porphyrin. *Chem. Commun.* **2000**, 2301-2302.

37.   Nasri, H.; Wang, Y.; Huynh, B. H.; Scheidt, W. R., Nitrite-Bound Five-Coordinate Low-Spin Iron(II) Model Complex for the Prosthetic Group of Nitrite Reductase with an Unusually Large Quadropole Splitting. Synthesis, Mossbauer Properties, and Molecular Structure of the Complex (Nitro)(a,a,a,a-tetrakis(o-pivalamidophenyl)porphinato)iron(II). *J. Am. Chem. Soc.* **1991,** 113, (2), 717-719.

38.   Nasri, H.; Haller, K. J.; Wang, Y.; Huynh, B. H.; Scheidt, W. R., Reactions of Bis(nitro)[α,α,α,α-*meso*-tetrakis(*o*-pivalamidophenyl)porphinato]iron(III) with 2,3,5,6-Tetrafluorothiophenol and 2,3,5,6-Tetrafluorothiophenolate. EPR and Mössbauer Spectra and Molecular Structures. *Inorg. Chem.* **1992,** 31, (16), 3459-3467.

39.   Nasri, H.; Ellison, M. K.; Chen, S.; Huynh, B. H.; Scheidt, W. R., Sharing the π-Bonding. An Iron Porphyrin Derivative with Trans, π-Accepting Axial Ligands. Synthesis, EPR and Mossbauer Spectra, and Molecular Structure of Two Forms of the Complex Nitronitrosyl(α,α,α,α-tetrakis(*o*-pivalamidophenyl)porphinato)ferrate(II). *J. Am. Chem. Soc.* **1997,** 119, (27), 6274-6283.

40.   Nasri, H.; Ellison, M. K.; Krebs, C.; Huynh, B. H.; Scheidt, W. R., Highly Variable π-Bonding in the Interaction of Iron(II) Porphyrinates with Nitrite. *J. Am. Chem. Soc.* **2000,** 122, 10795-10804.

41.   Nasri, H.; Ellison, M. K.; Shang, M.; Schultz, C. E.; Scheidt, W. R., Variable pi-Bonding in Iron(II) Porphyrinates with Nitrite, CO, and tert-Butyl Isocyanide: Characterization of [Fe(TpivPP)(NO2)CO]-. *Inorg. Chem.* **2004,** 43, 2932-2942.

42.   Ellison, M. K.; Scheidt, W. R., Synthesis, Molecular Structures, and Properties of Six-Coordinate [Fe(OEP)(L)(NO)]+ Derivatives. Elusive Nitrosyl Ferric Porphyrins. *J. Am. Chem. Soc.* **1999,** 121, (22), 5210-5219.

43.   Kadish, K. M.; Adamian, V. A.; Caemelbecke, E. V.; Tan, Z.; Tagliatesta, P.; Bianco, P.; Boschi, T.; Yi, G.-B.; Khan, M. A.; Richter-Addo, G. B., Synthesis, Characterization, and Electrochemistry of Ruthenium Porphyrins Containing a Nitrosyl Axial Ligand. *Inorg. Chem.* **1996,** 35, (5), 1343-1348.

44.   Bohle, D. S.; Hung, C.-H.; Smith, B. D., Synthesis and Axial Ligand Substitution Chemistry of Ru(TTP)(NO)X. Structures of Ru(TTP)(NO)X (X = ONO, OH). *Inorg. Chem.* **1998,** 37, 5798-5806.

45.   Miranda, K. M.; Bu, X.; Lorkovic, I.; Ford, P. C., Synthesis and Structural Characterization of Several Ruthenium Porphyrin Nitrosyl Complexes. *Inorg. Chem.* **1997,** 36, (21), 4838-4848.

46. Suslick, K. S.; Watson, R. A., Photochemical Reduction of Nitrate and Nitrite by Manganese and Iron Porphyrins. *Inorg. Chem.* **1991,** 30, 912-919.

47. Goldner, M.; Geniffke, B.; Franken, A.; Murray, K. S.; Homborg, H., Mononitrosyl and trans-Dinitrosyl Complexes of Phthalocyaninates of Manganese and Rhenium. *Z. Anorg. Allg. Chem.* **2001,** 627, 935-947.

48. Sievertsen, S. e. a., *Z. Anorg. Allg. Chem.* **1996**, (622), 1685.

49. Leal, F. A.; Lorkovic, I. M.; Ford, P. C.; Lee, J.; Chen, L.; Torres, L.; Khan, M. A.; Richter-Addo, G. B., Synthesis, Characterization, and Molecular Structures of Nitrosyl Nitrito Complexes of Osmium Porphyrins: Disproportionation of Nitric Oxide in its Reaction with Os(P)(CO) (P = porphyrinato dianion). *Can. J. Chem.* **2003,** 81, 872-881.

50. Nasri, H., et al, Variable pi-Bonding in Iron(II) Porphyrinates with Nitrite, CO, and tert-butyl isocynide: Characterization of [Fe(TpivPP)(NO2)(CO)-. *Inorg, Chem.* **2004,** 43, 2932-2942.

51. Adachi, H.; Suzuki, H.; Miyazaki, Y.; Iimura, Y.; Hoshino, M., Structure and Photochemistry of Nitrocobalt(III) Tetraphenylporphyrin with Axial Triphenylphosphine in Toluene Solution. *Inorg. Chem.* **2002,** 41, 2518-2524.

52. Ohba, S. S., H., *Acta Crystallogr.,Sect.E:Struct.Rep.Online* **2002,** 58, 169.

53. Ohba, S. M. E. H. S., *Acta Crystallogr.,Sect.C:Cryst.Struct.Commun.* **2000,** 56, 555.

54. Sievertsen, S. e. a., *Z. Anorg. Allg. Chem.* **1996,** 622, 1685.

55. Copeland, D. M.; West, A. H.; Richter-Addo, G. B., Crystal Structures of Ferrous Horse Heart Myoglobin Complexed with Nitric Oxide and Nitrosoethane. *Proteins: Struct. Func. Genet.* **2003,** 53, 182-192.

56. Pflugrath, J., The Finer Things in X-Ray Diffraction Data Collection. *Acta Crystallogr., Section D* **1999,** D55, 1718-1725.

57. Otwinowski, Z.; Minor, W., Processing of X-Ray Diffraction Data Collected in Oscillation Mode. *Methods Enzymol.* **1997,** 276, 307-326.

58. McRee, D. E., XtalView/Xfit - A Versatile Program for Manipulating Atomic Coordinates and Electron Density. *J. Struct. Biol.* **1999,** 125, 156-165.

59. Sono, M.; Dawson, J. H., Formation of Low Spin Complexes of Ferric Cytochrome P-450-CAM with Anionic Ligands. Spin State and Ligand Affinity Comparison to Myoglobin. *J. Biol. Chem.* **1982,** 257, (10), 5496-5502, and references therein.

60. Laskowski, R. A.; MacArthur, M. W.; Moss, D. S.; Thornton, J. M., PROCHECK: A Program to Check the Stereochemical Quality of Protein Structures. *J. Appl. Cryst.* **1993,** 26, 283-291.

61. Hitchman, M. A.; Rowbottom, G. L., Transition Metal Nitrite Complexes. *Coord. Chem. Rev.* **1982,** 42, 55-132.

62.   Wyllie, G. R. A.; Scheidt, W. R., Solid-State Structures of Metalloporphyrin NOx Compounds. *Chem. Rev.* **2002,** 102, (4), 1067-1089.

63.   Lee, J.; Kovalevsky, A. Y.; Novozhilova, I. V.; Bagley, K. A.; Coppens, P.; Richter-Addo, G. B., Single- and Double-Linkage Isomerism in a Six-Coordinate Iron Porphyrin Containing Nitrosyl and Nitro Ligands. *J. Am. Chem. Soc.* **2004,** 126, 7180-7181.

64.   Novozhilova, I. V.; Coppens, P.; Lee, J.; Richter-Addo, G. B.; Bagley, K. A., Experimental and Density Functional Theoretical Investigations of Linkage Isomerism in Six-Coordinate {FeNO}6 Iron Porphyrins with Axial Nitrosyl and Nitro Ligands. *J. Am. Chem. Soc.* **2006,** 128, 2093-2104.

65.   Silaghi-Dumitrescu, R., Linkage Isomerism in Nitrite Reduction by Cytochrome cd1 Nitrite Reductase. *Inorg. Chem.* **2004,** 43, 3715-3718.

66.   Garber, E. A. E.; Hollocher, T. C., ^{15}N, ^{18}O Tracer Studies on the Activation of Nitrite by Denitrifying Bacteria. *J. Biol. Chem.* **1982,** 257, (14), 8091-8097.

67.   Herold, S.; Rehmann, F.-J. K., Kinetic and Mechanistic Studies of the Reactions of Nitrogen Monoxide and Nitrite with Ferry Myoglobin. *J. Biol. Inorg. Chem.* **2001,** 6, 543-555.

68.   Herold, S.; Rehmann, F.-J. K., Kinetics of the Reactions of Nitrogen Monoxide and Nitrite with Ferryl Hemoglobin. *Free Radical Biol. Med.* **2003,** 34, (5), 531-545.

69.   Yi, G.-B.; Chen, L.; Khan, M. A.; Richter-Addo, G. B., Activation of Thionitrites and Isoamyl Nitrite by Group 8 Metalloporphyrins and the Subsequent Generation of Nitrosyl Thiolates and Alkoxides of Ruthenium and Osmium Porphyrins. *Inorg. Chem.* **1997,** 36, (18), 3876-3885.

70.   Richter-Addo, G. B., Binding of Organic Nitroso Compounds to Metalloporphyrins. *Acc. Chem. Res.* **1999,** 32, (6), 529-536.

71.   Lee, J.; Chen, L.; West, A. H.; Richter-Addo, G. B., Interactions of Organic Nitroso Compounds with Metals. *Chem. Rev.* **2002,** 102, (4), 1019-1065.

72.   Yi, G.-B.; Khan, M. A.; Richter-Addo, G. B., Formal Addition of *S*- and *O*-Nitroso Compounds to Metalloporphyrins. *Chem. Commun.* **1996**, 2045-2046.

4 Nitrosoalkane and Nitrosoarene Complexes of Horse Heart Myoglobin, and Extensions to the Nitrosoalkane Adducts of Cytochrome P450

4.1 Introduction

4.1.1 *C*-nitroso Compounds and Heme proteins

Nitrosoalkanes and nitrosoarenes (R-N=O; R = alkyl or aryl group) are biologically important compounds that are generated in physiological media by oxidative metabolism of the precursor amines RNH_2 (or hydroxylamines RNHOH) or by reduction of the organic nitro RNO_2 compounds, and these resulting RNO compounds are known to interact with several heme-containing biomolecules by binding to the heme iron [4-16].
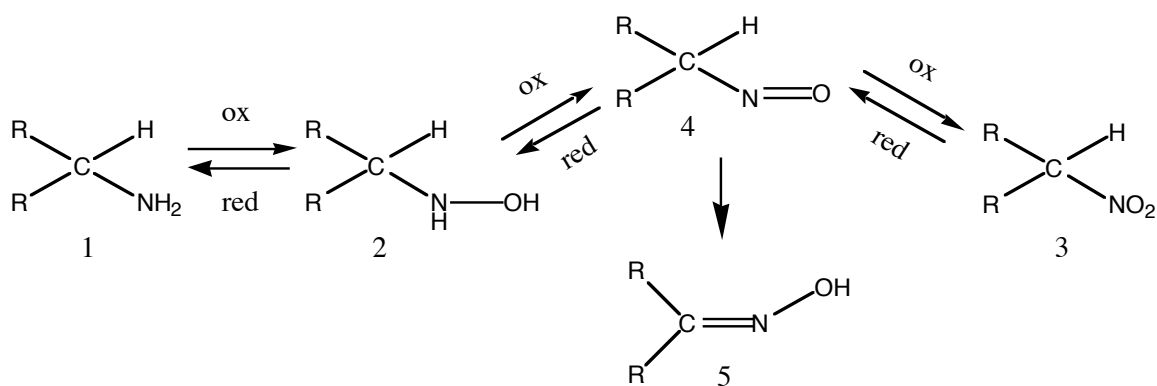
In the case of 1° and 2° nitroso compounds (4), irreversible isomerization to the oxime (5) occurs. The rate of this conversion is dependent on the availability of hydrogen on the alpha carbon. Once the nitroso compound is converted to the oxime it is no longer able to bind the heme iron. Therefore, one would assume that the binding of nitrosoarenes to heme proteins would be more efficient than that of nitrosoalkanes. However, Mansuy

and coworkers [17] showed that nitrosoarenes, because of the electron poorer NO species, are easier to reduce to the phenylhydroxylamine and then the amine complex than are similar nitrosoalkane complexes. Therefore, in a reducing environment the nitrosoalkanes appear more stable than do nitrosoarenes because of the relative difficulty to reduce them to the amine complex.
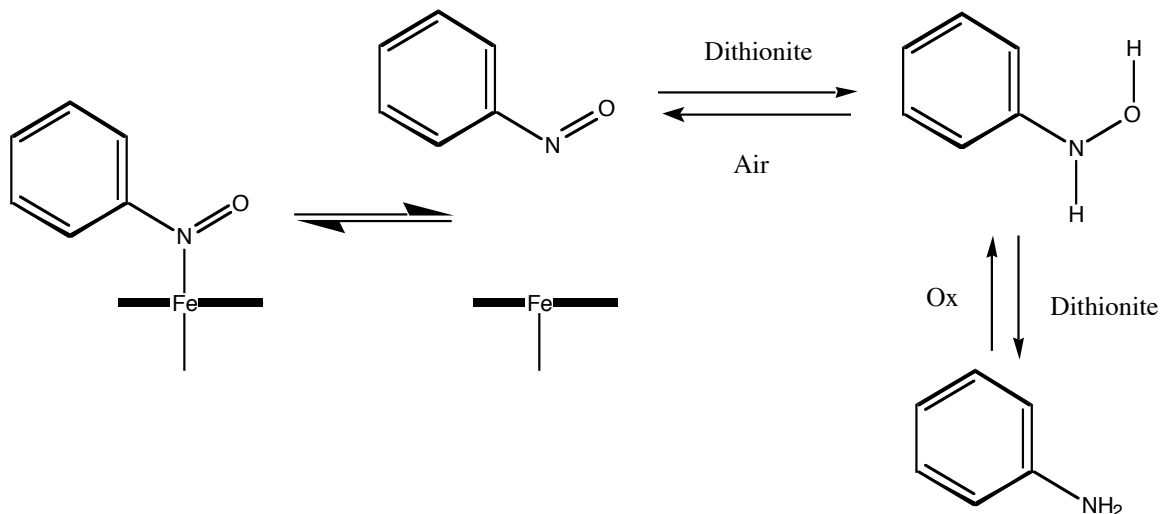
In cases where the heme proteins contain exposed cysteine residues (e.g., hemoglobin), interactions of RNO compounds with the cysteine residues are possible generating sulfinamines [18, 19]. RNO binding to histidine-liganded hemes are biologically relevant. For example, Hb(RNO) formation was shown to be associated with nitrobenzene poisoning more than a century ago [20, 21]. In our lab, we previously demonstrated, by single-crystal X-ray crystallography, that in heme model complexes containing RNO ligands, the ligands can bind to the iron center either through the N or O atoms [22]. Other reports have been published that show *N*-binding of RNO ligands to the iron center in heme model complexes [23, 24]. Surprisingly, however, there is very little information to date on the structural consequences of RNO binding to the iron center in heme proteins. Thus, despite the importance of RNO binding to heme proteins (e.g., in

the inhibition of heme protein function) [16], ours are the only reports to date of the single-crystal X-ray structural characterization of heme-nitrosoalkane adducts. There is only one structural example of a related heme-nitrosoarene complex, namely that of the nitrosobenzene adduct of leghemoglobin from *Lupinus luteus* [25] which is shown in Figure 4.1.
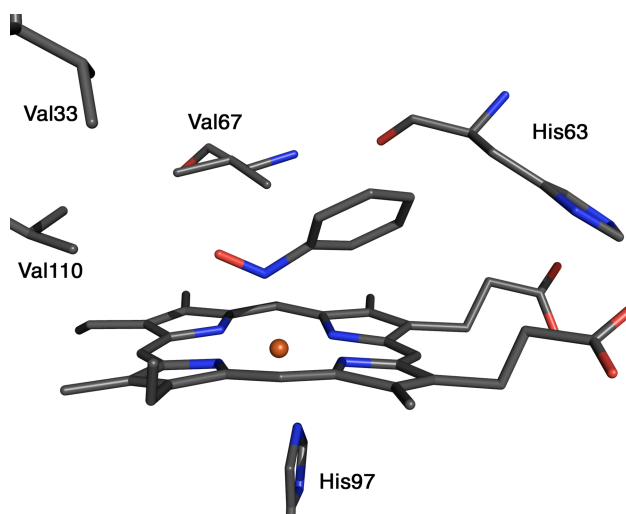
Figure 4.1　　　The heme site of the Leg Hb (nitrosobenzene) complex[3]. Exterior of protein shown to the right side of the figure, hydrophobic core of the protein is shown on the left. There is no possibility of hydrogen bonding between the ligand and the heme pocket with side chain or backbone atoms. The only interaction between the ligand and the protein is through the metal.

There has, however, been a long history of spectroscopic studies that have been carried out on the interactions of nitrosoalkanes and nitrosoarenes with heme proteins. Some of the first studies on C-nitroso compounds and heme proteins were undertaken to study nitrosobenzene poisoning [21]. Murayama used UV/Vis spectroscopy to study the interaction of nitrosobenzene and hemoglobin [26] concluding that nitrosobenzene does bind human hemoglobin, and that the addition of bulkier groups caused steric clashes that raised the energy barrier of forming the complex. Soon after, Gibson published studies

95

looking at the "rates of combination" of several nitrosoarenes with hemoglobin and myoglobin [27] and determined rate constants for the formation of several substituted nitrosobenzenes.

In the early 1970s, several studies examined the interactions of amine containing drugs, specifically amphetamines, with rat and rabbit liver microsomal cytochromes and a distinctive peak in the UV/Vis spectrum was observed [28, 29] but not identified until 1975 when Mansuy and coworkers identified the species as a bound nitrosoalkane [2]. The species was determined because it could be made by two distinct routes; (i) the oxidation of amphetamines, and (ii) the reduction of the nitro species to the nitroso species [2]. Shortly after, these studies were extended from interactions only with cytochromes to the interactions of nitrosoalkanes with hemoglobin and myoglobin [15].

RNO compounds are now known to bind the heme iron in several proteins including prostaglandin synthase where the R group was one of several options (methyl, ethyl, isopropyl and phenyl)[12], soluable guanylate cyclase (R = methyl)[30], microperoxidase (R = methane, ethane, propane, benzene, hexane, cyclohexane, tert-butane)[6, 31], P450 (R = phenyl)[17, 32], hemoglobin and myoglobin (R = methyl, ethyl, isopropyl, tert-butyl, pentane, and cyclopentane)[15], and nitric oxide synthase (R = methyl, ethyl, isopropyl, tert-butyl, hexyl, cyclohexyl, phenyl, and various substituted phenyl groups)[13]. The binding of all of these various RNO compounds to these varied proteins was determined by UV/Vis spectroscopy. However, with the exception of the leghemoglobin/nitrosobenzene complex there is a complete lack of structural information available in this research field.

The most important research discussed in this chapter are the 3-dimensional crystal structures of the horse heart myoglobin/nitrosoethane complex, horse heart myoglobin/nitrosomethane complex and horse heart myoglobin/nitrosobenzene complex, which are the first two nitrosoalkane/heme protein complexes reported in the literature and the hh Mb(PhNO) structure displays an alternative binding mode to that observed in the leg Hb(PhNO) complex.

4.1.2 *C*-nitroso Compounds and Synthetic Metalloporphyrins as Heme Models

Nitrosoalkane and nitrosoarene binding have both been studied extensively in heme model systems with Fe, Mn, Ru, Os, and Co [16]. While many of the metal complexes are interesting in their own right, only complexes with iron porphyrins will be discussed here. The two major groups of model porphyrins that exist are symmetrical and asymmetrical porphyrins, and both of these types of porphyrins have been employed to study these complexes [22, 24, 33, 34].

The symmetrical porphyrins can, as above with the porphyrins, be divided into two groups, the tetra-substituted and the octa-substituted. The two tetra-substituted porphyrins that have been used in the study of RNO binding have been 5,10,15,20-tetraphenylporphyrin (TPP) and 5,10,15,20-tetra-p-tolylporphyrin (TTP) [24, 33]. The ferric and ferrous derivitives have been used to study bound nitrosoalkanes and nitrosoarenes.

The first binding studies that were carried out with nitrosoalkanes and FeTPP were performed by Mansuy and coworkers in 1983 [23]. These showed that TPP was a

reasonably good model for biological heme systems and was the first structural evidence that showed RNO binding to a heme or heme model system. One of the more important finding made using the FeTPP system was that the oxidation state of the metal determines the mode of binding of the ligand [22]. Our group showed in 1996 that nitrosoarenes would bind through the nitrogen of the NO moiety to ferrous porphyrins and through the oxygen with ferric porphyrins[22].

(OEP)Fe(i-PrNO)(I-MeIm)   [(TPP)Fe(Et$_2$NC$_6$H$_4$NO)$_2$]SbF$_6$
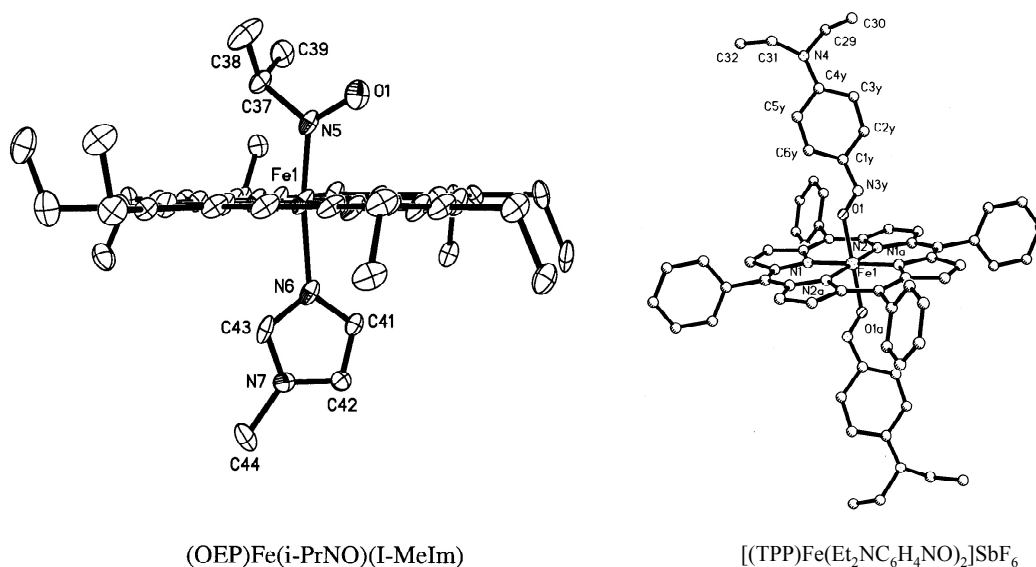
Figure 4.2 Examples of two iron porphyrin RNO complexes. (left) (OEP)Fe(II)(i-PrNO)(1-MeIm) showing the N-bound mode of binding of the RNO with an Fe(II) porphyrin[33]. (right) [(TPP)Fe(Et$_2$NC$_6$H$_4$NO)$_2$]SbF$_6$ showing the O-bound mode of binding for that RNO compound with and Fe(III) center[22].

Fe(II) porphyrin RNO complexes are usually formed in model systems by reacting the hydroxylamine species of interest with the oxidized iron porphyrin. The reduction of the metal from Fe(III) to Fe(II) and the oxidation of the hydroxylamine to the nitroso compound results in the generation of the final product Fe(II) RNO complex.

However, Mansuy and coworkers determined that in proteins, the PhNO ligand alone was enough to reduce the Fe and bind to the heme and that the phenylhydroxylamine was not necessary, but its presence did speed up the reaction [17].

Fe(III) porphyrin RNO complexes have only been made with *para*-substituted nitrosoarenes that are fairly stable in solution, and are usually made by adding the nitroso compound of interest directly to the Fe(III) porphyrin [22]. This method could shed some light on the above method of having the RNO itself reduce the metal and form the Fe(II) complex. One could postulate that the *O*-bound Fe(III) complex is initially formed and is slowly converted to the N-bound Fe(II) complex.

4.2   Materials and Methods

4.2.1 P450BM-3 hd Expression

The expression vector for the heme domain of cytochrome P450BM-3 (P450BM-3hd), from *Bacillus megaterium,* was given to us by Dr. Thomas Poulos at the University of California, Irvine.   The plasmid pT7BMHD has the DNA encoding P450BM-3hd inserted into a pET21 vector.   This vector uses the strong T7 promoter to obtain high expression levels of the protein in *E. coli*.   The protein was expressed in a BL21-DE3 strain of *E. coli* and approximately 50 mg of P450BM-3hd was obtained from a 2 L preparation.

The purification of the protein was performed using a Q-sepharose (Amersham Pharmacia) column followed by an sephacryl S-200 (Amersham Pharmacia) column run as described in the Li and Poulos paper, which describes the initial characterization[35].

4.2.2 UV/Vis Spectroscopic Techniques

Experiments were carried out on a Hewlett Packard 8453 spectrophotometer equipped with a diode array detector.   Samples were contained in screw top quartz cuvettes so data could be collected both aerobically and under anaerobic conditions if the need arose.

4.2.3 Crystallization Techniques

4.2.3.1   Horse Heart Myoglobin Nitrosoalkane Complexes

In the case of the nitrosoalkane structures, cocrystallization was used instead of soaking the ligand into the preformed crystals. A 30 mg/mL solution of horse heart myoglobin was prepared in 100 mM Tris-HCl at pH 7.4. An excess of nitroethane or nitromethane (10 μL) and sodium dithionite (50 mg) were added to the solution, and an immediate color change of the solution from brown to reddish-purple occurred, indicative of the formation of the desired Mb(EtNO) or Mb(MeNO) product (λ_{max} 425 nm) [15]. The solution was then applied to a desalting column (Sephadex G25, 10 mL) to remove the excess dithionite, and the flow-through sample was reconcentrated in an aerobic atmosphere to 30 mg/mL using a Centricon YM-10 membrane.

Crystals were obtained by the hanging drop vapor diffusion method at room temperature (21°C). The droplets were 10 μL each in volume, and were prepared by mixing 5 μL of the 30 mg/mL protein solution in 100 mM Tris-HCl at pH 7.4 with 5 μL of 3.4-4.0 M ammonium sulfate in 100 mM Tris-HCl at pH 7.4. The droplets were suspended over reservoirs containing 1 mL of 3.1–3.3 M ammonium sulfate (100 mM Tris-HCl at pH 7.4). Crystals of suitable size (1.0 x 0.4 x 0.05 mm) grew in 5 days and were harvested as soon as they were of suitable size due to the instability of the nitrosoalkane complexes in the crystallization buffer, which will be discussed later. These were harvested and passed through a solution of the artificial mother liquor

101

containing 7.5-15% glycerol (v/v) as a cryoprotectant. The crystals were then flash frozen in liquid nitrogen.

4.2.3.2   Horse Heart Myoglobin Nitrosobenzene Complex

MetMyoglobin crystals were grown using the same method as described previously[36]. The droplets were prepared by mixing 5 μL of the 30 mg/mL protein solution in 100 mM Tris-HCl at pH 7.4 with 5 μL of 3.4-4.0 M ammonium sulfate (100 mM Tris-HCl at pH 7.4). The droplets were suspended over reservoirs containing 1 mL of 3.1–3.3 M ammonium sulfate (100 mM Tris-HCl at pH 7.4).

Crystals grew to a suitable size (0.5 x 0.2 x 0.05 mm) in 3-5 days and were transferred to a solution of artificial mother liquor, 15% glycerol and 300 mM phenylhydroxylamine. The phenylhydroxylamine was synthesized from nitrobenzene according to Kamm's method.[37]

4.2.4   Data Collection, Processing and Refinement

All X-ray data sets were collected on our in-house diffractometer at 100 K on a RigakuMSC RU-H3R X-ray generator operated at 50 kV/100 mA to produce CuKα radiation (λ = 1.5418 Å). Diffracted X-rays were detected using an R-AXIS 4++ dual image plate detector system. For the hh Mb(EtNO) crystal, the crystal-to-detector distance was set at 100 mm and 148 frames were collected using a 1.0° oscillation to a resolution of 1.7 Å. For the hh Mb(MeNO) crystal data, 1° oscillation images were collected over a range of 180° with the crystal-to-detector distance of 150 mm and an exposure time of 300 sec. For the hh Mb(PhNO) crystal data, 1° oscillation images were

collected over a range of 210° with the crystal-to-detector distance of 70 mm and an exposure time of 300 sec.

Data sets were processed using the stand-alone d*TREK program (Macintosh v.2D) [38] or with the *d*TREK* program as implemented in the *Crystal Clear* suite [39], both available from Molecular Structure Corporation.

4.2.4.1   Horse Heart Myoglobin Nitrosoethane Complex

After the rotation and translation search, (using the 1.45 Å resolution structure of ferrous MbCO, PDB access code 1DWR[40] with CO and solvent molecules removed) the initial model had a R-factor of 30.70%. Rigid body refinement lowered the R-factor to 28.91%. Well-defined electron density for the nitrosoethane ligand was apparent in the initial F_o-F_c electron density map. The nitrosoethane ligand was then modeled into this density, and its position and geometric parameters were unrestrained throughout refinement. Further rounds of refinement and model adjustment were performed until the R-factor stabilized (at ~26%). An F_o-F_c electron density map showed negative density in the vicinity of the nitrosoethane ligand indicating partial occupancy of the ligand. Consequently, unrestrained individual occupancy refinement was performed. All atoms of the nitrosoethane ligand refined to occupancies of ~0.6.   The ligand occupancy was consistent with our UV-vis spectroscopic data (see later) which suggested a ~40% conversion of the ferrous Mb(EtNO) complex to *aqua-met*Mb under the crystallization conditions. This led to the modeling of a water molecule as an alternate sixth ligand to iron (for the *aqua-met*Mb contribution) with an occupancy of 0.4. Water molecules and two sulfate anions were added to the structure using an F_o-F_c electron density map. Further cycles of conjugate gradient energy minimization and model adjustment were

subsequently performed. As with the hh MbNO structure, poor electron density was observed for the two C-terminal residues Gln152 and Gly153.

The final crystallographic R-factor (R_{free} calculated using 10% of randomly selected reflections) was 19.8% (R_{free} = 22.7%). Coordinates for this structure have been deposited at the Protein Data Bank [41] with access code 1NPG.

4.2.4.2   Horse Heart Myoglobin Nitrosomethane Complex

After the rotation and translation search, (using the 1.90 Å resolution structure of ferrous MbNO, PDB access code 1NPF[36] with NO and solvent molecules removed) the initial model had a R-factor of 27.86%. Ten cycles of restrained refinement lowered the R-factor to 21.03%. Well-defined electron density for the nitrosomethane ligand was apparent in the initial F_o-F_c electron density map and the nitrosomethane ligand was then modeled into this density. An F_o-F_c electron density map showed negative density in the vicinity of the nitrosomethane ligand indicating partial occupancy of the ligand and the final occupancy of the nitrosomethane ligand was determined to be 80%. The ligand occupancy was consistent with our UV-vis spectroscopic data which suggested a ~10-20% conversion of the ferrous Mb(MeNO) complex to *aqua-met*Mb under the crystallization conditions. Water molecules and two sulfate anions were added to the structure using an F_o-F_c electron density map. Further cycles of refinement and model adjustment were subsequently performed. As with most hh Mb structures, poor electron density was observed for the two C-terminal residues therefore Gly153 was omitted from the model.[42-46]

The final crystallographic R-factor (R_{free} calculated using 10% of randomly selected reflections) was 16.2% (R_{free} = 22.9%). Coordinates for this structure will be deposited in the Protein Data Bank [41].

4.2.4.3   Horse Heart Myoglobin Nitrosobenzene Complex

After the rotation and translation search, (using the 1.90 Å resolution structure of ferrous MbNO, PDB access code 1NPF[36] with NO and solvent molecules removed) the initial model had an R-factor of 41.0%. Restrained refinement was carried out for 10 cycles in Refmac5 prior to the addition of any solvent, which lowered the *R-factor* to 23.1%. At this point nitrosobenzene as well as two sulfate ions were added to the model based on an F_o-F_c electron density map. After cycling with ARP/wARP and 10 additional cycles of restrained refinement, 98 water molecules were added and the *R-factor* dropped to 18.4%. 100 more cycles of restrained refinement using data between 20 Å and 2.0 Å led to an *R-factor* of 18.2%. As with previous horse heart myoglobin structures poor electron density was seen at the C-terminal of the protein for residues Gln152 and Gly153 and residue 153 was omitted from the structure [42-46].

The final crystallographic R-factors (R_{free} calculated using 5% of randomly selected reflections) 18.1% (R_{free} = 26.5%) for the hh Mb(PhNO) structure. Coordinates will be deposited in the Protein Data Bank [41].

4.3 Results

4.3.1 UV/Vis Spectroscopic Studies of the Bindiong of Simple Nitrosoalkanes to the Heme Domain of Cytochrome P450BM-3

The heme domain of cytochrome P450BM-3 from *Bacillus megaterium* was complexed with a series of simple nitrosoalkanes in an attempt to find a suitable complex for crystallographic work. The results show that the R-group on the nitrosoalkane can greatly influence the extent of binding of the RNO compounds to the heme domain of P450 BM-3.

The differences in the extent of formation of these complexes as seen in Figure 4.3 is what initially interested us in these ligands. There were dramatic differences observed with the only variation between the experiments being the identity of the ligand. The next step taken was to monitor the extent of formation over time to see if all of the complexes would eventually proceed to 100% complex formation.

All of the complexes were made the same way, by adding a given amount of the corresponding nitro compound to the protein solution and then adding enough reducing agent to reduce both the protein and the ligand. The method used to study these complexes was originally used by Mansuy and coworkers to determine the interaction of these RNO compounds with rat liver microsomal P450[2]. Our results are very similar to those that were seen by Mansuy.

Our reaction mixture consists of 5 μM P450BM-3hd, 10 mM nitroalkane (any of the nitroalkanes), and 20 mM sodium dithionite in a total of 1 mL of solution. For the time courses, time was started as soon as the sodium dithionite was added to the mixture

and spectra were taken at time points (15s, 30s, 1, 2, 3, 4, 5, 10, 15, 20, 30, 45, and 60m) for up to 1 hour. The experiment was repeated at least three times for each nitroalkanes used.

We determined that the best way to monitor this reaction was to monitor the change in the 419 nm and to divide that by the original absorbance at 419 nm and to express that number as the extent of complex formation. The appearance of the new peak at 453 nm was also monitored, and similar extent of formation values were obtained when it was divided by the original absorbance at 419 nm. While the extinction coefficient for the P450(nitrosoalkane) complexes are not known, it can be assumed the they will not be the same as the extinction coefficient for the unbound protein and therefore, the absorbance values would not directly relate to each other, and simply monitoring the 419 nm peak was the most accurate and the only way to relate the values to each other.
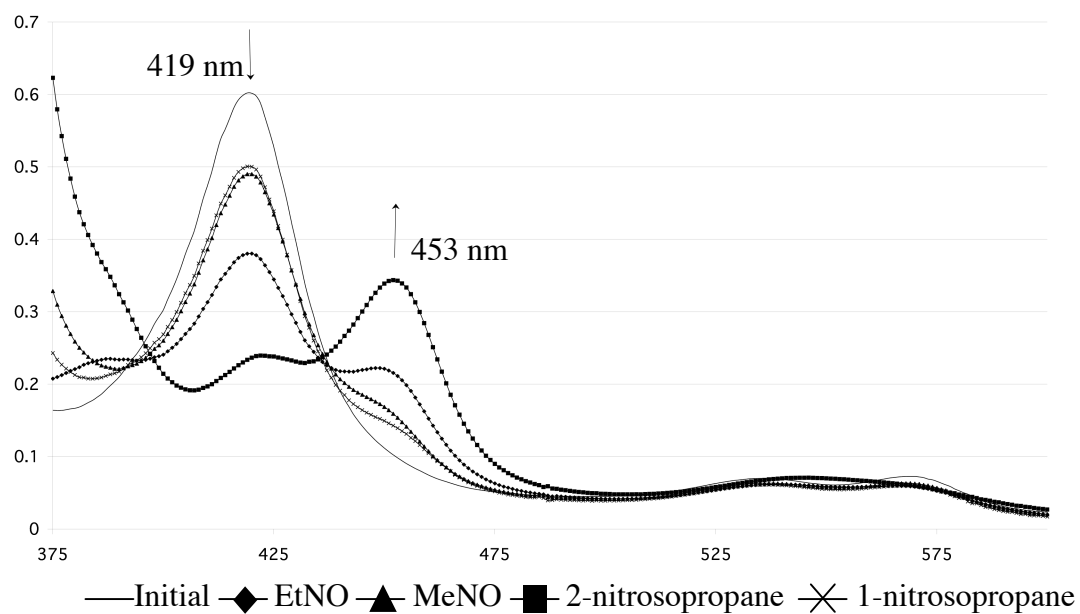
Figure 4.3 Overlay of five spectra showing the different changes in absorbance based on the identity of the R-group on the nitrosoalkane ligand. The x-axis is in units of wavelength and the y-axis is absorbance units. The highest peak at 419 nm corresponds to the nonbound form of P450BM-3hd. The addition of ligand causes a disappearance of the 419 nm peak and the appearance of a new peak at 453 nm. The identities of the different lines are shown in the legend at the bottom of the graph.

Table 4.1 Extent of Formation as a Function of Time Expressed a Percentage

Time(min)	0.16	0.5	1	2	5	10	20	30	45	60
Nitrosomethane	10	12	14	16	19	**20**	20	19	17	16
Nitrosoethane	10	14	17	21	26	30	33	34	35	**36**
1-nitrosopropane	10	11	12	13	15	17	18	19	19	**19**
2-nitrosopropane	10	19	24	31	41	49	54	57	59	**60**

Calculations Based on $\Delta419/419$(original) X 100
Highest values shown in bold

Table 4.1 shows that the R-group on the nitrosoalkane does make a significant difference in its binding to the heme domain of cytochrome P450BM-3. Varying only the R-group we see a range of extents of formation from 19% all the way to 60% in a 1 hour time course.

This shows that the heme pocket of cytochrome P450 BM-3 can influence the binding of these ligands, and that simple changes in the R-group can drastically influence the binding. We can be certain that the 453 nm peak is due to the P450-RNO complex because Cho and coworkers[32] formed the P450(nitrosobenzene) complex, which displayed the characteristic 453 nm peak and then added CO to the solution and saw no change in the spectrum, indicating that the heme site was blocked. It can also be inferred from the data obtained here that there will not be a complete conversion from the unbound form to the bound form. In this experiment, a 2000 fold excess of ligand was used to try to achieve 100% conversion, and with that huge excess only a 60% conversion was seen in one of the ligands. The most likely conclusion that can be drawn from this data is that a much higher excess of ligand is needed to achieve 100% conversion to product. However, this can be somewhat dismissed because this experiment was performed with larger excesses of ligand and dithionite and no increase in complex formation was seen, however, too large of an excess caused precipitation of the protein.

4.3.2 UV/Vis Spectroscopy Showing The Instability of Complexes in the Presence of Ammonium Sulfate

Both of the complexes that are discussed in this chapter, the myoglobin nitrosoethane complex and the myoglobin nitrosomethane complex, are unstable in the crystallization solution. Although both complexes are stable in aqueous buffer in the presence of oxygen for several weeks (showing no signs of decomposition as judged by UV/Visible spectroscopy), the complex slowly converts to the *aqua*-metmyoglobin in the presence of ammonium sulfate.

4.3.2.1 Myoglobin Nitrosoethane Complex

As seen in Figure 4.4, the horse heart myoglobin nitrosoethane complex was converted completely to the *aqua*-metmyoglobin form over the course of 15 days.

The importance of this is, for the crystallographic experiment, the myoglobin nitrosoethane complex was pre-formed and then cocrystallized and thus the instability of the myoglobin nitrosoethane complex in the crystallization solution becomes important.

The crystals only grew to a suitable size for data collection after five days at which time they were immediately harvested and frozen in liquid nitrogen for data collection. From this spectroscopic data we can calculate that only 58% (as seen in Table 4.2) of the original complex remains after 5 days, which corresponds well to the data that was obtained crystallographically.
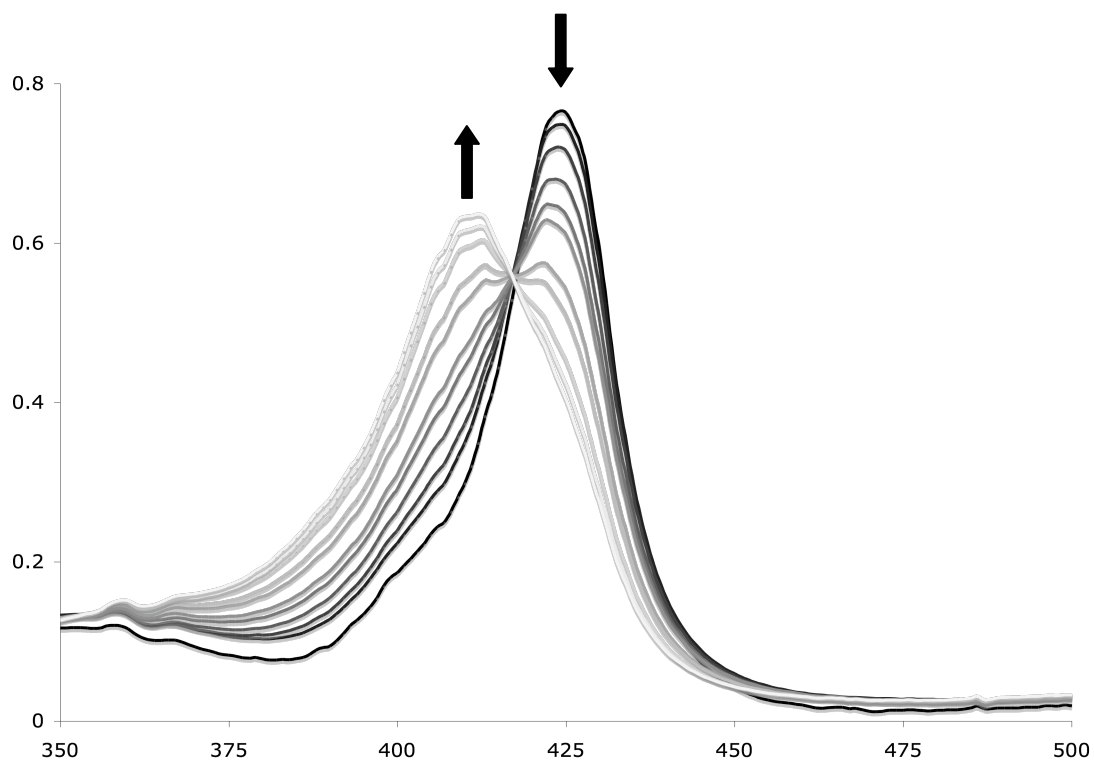
Figure 4.4   Time course of UV/Vis spectra showing the conversion of Mb(EtNO) back to Mb(H$_2$O) over the course of 15 days in the presence of ammonium sulfate. Darkest line with peak at 425 nm is the initial spectrum. As time course proceeds the 425 nm peak disappears and the 409 nm peak is formed. Time course proceeds from darkest line to the lightest line.

The group of overlaid UV/Vis spectra clearly show the disappearance of the 425 nm peak that corresponds to the bound myoglobin/nitrosoethane complex and over time the reappearance of the 409 nm peak representative of the *aqua*-metmyoglobin. This degradation of the 425 nm peak is not observed in the absence of the ammonium sulfate. In fact, the complex is stable in air for several months when NOT in the crystallization buffer (data not shown).

Table 4.2 Degradation of Mb(EtNO) Complex

	% of Initial Complex Remaining		
Time (days)	425 nm	425 nm corrected[1]	% Complex Remaining
0	0.7630	0.3604	100
1	0.7463	0.3436	95
2	0.7154	0.3128	87
3	0.6728	0.2701	75
4	0.6349	0.2323	64
5	0.6101	0.2074	58
8	0.5409	0.1383	38
10	0.5090	0.1064	30
12	0.4522	0.0495	14
14	0.4223	0.0197	5
15	0.4027	0.0000	0

[1] Corrected value has contribution of 409nm peaks
   shoulder subtracted out.
After day 15 no changes were seen in the spectra
   therefore this data was set to zero, implying all of the
   absorbance came from the shoulder of the 409nm
   peak.

4.3.2.2 Myoglobin Nitrosomethane Complex

UV/Vis spectroscopy was also used to study the horse heart myoglobin nitrosomethane complex. There is similar but reduced instability of the nitrosomethane complex in the presence of ammonium sulfate as was observed with the nitrosoethane complex. Where the nitrosoethane complex degraded by approximately 40% over the course of the 5 days required for crystal growth, the nitrosomethane complex only lost 10-20% of the complex in the same amount of time under the same conditions. Although the difference between these two compounds is minor ($-CH_2-$) there is a significant difference in the stability of these complexes that cannot be easily explained with only the spectroscopic data. The crystal structures of these two compounds however do shed light on the difference in stability and will be discussed in detail in the next section of this chapter.

Table 4.3 Degradation of Mb(MeNO) Complex

	% of Initial Complex Remaining		
Time (days)	425 nm	425 nm corrected[1]	% Complex Remaining
0	0.1507	0.0712	100
3	0.1429	0.0634	89
6	0.1378	0.0582	82

[1] Corrected value has contribution of 409nm peaks shoulder subtracted out.

4.3.3 Myoglobin Nitrosobenzene Complex

The stability of the myoglobin nitrosobenzene complex in the crystallization buffer was not examined because this complex was formed using a soaking method instead of the cocrystallization method. Full occupancy of the ligand was observed in the crystal structure and it was therefore unnecessary to determine using UV/Vis spectroscopy if the crystallization solution was causing instability in the complex.

4.3.4 Crystallographic Results

4.3.4.1 Crystallization and Structure Solution of Nitrosoalkane Complexes of Myoglobin

Both Mb/nitrosoethane (Mb(EtNO)) and Mb/nitrosomethane (Mb(MeNO)) were crystallized as stated in the Methods section of this work. The reservoir contained 3.00-3.20 M ammonium sulfate in 100 mM Tris-HCl pH 7.4 and the drop contained 5 μL of Mb(EtNO) or Mb(MeNO) at 30 mg/mL (in 100 mM Tris-HCl pH 7.4) and 5 μL of 3.48 – 3.60 M ammonium sulfate in 100 mM Tris-HCl pH 7.4. As this final condition was worked out, the crystal morphology slowly improved from needles to thin plates to finally plates that were thick enough to work with without damaging them as seen below in Figure 4.5.
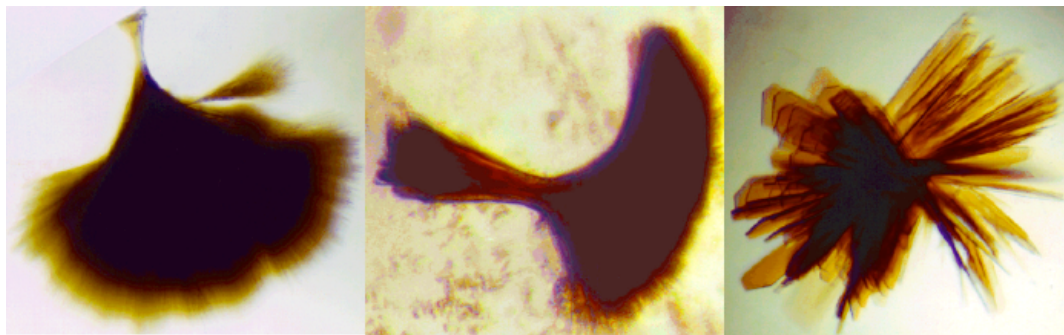

Figure 4.5. Left to right shows the improvement of crystal quality as the crystallization conditions got closer to ideal. The crystals on the right had several leaflets that were used to collect data for myoglobin/nitrosoethane complexes.

Table 4.4 X-ray Data Collection and Refinement Statistics

	Mb(EtNO)	Mb(MeNO)	Mb(PhNO)
Method of prepn.	*cocrystallized*	*cocrystallized*	*Phenylhydroxylamine soak*
Data Collection[a]			
Space Group	$P2_1$	$P2_1$	$P2_1$
Source	In-House	In-House	In-House
λ (Å)	1.5418	1.5418	1.5418
Cell Dimensions			
a, b, c (Å)	35.16, 28.71, 63.03	35.34, 28.74, 63.47	35.25, 28.85, 65.98
β (°)	106.2	106.0	105.63
Resolution(Å)	1.70	1.90	2.0
Mean $I/\sigma(I)$	24.4 (5.1)	16.3 (4.0)	12.5 (4.2)
No. Reflections			
Observed	39336 (3655)	33510 (1904)	42160 (3872)
Unique	13504 (1323)	9925 (974)	8797 (896)
Completeness (%)	99.4 (98.2)	94.5 (66.6)	97.5 (97.5)
R_{merge} (%)[b]	3.8 (20.1)	7.2 (26.4)	7.9 (31.4)
Refinement Statistics[a]			
Resolution Range (Å)	40-1.70	20-1.90	25-2.0
R-factor (%)[c]	19.8 (41.8)	16.2 (23.8)	18.1 (24.1)
R_{free} (%)[d]	22.7 (41.2)	22.9 (24.4)	26.5 (44.4)
r.m.s.d. bond distances (Å)	0.005	0.018	0.024
r.m.s.d. angles (°)	1.414	1.504	1.950
B factor (Å^2)			
Mean	15.76	18.18	26.20
r.m.s.d. mainchain	1.03	0.60	0.80
r.m.s.d. sidechain	1.95	2.01	2.13
Ramachandran Plot[e]			
% Residues in			
Most Favored	93.2	92.5	92.5
Allowed	6.8	7.5	7.5

[a] Values in parentheses correspond to the highest resolution shells for Mb(EtNO) (1.76-1.70 Å), Mb(MeNO) (1.97-1.90 Å) and Mb(PhNO) (2.09-2.00 Å)..

[b] $R_{merge} = \Sigma|I - <I>|/\Sigma(I)$ where I is the individual intensity observation and $<I>$ is the mean of all measurements of I.

[c] R-factor $= \Sigma||F_o| - |F_c||/\Sigma|F_o|$ where F_o and F_c are the observed and calculated structure factors, respectively.

[d] R_{free} is calculated using randomly selected reflections comprising 10% Mb(EtNO) and Mb(MeNO) and 5% Mb(PhNO)) of the data not used throughout refinement.

[e] As calculated using PROCHECK.

4.3.4.1.1　　Horse Heart Myoglobin Nitrosoethane Complex

X-ray crystal structural analysis of hh Mb(EtNO) revealed that the protein retained its normal Mb fold, as observed in the previous structure of hh MbNO. Initial electron density maps clearly indicated the presence of the nitrosoethane ligand, which refined to a final occupancy of 60%.   Although the hh Mb(EtNO) complex is stable in aqueous buffer in air for several weeks (showing no signs of decomposition as judged by UV-vis spectroscopy), it slowly converts to *aqua-met*Mb under our crystallization conditions in the presence of ammonium sulfate as was seen in the spectroscopic data presented above.   Suitable-sized crystals took ~5 days to form, during which a ~40% conversion to *aqua*-metMb occurred.   This partial occupancy of the EtNO ligand in the hh Mb(EtNO) crystal structure is consistent with the spectroscopic data that was presented above.

The EtNO ligand is N-bound to the ferrous center with an Fe-N(EtNO) distance of 2.14 Å. The Fe-N(His93) distance is 2.14 Å, and the Fe-N(porphyrin) distances fall in the 1.98-2.00 Å range. The axial (His93)N-Fe-N(EtNO) angle is 166°, and the Fe atom is positioned in the mean porphyrin plane. The N-O distance is 1.26 Å, and the Fe-N-O and C-N-O angles are 117° and 119°, respectively. Unlike the case for hh MbNO, however, the NO moiety in Mb(EtNO) is oriented towards the distal His64 residue with a 2.74 Å distance between the nitrosoethane O atom and the N^ε atom of His64, suggestive of a

hydrogen-bonding interaction between these groups. The ethyl group of the EtNO ligand is oriented in the direction in-between the hydrophobic residues Phe43 and Ileu107.

The closest non-bonding interactions of the ethyl group of EtNO with the distal residues of the protein are between the C2 atom of EtNO and Leu29 (3.2 Å) and that between the C1 atom of EtNO and Val68 (3.5 Å). There is a considerable off axis tilt of the nitrosoethane ligand to the 4-N heme normal. The angle from the heme normal through the Fe to the N of EtNO is 18°, and the CNO plane of the ligand is tilted a further 3° off of the heme normal to 21°. This unusual tilt will be discussed in detail later in this chapter.

Figure 4.6 (Top) Final model and F_o-F_c omit electron density map contoured at 3σ showing a side view of the heme environment in hh Mb(EtNO). The dashed yellow line represents a 2.73 Å distance between the N^ε atom of the distal His64 residue and the O atom of the nitrosyl ligand. (Bottom) Top view of the heme environment in hh Mb(EtNO). The EtNO ligand is on the side of the porphyrin ring facing the viewer.

4.3.4.1.2   Horse Heart Myoglobin Nitrosomethane Complex

Suitable-sized crystals took ~5 days to form, during which a ~15-20% conversion to *aqua-met*Mb occurred. This observation is consistent with the partial occupancy of the MeNO ligand determined from the spectroscopic data. The MeNO ligand is N-bound to the ferrous center with an Fe-N(MeNO) distance of 1.96 Å. The Fe-N(His93) distance is 2.18 Å, and the Fe-N(porphyrin) distances fall in the 2.02-2.1 Å range. The axial (His93)N-Fe-N(MeNO) angle is 170°, and the Fe atom is positioned in the mean porphyrin plane. The N-O distance is 1.22 Å, and the Fe-N-O and C-N-O angles are 116° and 121°, respectively. Similarly to the hh Mb(EtNO), the NO moiety in Mb(MeNO) is oriented towards the distal His64 residue with a 2.41 Å distance between the nitrosoethane O atom and the N^ε atom of His64, suggestive of a hydrogen-bonding interaction between these groups. The methyl group of the MeNO ligand is oriented in the direction in-between the hydrophobic residues Phe43 and Ileu107. The closest non-bonding interactions of the methyl group of MeNO with the distal residues of the protein are between the C atom of MeNO and Leu29 (3.6 Å) and that between the C atom of MeNO and Val68 (3.5 Å).
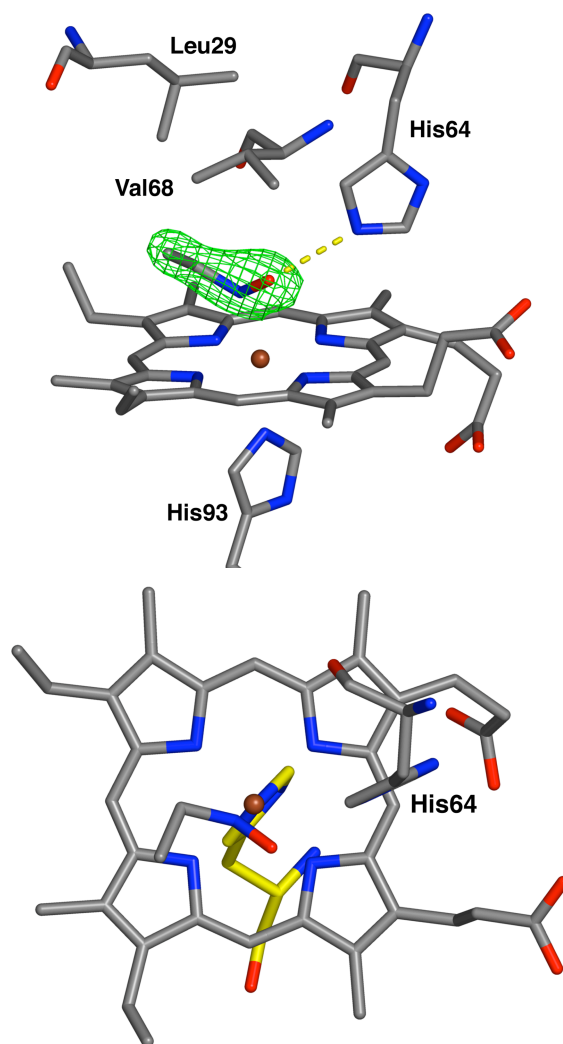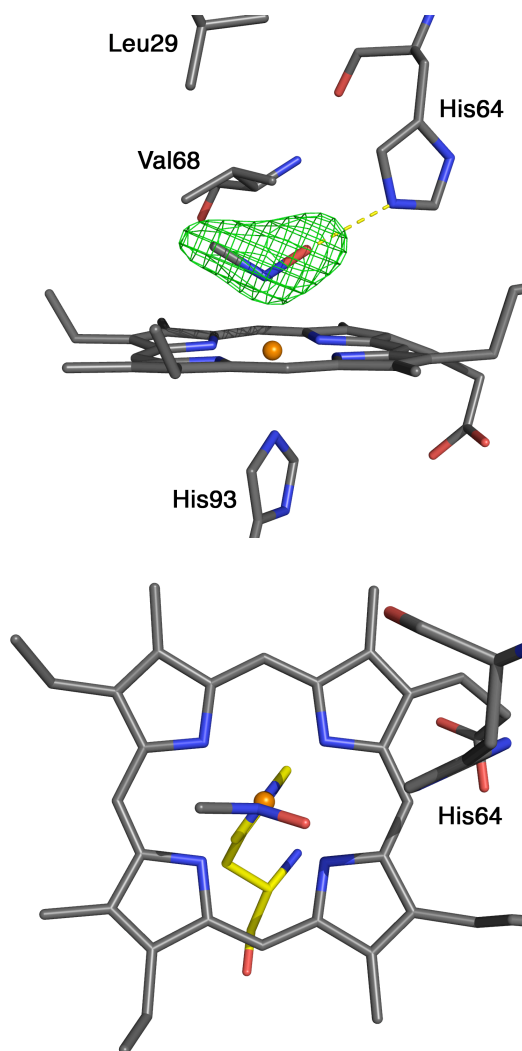
Figure 4.7 (Top) F_o-F_c omit electron density map contoured at 3σ showing a side view of the heme environment in hh Mb(MeNO). The dashed yellow line represents a 2.41 Å distance between the N^{ε} atom of the distal His64 residue and the O atom of the nitrosomethane ligand. (Bottom) Top view of the heme environment in hh Mb(MeNO). The MeNO ligand is on the side of the porphyrin ring facing the viewer. Histidine 93 is colored yellow for clarity.

4.3.4.2 Crystallization and Structure Solution of a Nitrosobenzene Complex of Myoglobin

The Mb(PhNO) complex was crystallized as stated in the Methods section of this work; the reservoir contained 3.00-3.20 M ammonium sulfate in 100 mM Tris-HCl pH 7.4 and the drop contained 5 μL of *met*Mb at 30 mg/mL in 100 mM Tris-HCl pH 7.4 and 5 μL of 3.48 – 3.60 M ammonium sulfate in 100 mM Tris-HCl pH 7.4. The complex was formed by soaking *met*Mb crystals in artificial mother liquor with added phenylhydroxylamine (138 mM). The substrate reduced the ferric iron to ferrous, and itself was oxidized to nitrosobenzene.

X-ray crystal structural analysis of hh Mb(PhNO) revealed that the protein retained its normal Mb fold, with the exception of the distal histidine which is in a different position from that observed in *met*Mb. Initial electron density maps clearly indicated the presence of the nitrosobenzene ligand which refined to full occupancy.

The PhNO ligand is N-bound to the ferrous center with an Fe-N(PhNO) distance of 2.20 Å. The Fe-N(His93) distance is 2.30 Å, and the Fe-N(porphyrin) distances fall in the 2.02-2.13 Å range. The axial (His93)N-Fe-N(PhNO) angle is 158°, and the Fe atom is positioned in the mean porphyrin plane. The N-O distance is 1.20 Å, and the Fe-N-O and C-N-O angles are 127° and 119°, respectively. Similar to the Mb(EtNO), the NO moiety in Mb(PhNO) is oriented towards the distal His64 residue with a 2.91 Å distance between the nitrosoethane O atom and the N^ε atom of His64, suggestive of a hydrogen-bonding interaction between these groups. The phenyl group of the PhNO ligand is oriented in the direction in-between the hydrophobic residues Phe43, Val68 and Ileu107.

The closest non-bonding interactions of the phenyl group of PhNO with the distal residues of the protein are between the C5 and C6 atom of PhNO and Phe 43 (2.71 and 2.87 Å respectively) and that between the C2 atom of PhNO and Val68 (3.30 Å). There is a considerable off axis tilt of the nitrosobenzene ligand to the 4-N heme normal. The angle from the heme normal through the Fe to the N of PhNO is 18°, and the CNO plane of the ligand is tilted a further 3° off of the heme normal to 21°.
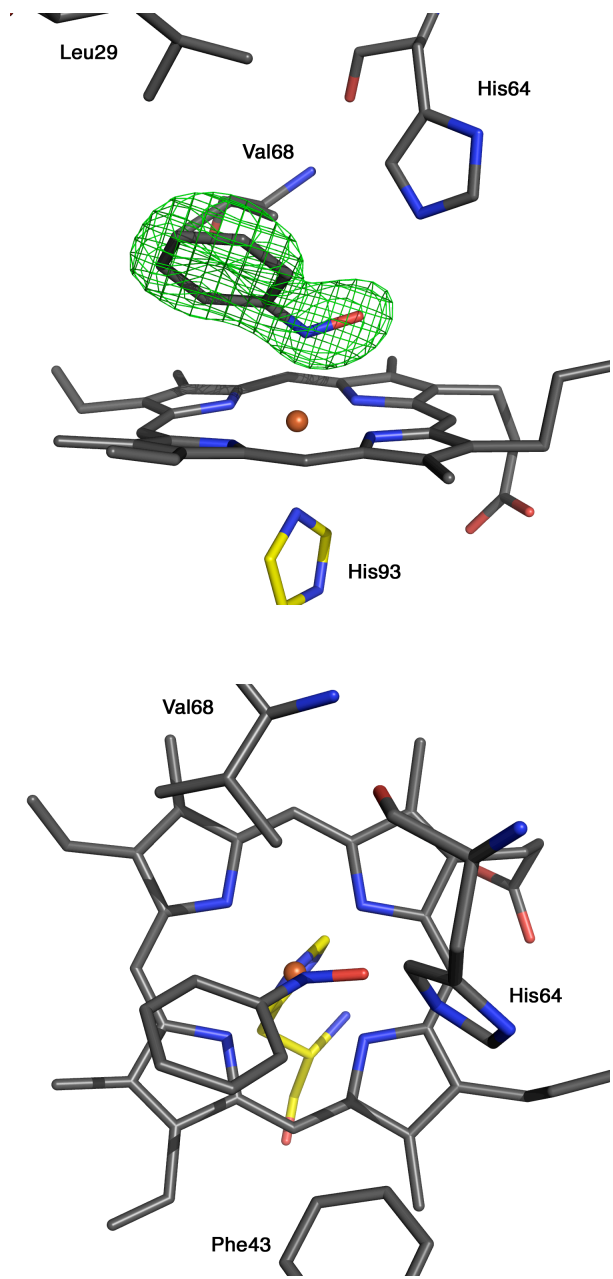
Figure 4.8 (Top) Side view of the structure of hh Mb(PhNO) formed by soaking phenyl hydroxylamine into preformed *met*Mb crystals. Electron density was calculated as an F_o-F_c omit electron density map and is contoured at 3σ. (Bottom) View from above the PhNO ligand showing the orientation in the heme pocket with respect to His93 (shown in yellow)

124

4.4   Discussion

4.4.1   Binding of Nitrosoalkanes to the Heme Domain of Cytochrome P450BM-3

This time course revealed that it was not "only a matter of time" until the complexes were 100% formed and in fact it does not appear that any of the complexes will completely form under the conditions used in these experiments. For the nitrosomethane complex, a maximum of 20% formation was observed at 10 minutes and began to decay thereafter.   For the nitrosoethane complex, a maximum of 35% conversion was observed at 1 hour. The 1-nitrosopropane complex formation was the poorest with only 19% conversion after 1 hour. Finally, the highest extent of formation at 60% was observed with 2-nitrosopropane at 1 hour. The data is presented in Figure 4.9(B). The data also shows that some of the complexes form more quickly under these condition than others, however, these values do not show rates of formation. What this data tells us is that cytochrome P450 BM-3 is a suitable model for other microsomal P450s and their interactions with these ligands because of its similar behavior toward them. Mansuy and coworkers [2] showed very similar results to the ones presented above when studying rat liver microsomal P450s as seen in Figure 4.9.
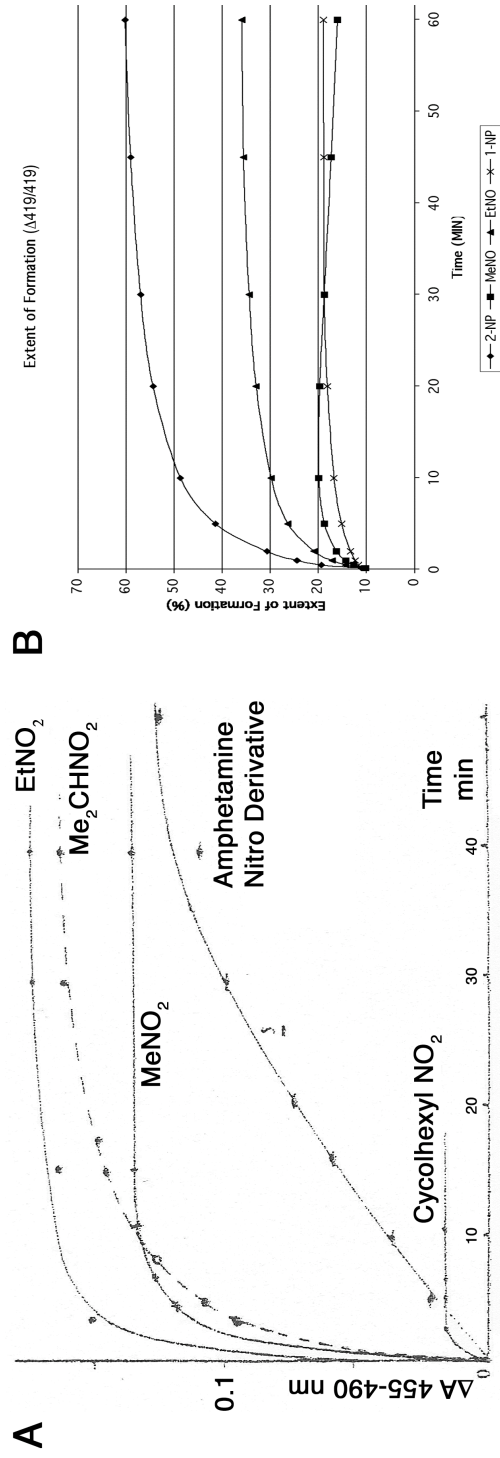
Figure 4.9 Side by side view of graph of Mansuy's 1975 work with nitro compounds and rat liver microsomal P450 and current work with nitro compounds and the heme domain of P450 BM-3. (A) Mansuy's graph [2] showing changes in absorbance of heme RNO compounds made from 5 different RNO_2 precursors. (B) Our work showing extents of formation of four different heme RNO compounds made from RNO_2 precursors. We see that in Mansuy's work the nitroethane showed the most change, which can be correlated to the highest extent of formation, followed by the 2-nitropropane, nitromethane, amphetamine nitro derivative and finally the cyclohexyl nitro compound. In our case with P450 BM-3 the three compounds we have in common show a slightly different order with the highest being the 2-nitropropane, followed by the nitroethane, nitromethane and then the lowest was 1-nitropropane.

126

When one looks closely at the work done by Mansuy [2] and compare it with the work that was done here, we see similar patterns in the binding, however there are some differences. The main difference is in the extent of binding of the ligands to the two proteins. In the rat liver microsomal P450, the ligand with the highest extent of formation is nitrosoethane followed by the 2-nitropropane, nitromethane, amphetamine nitro derivative and finally the cyclohexyl nitro compound. While with P450BM-3, the ligand with the highest extent of formation was 2-nitrosopropane, followed by the nitroethane, nitromethane and then the lowest was 1-nitropropane. These slight differences in the way these ligands bind are most likely due to the active site configuration. While there is no crystal structure of rat liver microsomal P450 available, there are published crystal structures of P450BM-3[1] and we can therefore model one of the RNO compounds into the heme site of a ligand bound form of P450BM-3 [1] to predict a possible conformation of the complex, as seen below in Figure 4.10.
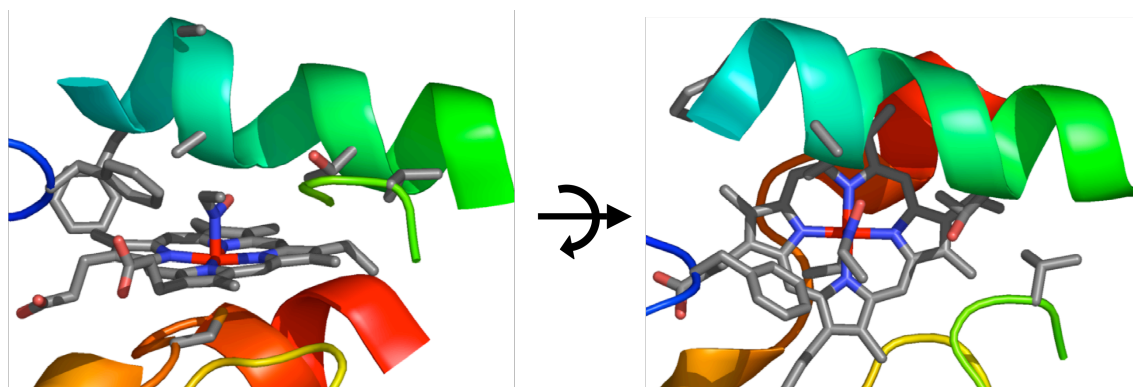

Figure 4.10 Theoretical model of active site of the heme domain cytochrome P450BM-3 [1] complexed with nitrosoethane. There is possible hydrogen bonding with a threonine sidechain as well as hydrophobic interactions with a phenylalanine sidechain.

4.4.2 Comparison of Nitrosoalkanes and Nitrosoarenes Myoglobin Complexes to Porphyrin Model Complexes

As stated in the introduction, the majority of the structural information available for the interactions of nitrosoalkanes and nitrosoarenes with porphyrins is based on the small molecule crystal structures available. The most obvious concern about this is the fact that in the model systems the ligand has little or no interaction with anything outside of the metal. Both of the myoglobin nitrosoalkane complexes [36] and the myoglobin nitrosobenzene complex discussed here, as well as the only other published protein structure, the leghemoglobin nitrosobenzene complex [3], show that there is at least some minimal interaction of the ligand with the heme pocket. However, this discussion will begin by examining the porphyrin complexes that have been used to model this interaction.

Mansuy and coworkers reported the crystal structure of (TPP)Fe(i-PrNO)(i-PrNH$_2$) in 1983 [23]. Recent studies in our lab have employed similar synthetic techniques to synthesize the (OEP)Fe($cyclo$-C$_6$H$_{11}$NO)(1-MeIm) complex to further this area of research. Our group and others have also published structural reports on nitrosoarene complexes with symmetrical iron porphyrins [22, 24, 33]. Our group has previously shown that the mode of binding is determined by the oxidation state of the metal. That study showed that RNO compounds preferred an η^1-N binding mode with ferrous centers and an η^1-O binding mode to ferric centers [22].

Two structures completed in our lab recently that are of particular interest to this work are the (OEP)Fe($cyclo$-C$_6$H$_{11}$NO)(1-MeIm) complex and the (PPDME)Fe(i-PrNO)(1-MeIm) complex. We also observe that in the (OEP)Fe($cyclo$-C$_6$H$_{11}$NO)(1-

MeIm) complex $cyclo$-$C_6H_{11}NO$ ligand is in a staggered conformation with respect to the porphyrin N-Fe-N with a torsion angle of 44.3° which is consistent with previously published (por)Fe(RNO) complexes [22, 24, 33]. We also observed that the orientation of the 1-MeIm (0.85° torsion angle to the porphyrin) is consistent with previously reported structures. In general, with octa-substituted porphyrins the 1-MeIm ligand is close to if not eclipsing the N-Fe-N plane of the porphyrin, and in tetra-substituted porphyrins the 1-MeIm is staggered with a torsion angle of approximately 45° [24, 33].

This structure presents very little porphyrin distortion and the Fe was only slightly out of plane towards the $cyclo$-$C_6H_{11}NO$ ligand. This finding is consistent with Oldfield's claim that bulky groups on both sides of the porphyrin would yield no net distortion [24], however it is inconsistent with more recent work done in our lab with (por)Fe(i-PrNO)(1-MeIm) that shows saddled porphyrins with TTP and OEP and a ruffled porphyrin when using TPP.[33] Therefore other factors may come into play that can cause porphyrin distortions.

The other recent small molecule structure of interest is (PPDME)Fe(i-PrNO)(1-MeIm). This complex has striking similarities to the (OEP)Fe($cyclo$-$C_6H_{11}NO$)(1-MeIm) complex described above, with the only major difference being that this porphyrin is asymmetric and polar, making it more similar to what is seen in biological heme systems. The NO group of i-PrNO is oriented toward the polar side of the porphyrin and the i-PrNO group has again adopted a staggered conformation with respect to the heme (torsion angle of 46.2°) very similar to all other RNO compounds. The 1-MeIm ligand has again adopted a fairly eclipsed orientation with a torsion angle of 12.4°. There is no porphyrin distortion in this structure. When this is compared to the saddled distortion of

the (OEP)Fe(i-PrNO)(1-MeIm) [33] our group previously published, it is evident that the identity of the porphyrin seems to have a larger impact than do the bound ligands, in this case at least.

Both model compounds presented above are fairly good models for Myoglobin RNO complexes. In fact, there are many more similarities than differences in the structures. The Mb(MeNO) and Mb(EtNO) have heme active sites that are strikingly similar to the (OEP)Fe($cyclo$-$C_6H_{11}NO$)(1-MeIm) and (PPDME)Fe(i-PrNO)(1-MeIm) complexes presented above. First, both the MeNO and the EtNO ligands are in similar orientations to the i-PrNO ligand in the model compound with a staggered conformation with respect to the heme (54.5˚ and 64.2˚ respectively), the NO group of MeNO is directed toward the polar side of the porphyrin (exterior of the protein) and the methyl group is oriented toward the nonpolar portion of the heme (which is in the heme pocket). The 1-MeIm ligand in the model compound is a good mimic for histidine and both of the orientation are along a N-Fe-N plane, although the histidine in hh Mb is ~90˚ away from the 1-MeIm on the other N-Fe-N plane.

When we compare the hh Mb(PhNO) structure and the leg Hb(PhNO) structure to that of Godbout and coworkers (OEP)Fe(PhNO)(1-MeIm) [24], we see that both of the protein structures are very similar to the small molecule structure. In the small molecule structure as well as in both protein structures (hh Mb(PhNO) and leg Hb(PhNO)) we see that the nitrosobenzene ligand has a (por)N-Fe-N-O torsion angle of ~45˚. In the legHb complex the N(por)-Fe-N-C torsion angle is 46˚ however the NO group is tilted off axis so the N(por)-Fe-N-O torsion angle is 24˚. In the hh Mb complex the N(por)-Fe-N-C torsion angle is 16.9° because this group is tilted off axis and the NO group has a torsion

angle (N(por)-Fe-N-O) of 40°. It is interesting to note that in both of the protein structures the group of the ligand that deviates the most from the model compound is the side that is oriented toward the protein pocket, not the outside of the protein, implying that the protein pocket severely affects the orientation of the ligand and thus, the importance of the protein pocket in determining the ligand orientation.
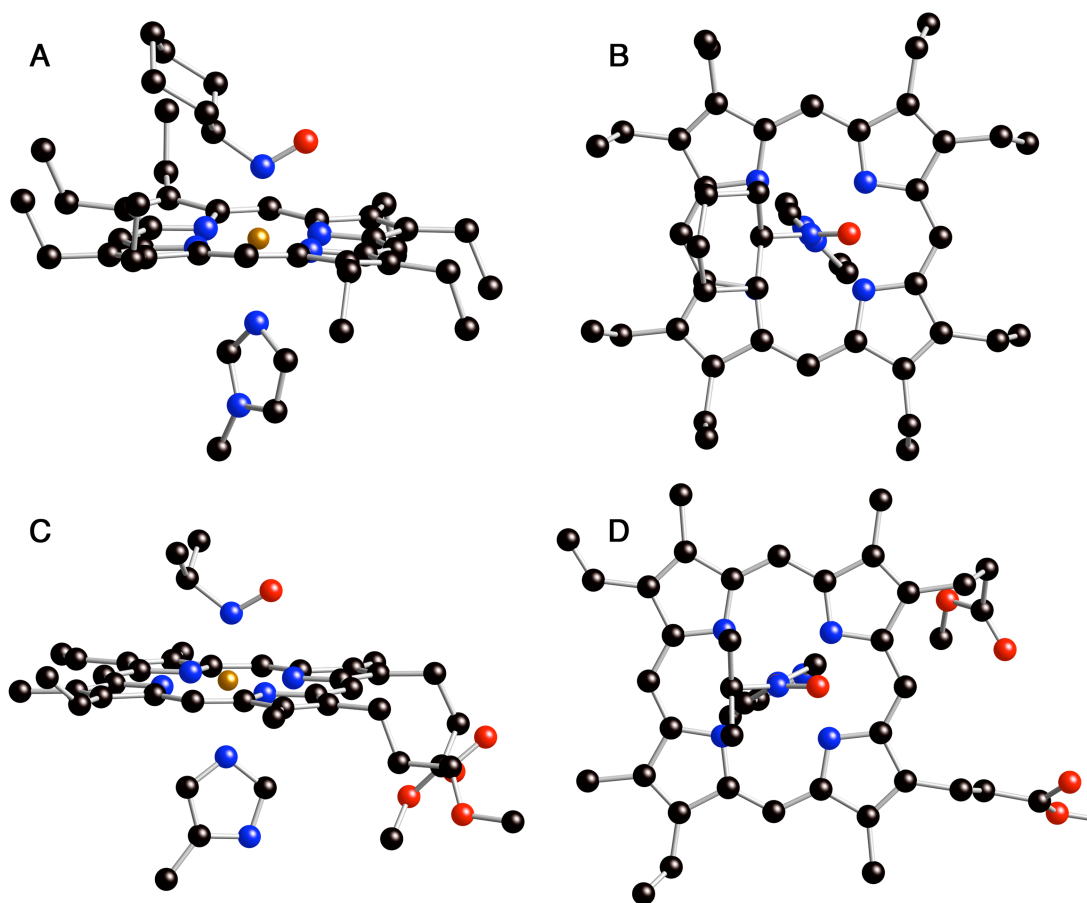

Figure 4.11 Side and top views of the two (OEP)Fe(RNO)(1-MeIm) model compounds discussed above. (A) Side view of (OEP)Fe(*cyclo*-$C_6H_{11}NO$)(1-MeIm) (B) Top View of (OEP)Fe(*cyclo*-$C_6H_{11}NO$)(1-MeIm), showing the orientation of both the RNO and the proximal 1-MeIm. (C) Side view of (PPDME)Fe(*i*-PrNO)(1-MeIm) and (D) top view of (PPDME)Fe(*i*-PrNO)(1-MeIm) again showing the orientation of both the RNO and the proximal 1-MeIm. From both top views it can be seen that the 1-MeIm is sitting on the N-Fe-N plane, similarly to what is seen in hh Mb and the RNO ligand is bisecting and ∠N-Fe-N with a torsion angle of ~45°. The compounds were prepared by Christal Sohl and the structure solutions were performed by Masood Khan.

4.4.3 Comparison of the Wild Type Horse Heart Myoglobin Nitrosoalkane and Nitrosoarene Complexes

4.4.3.1   Mb(Nitrosoalkane) Adducts

To the best of our knowledge, the X-ray crystal structure of hh Mb(EtNO) (Figure 4.6) is the first such determination to be reported for a nitrosoalkane complex of a heme protein. Results from model heme-nitrosoalkane complexes predict an N-binding mode in ferrous porphyrins, in which the RNO ligand acts as a π-acid ligand [16]. Selected structural data for ferrous nitrosoalkane and nitrosoarene hemes are collected in Table 4.5.

Table 4.5 X-ray Structural Data for Nitrosoalkane and Nitrosoarene Ferrous Porphyrin and Heme Complexes

	Fe-N(O) (Å)	N-O (Å)	∠Fe-N-O (°)	Fe-L(ax) (Å)	*ref*
nitrosoalkane					
(TPP)Fe(*i*-PrNO)(1-MeIm)	1.810(3)	1.245(4)	122.4(2)	2.046(3)	[47]
(TPP)Fe(*i*-PrNO)(*i*-PrNH$_2$)[a]	1.862(14)	1.26(2)	124(1)	2.105(15)	[23]
	1.867(13)	1.26(2)	124(1)	2.094(13)	
hh Mb(EtNO)	2.14	1.23	123.08	2.14	[36]
hh Mb(MeNO)	1.95	1.22	115.8	2.18	*this work*
nitrosoarene					
(TPP)Fe(PhNO)(py)	1.819(3)	1.249(4)	123.9(3)	2.106(3)	[24]
(TPP)Fe(PhNO)(1-MeIm)[a]	1.800(8)-	1.254(8)-	122.8(3)-	2.03(1)	[24]
	1.812(3)	1.267(3)	124.8(7)		
(TPP)Fe(ONC$_6$H$_4$NMe$_2$-*p*)(py)	1.859(6)	1.252(6)	119.8(5)	2.095(5)	[24]
(OEP)Fe(PhNO)(1-MeIm)[a]	1.809(4)	1.269(5)	122.8(3)	2.092(4)	[24]
	1.802(4)	1.258(4)	123.8(3)	2.094(4)	
(TPP)Fe(PhNO)$_2$	1.874(2)	1.237(3)	123.6(2)		[22]
	1.899(2)	1.227(3)	123.4(2)		
leg Hb(PhNO)[b]	2.10	1.26	120.6	2.17	[25]
Hh Mb(PhNO)	2.20	1.20	127	2.30	*this work*

[a] Two independent molecules in the asymmetric unit.

[b] The structure was determined at 2.0 Å resolution. Metrical data were obtained using coordinates from the Brookhaven Protein Data Bank [41].

The structure of hh Mb(EtNO) reveals an N-bound nitrosoalkane ligand as shown in Figure 4.6. In high-resolution X-ray crystal structures of model heme complexes containing nitrosoalkane or nitrosoarene ligands, the Fe-N(nitroso) distances are found to be generally shorter (1.8-1.9 Å) than the *trans* Fe-N(axial) bond lengths (2.0-2.1 Å). While this is not the case for hh Mb(EtNO), the Fe-N(nitroso) and the *trans* Fe-N(His) distances are both 2.14 Å, the distances in the hh Mb(MeNO) do fit within these bounds, with a Fe-N(nitroso) distance of 1.95 Å and a Fe-N(histidine) distance of 2.18 Å. The axial distances in hh Mb(EtNO) are, however, similar to those determined in the structure of the nitrosobenzene complex leg Hb(PhNO) (2.10 and 2.17 Å, respectively) [3].

The ethyl group of the EtNO and the methyl group of MeNO ligands are positioned on the side of the distal pocket away from the His64 toward the interior hydrophobic core of the protein. The axial ligand orientation of the EtNO and MeNO groups does appear to be influenced by the distal His64 residue, whose presence causes the CNO plane to be tilted off of the heme normal by 21° in the case of EtNO and 10.5° in the case of MeNO (Figure 4.12) in a direction toward Phe 43, and the bound nitrogen is tilted 18° and 12° respectively, to the heme normal calculated from the heme 4-N-plane. The result is a hydrogen-bonding distance of 2.74 Å between the nitroso O atom and the N^ε atom of His64 in the EtNO complex and 2.41 Å in the MeNO complex.
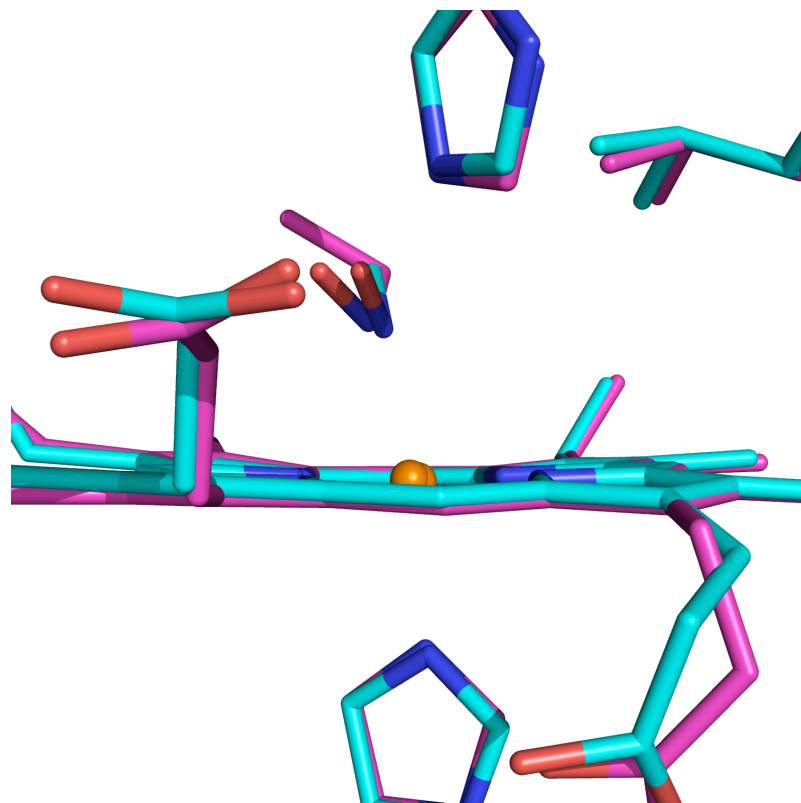
Figure 4.12 Overlay of the heme sites in Mb(EtNO) (magenta) and Mb(MeNO) (cyan) shown from the propionate side of the heme. This orientation shows the off-axis tilt that the ligands are forced into because of the hydrogen bonding of His 64.

In contrast, the dominant hydrogen-bonding interaction between the nitrosyl group in hh MbNO and the distal His64 is via the nitrosyl N-atom, although the participation of nitrosyl O atoms in distal hydrogen-bond interactions has been observed in the NO adducts of cyt c' from *A. xylosoxidans* (with Arg124) [48], cyt cd_1 nitrite reductase from *P. aeruginosa* (with His369) [49], and sulfite reductase heme protein (with Arg153 and Lys215) [50]. As stated before, the only other structure of a C-nitroso compound bound to a heme protein is that of nitrosobenzene bound to leghemoglobin and although the ligands are similar between the hh Mb(EtNO) and the leghemoglobin/nitrosobenzene (leg Hb(PhNO)) structures there is no hydrogen bonding between the PhNO and any of the heme pocket residues because of the orientation of the ligand [3]. In both the nitrosoethane and nitrosomethane structures, the R-group is oriented toward the interior of the protein, however in the leg Hb(PhNO) structure, the phenyl group is oriented toward the distal histidine and the oxygen from the NO directed toward the interior of the protein. This forces the distal histidine to be oriented in a position away from the heme pocket, in the "flipped out" position. The remainder of the heme pocket has no residues that are capable of hydrogen bonding to the ligand. Even without the influence of hydrogen bonding the PhNO ligand does not sit perfectly linearly on top of the heme it is tilted of axis by 10° from the heme normal and the CNO plane is 13° of the heme normal, showing that the histidine is not the only residue in the heme pocket that affects the orientation of the RNO ligands.
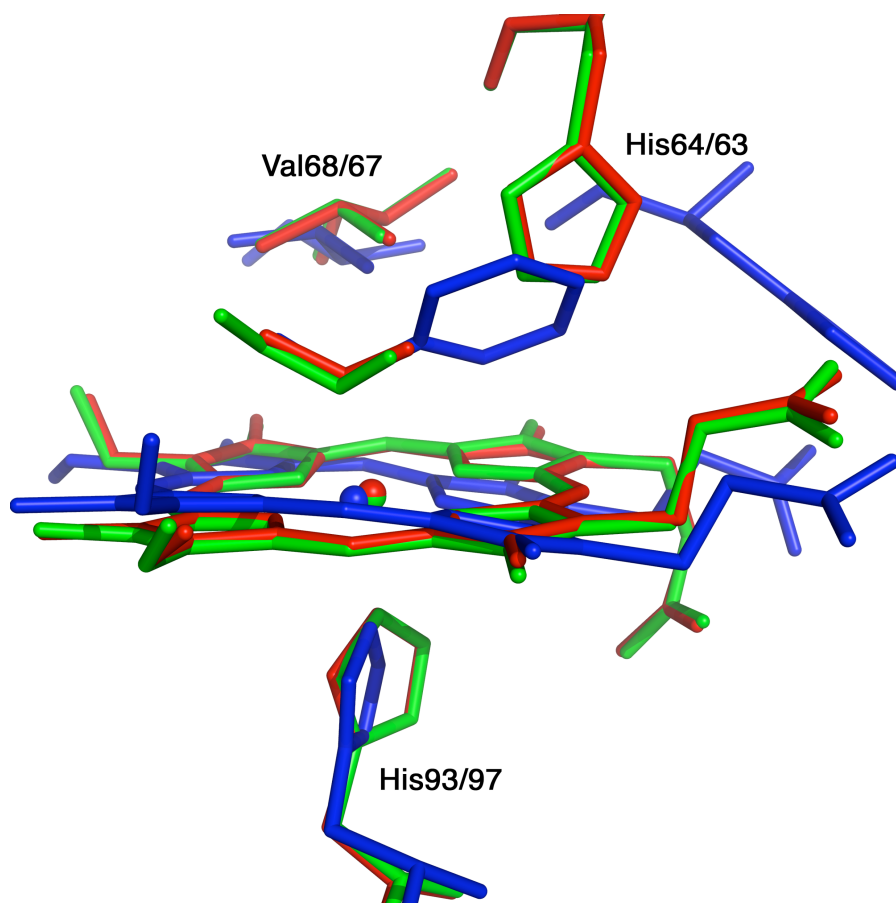
Figure 4.13   Overlay of Mb(EtNO) (green), Mb(MeNO) (red), and leg Hb(PhNO) (blue) showing the similar orientation of the two nitrosoalkane structures and the opposite orientation of the nitrosobenzene in the leghemoglobin structure. The R-group of the EtNO and MeNO structures are oriented to the left, the core of the molecule, allowing for hydrogen bonds between the ligands O atom and N^{ε} of His64. In the nitrosobenzene structure the ligand is oriented to the right, toward the outside of the molecule causing the distal histidine to flip out of the pocket and thus prevents hydrogen bonding.

The axial (His93)N-Fe-N(Et/MeNO) angle of 166° and 170° respectively, both deviate from strict linearity. However, off-axis tilts of axial ligands from the heme normal are frequently observed in natural and model heme complexes, and these off-axis tilts have been analyzed computationally, structurally, and spectroscopically by others [51-59].

4.4.3.2   Mb(PhNO) Complex

Over the years there has been a great deal of interest in the binding of aromatic

amine metabolites and nitro compounds to heme proteins. The effects of nitrobenzene

poisoning, known as "nitrobenzol" at the time, has been studied since 1878 [21, 26].   The

intermediate aromatic C-nitroso compounds are proposed to be involved in a variety of

reactions *in vivo* [8, 60, 61]. The published literature on all of the interactions of nitrosoarenes

and heme model systems and heme proteins are reviewed in a *Chemical Reviews* article

published in 2002 by Lee et al. [16].

To date, with the exception of the legHb(PhNO) protein structure, all of the

research looking at the interactions of nitrosoarenes and heme proteins has been by

spectroscopy. This leaves a large void with respect to the structural aspects of these

complexes.   As was discussed in the previous section when comparing the leg

Hb(PhNO) structure to that of the two Mb(nitrosoalkane) structures, the nitrosobenzene

ligand in the leg Hb structure is oriented opposite to the nitrosoalkane ligands.   We

believe that this orientation was favored because of the bulk of the phenyl ring. Thus, the

structure that was determined of the hhMb(PhNO) complex, described in this thesis was

somewhat of a surprise. We believe that because of the relatively smaller size of the

heme pocket with hh Mb vs. leg Hb that the ligand would be in the same orientation. As

can be seen in Figure 4.15, which is the overlay of the two complexes, hh Mb(PhNO) in

magenta and leg Hb(PhNO) in cyan, the orientation of the two ligands in the heme pocket

are approximately 180° apart. The major difference in these two orientations is that the

ligand in the hh Mb(PhNO) structure has a potential hydrogen bond with the His64

residue. In both proteins the heme pocket itself is hydrophobic, thus there are no side

chains in the pocket that are available for hydrogen bonding with the ligand in the orientation observed for the leg Hb structure.

Something else that is evident in the hh Mb(PhNO) structure that was soaked with a higher concentration of phenylhydroxylamine is that there are two disordered phenylhydroxylamine molecules at the mouth of the heme pocket, although we cannot be fully certain that these are phenylhydroxylamine ligands and not PhNOs. However nitrosobenzene is not very soluble in the monomeric form in water, so it is likely that the additional ligands are phenylhydroxylamine.
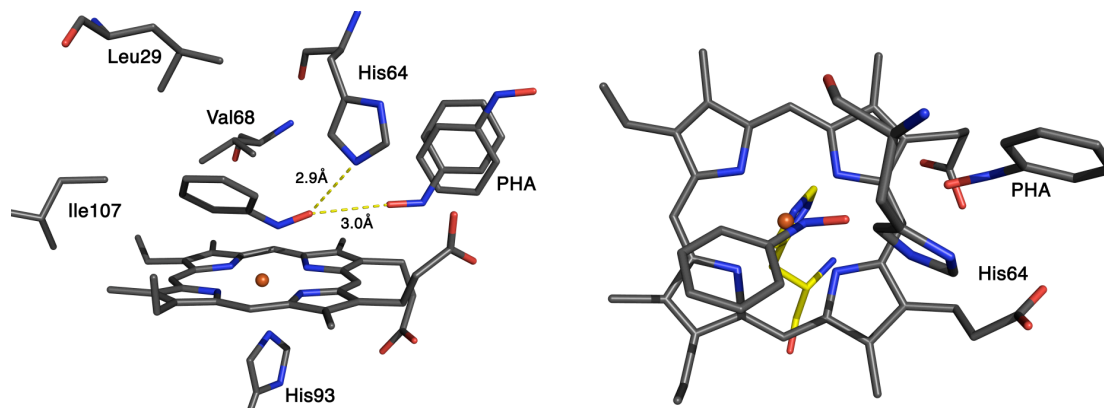

Figure 4.14 Side and top views of hh Mb(PhNO) formed with higher concentration of phenylhydroxylamine (PHA) showing additional PHA at the mouth of the heme pocket.

One potential significance of this new structure is that in proteins that more resemble the

hh Mb heme pocket than the leg Hb heme pocket the binding of nitrosobenzene could be

stronger than was previously believed because of the addition of the hydrogen bond that
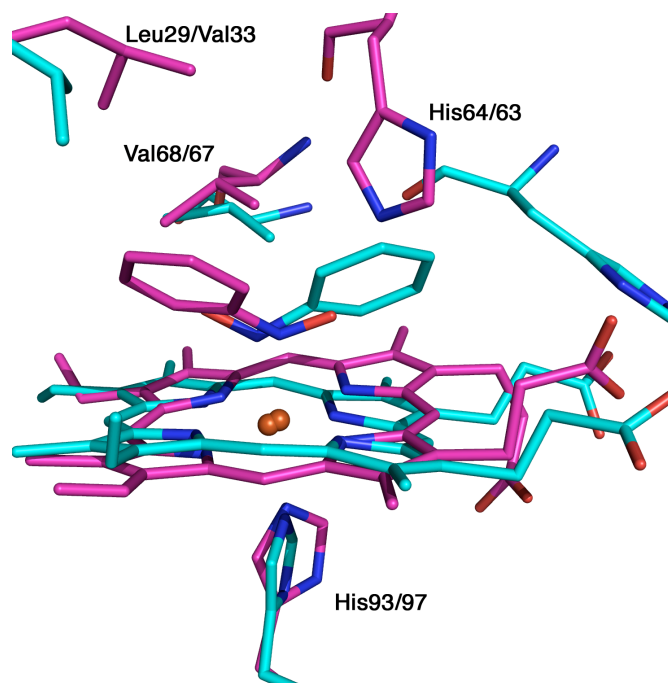
is not available in leg Hb.

Figure 4.15 Overlay of the two known heme protein nitrosobenzene structures. Shown in cyan is the leg Hb(PhNO) complex and in magenta is the hh Mb(PhNO) complex. The major difference between the two complexes is the orientation of the ligand in the heme pocket. In the leg Hb(PhNO) structure the phenyl ring is oriented toward the distal histidine, eliminating the possibility of hydrogen bonds. In the hh Mb(PhNO) the phenyl group is oriented toward the interior of the heme pocket allowing a hydrogen bond to the distal histidine.

4.5   Conclusions

RNO compounds are now recognized as important ligands to biological hemes because of their ability to bind heme and inhibit protein function [12, 14, 62]. Here we discuss the first structural studies reported of the interactions of any nitrosoalkane with a biological heme. We have definitively shown that the interaction with the ferrous ion is through the nitrogen of the RNO ligand as is observed in model complexes. We have also observed through both the crystal structures of the Mb(EtNO) complex and the Mb(MeNO) complex and the UV/Vis studies performed on the interactions of simple alkyl RNO compounds with cytochrome P450 BM-3hd that the R-group of the ligand does impact the binding and stability of the complexes.

Additionally, we have determined the crystal structure of horse heart myoglobin complexed with nitrosobenzene and compared it with the only other macromolecular crystal structure involving a heme/RNO interaction, specifically the leghemoglobin nitrosobenzene complex [3]. Our complex showed a binding mode that was oriented in the opposite direction to the previous legHb(PhNO) structure and thus had the ability to hydrogen bond to histidine 64. The comparison of these three structures, hh Mb(MeNO), hh Mb(EtNO) and hh Mb(PhNO), have shown that the formation of RNO complexes through two different synthetic routes give similar structures.

4.6 References

1. Haines, D. C.; Tomchick, D. R.; Machius, M.; Peterson, J. A., Pivotal Role of Water in the Mechanism of P450BM-3. *Biochemistry* **2001,** 40, 13456-13465.

2. Mansuy, D.; Beaune, P.; Chottard, J. C.; Bartoli, J. F.; Gans, P., The Nature of the "455 nm Absorbing Complex" Formed During the Cytochrome P450 Dependent Oxidative Metabolism of Amphetamine. *Biochem. Pharmacol.* **1976,** 25, 609-612.

3. Kuranova, I. P.; Teplyakov, A. V.; Obmolova, G. V.; Voronova, A. A.; Popov, A. N.; Kheiker, D. M.; Arutyunyan, E. G., X-ray Diffraction Study of Leghemoglobin in Complexes with Nitrosobenzene, Nicotinic Acid, and Acetate, Fluoride, and Cyanide Ions. *Bioorg. Khim.* **1982,** 8, 1625-1636 (in Russian). *Chem. Abstr.* CA98:48994. PDB codes 1LH7 and 2LH7.

4. Ullrich, V.; Schnabel, K. H., Formation and Binding of Carbanions by Cytochrome P-450 of Liver Microsomes. *Drug. Metab. Dispos.* **1973,** 1, (1), 176-183. *Chem. Abs.* **81**:164001z.

5. Eyer, P.; Kampffmeyer, H.; Maister, H.; Rosch-Oehme, E., Biotransformation of Nitrosobenzene, Phenylhydroxylamine, and Aniline in the Isolated Perfused Rat Liver. *Xenobiotica* **1980,** 10, (7/8), 499-516.

6. Ricoux, R.; Boucher, J.-L.; Mansuy, D.; Mahy, J.-P., Formation of Iron(II) Nitrosoalkane Complexes: A New Activity of Microperoxidase 8. *Biochem. Biophys. Res. Commun.* **2000,** 278, 217-223.

7. Ellis, M. K.; Foster, P. M. D., The Metabolism of 1,3-Dinitrobenzene by Rat Testicular Subcellular Fractions. *Toxicol. Lett.* **1992,** 62, 201-208.

8. O'Brien, P. J.; Wong, W. C.; Silva, J.; Khan, S., Toxicity of Nitrobenzene Compounds Towards Isolated Hepatocytes: Dependence on Reduction Potential. *Xenobiotica* **1990,** 20, (9), 945-955.

9. Kiese, M., Oxidation of Aniline to Nitrosobenzene *In Vivo. Arch. Exptl. Pathol. Pharmakol.* **1959,** 236, 19-20. *Chem. Abs.* **53**:9476b.

10. Werringloer, J.; Estabrook, R. W., Heterogeneity of Liver Microsomal Cytochrome P-450: The Spectral Characterization of Reactants with Reduced Cytochrome P-450. *Arch. Biochem. Biophys.* **1975,** 167, 270-286.

11. James, R. C.; Franklin, M. R., Comparisons of the Formation of Cytochrome P-450 Complexes Absorbing at 455 nm In Rabbit and Rat Microsomes. *Biochem. Pharmacol.* **1975,** 24, 835-838.

12. Mahy, J. P.; Mansuy, D., Formation of Prostaglandin Synthase-Iron-Nitrosoalkane Inhibitory Complexes upon in Situ Oxidation of N-Substituted Hydroxylamines. *Biochemistry* **1991,** 30, 4165-4172.

13. Renodon, A.; Boucher, J.-L.; Wu, C.; Gachhui, R.; Sari, M.-A.; Mansuy, D.; Stuehr, D., Formation of Nitric Oxide Synthase-Iron(II) Nitrosoalkane

Complexes: Severe Restriction of Access to the Iron(II) Site in the Presence of Tetrahydrobiopterin. *Biochemistry* **1998,** 37, (18), 6367-6374.

14. Mansuy, D.; Rouer, E.; Bacot, C.; Gans, P.; Chottard, J. C.; Leroux, J. P., Interaction of Aliphatic *N*-Hydroxylamines with Microsomal Cytochrome P450: Nature of The Different Derived Complexes and Inhibitory Effects on Monooxygenases Activities. *Biochem. Pharmacol.* **1978,** 27, 1229-1237.

15. Mansuy, D.; Chottard, J. C.; Chottard, G., Nitrosoalkanes as Fe(II) Ligands in the Hemoglobin and Myoglobin Complexes Formed from Nitroalkanes in Reducing Conditions. *Eur. J. Biochem.* **1977,** 76, 617-623.

16. Lee, J.; Chen, L.; West, A. H.; Richter-Addo, G. B., Interactions of Organic Nitroso Compounds with Metals. *Chem. Rev.* **2002,** 102, (4), 1019-1065.

17. Mansuy, D.; Beaune, P.; Cresteil, T.; Bacot, C.; Chottard, J.-C.; Gans, P., Formation of Complexes between Microsomal Cytochrome. *Eur. J. Biochem.* **1978,** 86, 573-579.

18. Eyer, P.; Gallemann, D., Reactions of Nitrosoarenes with SH Groups. In *The Chemistry of Amino, Nitroso, Nitro and Related Groups. Supplement F2*, Patai, S., Ed. John Wiley and Sons Ltd.: Chichester, 1996; pp 999-1039. Chapter 23.

19. Ringe, D.; Turesky, R. J.; Skipper, P. L.; Tannenbaum, S. R., Structure of the Single Stable Hemoglobin Adduct Formed by 4-Aminobiphenyl *in Vivo*. *Chem. Res. Toxicol.* **1988,** 1, 22-24.

20. Loeb, R. F.; Bock, A. V.; Fitz, R., Acute Nitrobenzene Poisoning, With Studies On The Blood in Two Cases. *Am. J. Med. Sci.* **1921,** 161, 539-546. CA15:1761.

21. Filehne, W., *Arch. Exptl. Pathol. Pharmakol.* **1878,** 9, 329.

22. Wang, L.-S.; Chen, L.; Khan, M. A.; Richter-Addo, G. B., The First Structural Studies of Nitrosoarene Binding to Iron-(II) and -(III) Porphyrins. *Chem. Commun.* **1996**, 323-324.

23. Mansuy, D.; Battioni, P.; Chottard, J.-C.; Riche, C.; Chiaroni, A., Nitrosoalkane Complexes of Iron-Porphyrins: Analogy between the Bonding Properties of Nitrosoalkanes and Dioxygen. *J. Am. Chem. Soc.* **1983,** 105, (3), 455-463.

24. Godbout, N.; Sanders, L. K.; Salzmann, R.; Havlin, R. H.; Wojdelski, M.; Oldfield, E., Solid State NMR, Mossbauer, Crystallographic, and Density Functional Theory Investigation of Fe-O_2 and Fe-O_2 Analogue Metalloporphyrins and Metalloproteins. *J. Am. Chem. Soc.* **1999,** 121, 3829-3844.

25. Vainshtein, B. K.; Harutyunyan, E. H.; Kuranova, I. P.; Borisov, V. V.; Sosfenov, N. I.; Pavlovsky, A. G.; Grebenko, A. I.; Konareva, N. V., Structure of Nitrosobenzene-Leghemoglobin. *Protein Data Bank* **1982,** Structure 1LH7 and 2LH7.

26. Murayama, M., The Combining Power of Normal Human Hemoglobin for Nitrosobenzene. *J. Biol. Chem.* **1960,** 235, (4), 1024-1028.

27. Gibson, Q. H., The Reactions of Some Aromatic *C*-Nitroso Compounds with Haemoglobin. *Biochem. J.* **1960,** 77, 519-526.

28. Hoffstrom, I.; Orrenius, S., The Interaction of Various *N*-Substituted Amphetamines with Cytochrome P-450 of Rabbit Liver Microsomes. *FEBS Lett.* **1973,** 31, (2), 205-208.

29. Franklin, M. R., The Formation of a 455 nm Complex During Cytochrome P-450-Dependent *N*-Hydroxyamphetamine Metabolism. *Mol. Pharmacol.* **1974,** 10, (6), 975-985.

30. Stone, J. R.; Marletta, M. A., The Ferrous Heme of Soluble Guanylate Cyclase: Formation of Hexacoordinate Complexes with Carbon Monoxide and Nitrosomethane. *Biochemistry* **1995,** 34, (50), 16397-16403.

31. Lefevre-Groboillot, D.; Dijols, S.; Boucher, J.-L.; Mahy, J.-P.; Ricoux, R.; Desbois, A.; Zimmerman, J.-L.; Mansuy, D., N-Hydroxyguanidines as New Heme Ligands: UV-Visible, EPR, and Resonance Raman Studies of the Interaction of Various Compounds Bearing a C=NOH Function with Microperoxidase-8. *Biochemistry* **2001,** 40, 9909-9917.

32. Fukuto, J. M.; Brady, J. F.; Burstyn, J. N.; VanAtta, R. B.; Valentine, J. S.; Cho, A. K., Direct Formation of Complexes between Cytochrome P-450 and Nitrosoarenes. *Biochemistry* **1986,** 25, (9), 2714-2719.

33. Sohl, C. D.; Lee, J.; Alguindigue, S. S.; Khan, M. A.; Richter-Addo, G. B., Synthesis and Solid-State Molecular Structures of Nitrosoalkane Complexes of Iron Porphyrins Containing Methanol, Pyridine, and 1-Methylimidazole Ligands. *J. Inorg. Biochem.* **2004,** 98, 1238-1246.

34. Copeland, D. M., Crystal Sohl, Ann H. West, George B. Richter-Addo, Crystal structures of the nitrosomethane and nitrosobenzene complexes of horse heart myoglobin and Two Small Molecule Nitrosoalkane Complexes. *In Prep.* **2006**

35. Li, H.; Darwish, K.; Poulos, T. L., Characterization of Recombinant Bacillus megaterium Cytochrome P450 BM3 and Its Two Functional Domains. *J. Biol. Chem.* **1991,** 266, (18), 11909-11914.

36. Copeland, D. M.; West, A. H.; Richter-Addo, G. B., Crystal Structures of Ferrous Horse Heart Myoglobin Complexed with Nitric Oxide and Nitrosoethane. *Proteins: Struct. Func. Genet.* **2003,** 53, 182-192.

37. Kamm, O., Organic Syntheses. In *b-Phenylhydroxylamine*, 2nd ed.; Gilman, H., Ed. John Wiley and Sons, Inc.: New York, Vol. 1, pp 445-447.

38. Pflugrath, J., The Finer Things in X-Ray Diffraction Data Collection. *Acta Crystallogr., Section D* **1999,** D55, 1718-1725.

39. Jacobson, R. *CrystalClear*, Rigaku Corporation: 1999.

40. Chu, K.; Vojtchovsky, J.; McMahon, B. H.; Sweet, R. M.; Berendzen, J.; Schlichting, I., Structure of a Ligand-Binding Intermediate in Wild-Type Carbonmonoxy Myoglobin. *Nature* **2000,** 403, 921-923.

41. Berman, H. M.; Westbrook, J.; Feng, Z.; Gilliland, G.; Bhat, T. N.; Weissig, H.; Shindyalov, I. N.; Bourne, P. E., The Protein Data Bank. *Nucleic Acids Research* **2000,** 28, 235-242.

42. Maurus, R.; Overall, C. M.; Bogumi, R.; Luo, Y.; Mauk, A. G.; Smith, M.; Brayer, G. D., A Myoglobin Variant with a Polar Substitution in a Conserved Hydrophobic Cluster in the Heme Binding Pocket. *Biochem. Biophys. Acta* **1997,** 1341, 1-13.

43. Maurus, R.; Bogumi, B.; Nguyen, N. T.; Mauk, A. G.; Brayer, G., Structural and Spectroscopic Studies of Azide Complexes of Horse Heart Myoglobin and the His64Thr Variant. *Biochem. J.* **1998,** 322, 67-74.

44. Bogumi, R.; Maurus, R.; Hildebrand, D. P.; Brayer, G. D.; Mauk, A. G., Origin of the pH-Dependent Spectroscopic Properties of Pentacoordinate Metmyoglobin Variants. *Biochemistry* **1995,** 34, 10483-10490.

45. Lloyd, E.; Burk, D. L.; Ferrer, J. C.; Maurus, R.; Doran, J.; Carey, P. R.; Brayer, G. D.; Mauk, A. G., Electrostatic Modification of the Active Site of Myoglobin: Characterization of the Proximal Ser92Asp Variant. *Biochemistry* **1996,** 35, 11901-11912.

46. Hildebrand, D. P.; Burk, D. L.; Maurus, R.; Ferrer, J. C.; Brayer, G. D.; Mauk, A. G., The Proximal Ligand Variant His93Tyr of Horse Heart Myoglobin. *Biochemistry* **1995,** 34, 1997-2005.

47. Sohl, C. D.; Lee, J.; Richter-Addo, G. B. In 225th National Meeting of the American Chemical Society; March 23-27, 2003, New Orleans, LA, U.S.A., 2003; New Orleans, LA, U.S.A., 2003; p INORG 166.

48. Lawson, D. M.; Stevenson, C. E. M.; Andrew, C. R.; Eady, R. R., Unprecedented Proximal Binding of Nitric Oxide to Heme: Implications for Guanylate Cyclase. *EMBO Journal* **2000,** 19, (21), 5661-5671.

49. Nurizzo, D.; Cutruzzola, F.; Arese, M.; Bourgeois, D.; Brunori, M.; Cambillau, C.; Tegoni, M., Conformational Changes Occurring upon Reduction and NO Binding in Nitrite Reductase from *Psudomonas aeruginosa*. *Biochemistry* **1998,** 37, (40), 13987-13996.

50. Crane, B. R.; Siegel, L. M.; Getzoff, E. D., Probing the Catalytic Mechanism of Sulfite Reductase by X-ray Crystallography: Structures of the *Escherichia coli* Hemoprotein in Complex with Substrates, Inhibitors, Intermediates, and Products. *Biochemistry* **1997,** 36, 12120-12137.

51. Leung, W.-H.; Hun, T. S. M.; Wong, K.-Y.; Wong, W.-T., Synthesis and Electrochemistry of Dialkylosmium-(IV) and -(V) Porphyrins. Crystal Structure of [Os(ttp)CH$_2$SiMe$_3$)$_2$] [H$_2$ttp = 5,10,15,20-tetra(*p*-tolyl)porphyrin]. *J. Chem. Soc., Dalton Trans*. **1994**, 2713-2718.

52. Smieja, J. A.; Omberg, K. M.; Breneman, G. L., Synthesis and Characterization of an Osmium Porphyrinato Bis(arylimido) Complex, Os(TTP)(NAr)$_2$, with Strongly Bent Osmium-Organoimido Bonds. *Inorg. Chem.* **1994,** 33, (3), 614-616.

53.   Waleh, A.; Ho, N.; Chantranupong, L.; Loew, G. H., Electronic Structure of Nitrosyl Ferrous Heme Complexes. *J. Am. Chem. Soc*. **1989,** 111, (8), 2767-2772.

54.   Hori, H.; Ikeda-Saito, M.; Yonetani, T., Single Crystal EPR of Myoglobin Nitroxide. *J. Biol. Chem*. **1981,** 256, (15), 7849-7855.

55.   Richter-Addo, G. B.; Wheeler, R. A.; Hixon, C. A.; Chen, L.; Khan, M. A.; Ellison, M. K.; Schulz, C. E.; Scheidt, W. R., Unexpected Nitrosyl Group Bending in Six-Coordinate {MNO}[6] σ-Bonded Aryl(iron) and -ruthenium Porphyrins. *J. Am. Chem. Soc*. **2001,** 123, 6314-6326.

56.   Chen, L.; Khan, M. A.; Richter-Addo, G. B.; Young, V. G., Jr.; Powell, D. R., Synthesis, Characterization, and Solid-State Molecular Structures of Nitrosoarene Complexes of Osmium Porphyrins. *Inorg. Chem*. **1998,** 37, (18), 4689-4696.

57.   Flores, M.; Wajnberg, E.; Bemski, G., Temperature Dependence of Q-Band Electron Paramagnetic Resonance Spectra of Nitrosyl Heme Proteins. *Biophys. J*. **1997,** 73, 3225-3229.

58.   Wyllie, G. R. A.; Scheidt, W. R., Solid-State Structures of Metalloporphyrin NOx Compounds. *Chem. Rev*. **2002,** 102, (4), 1067-1089.

59.   Yang, S.-Y.; Leung, W.-H.; Lin, Z., Geometric Features and Electronic Structure of Six-Coordinated Dialkyl and Dithiolate Complexes of Osmium(IV) Porphyrins. *Organometallics* **2001,** 20, (14), 3198-3201.

60.   Eyer, P., Detoxification of N-Oxygenated Arylamines in Erythrocytes. A Review. *Xenobiotica* **1988,** 18, (11), 1327-1333.

61.   Kiese, M., The Biochemical Production of Ferrihemoglobin-Forming Derivatives from Aromatic Amines, and Mechanisms of Ferrihemoglobin Formation. *Pharmacol. Rev*. **1966,** 18, (3), 1091-1161.

62.   Mittal, C. K.; Arnold, W. P.; Murad, F., Characterization of Protein Inhibitors of Guanylate Cyclase Activation from Rat Heart and Bovine Lung. *J. Biol. Chem*. **1978,** 253, (4), 1266-1271.

Copyright Releases